University of Nevada, Reno

Gold and Base Metal Mineralization, Hydrothermal Alteration and Vein Paragenesis in the Spring Valley Deposit, Pershing County, Nevada

A thesis submitted in partial fulfillment of the requirements for the degree of Master of Science in Geology

by

Betsy L. Crosby

Dr. Tommy B. Thompson/Thesis Advisor

December, 2012

ProQuest LLC.
789 East Eisenhower Parkway
P.O. Box 1346
Ann Arbor, MI 48106 - 1346

University of Nevada, Reno
Statewide • Worldwide

THE GRADUATE SCHOOL

We recommend that the thesis
prepared under our supervision by

BETSY CROSBY

entitled

Gold And Base Metal Mineralization, Hydrothermal Alteration And Vein Paragenesis In The Spring Valley Deposit, Pershing County, Nevada

be accepted in partial fulfillment of the
requirements for the degree of

MASTER OF SCIENCE

Tommy B. Thompson, Ph.D., Advisor

Peter Vikre, Ph.D., Committee Member

Victor Vasquez, Ph.D., Graduate School Representative

Marsha H. Read, Ph. D., Dean, Graduate School

December, 2012

Abstract

Spring Valley is a gold-base metal deposit located on the eastern flank of the Humboldt Range in Pershing County, Nevada. Mineralization is primarily hosted within the Feldspar Porphyry, Agglomerate, Welded Tuff, Volcaniclastic Siltstone and Quartz-eye Rhyolite units of the Rochester Formation and in lithic tuffs and greenstones of the Limerick Formation. It occurs in a series of crosscutting quartz-carbonate ± pyrite ± tourmaline ± sphalerite ± galena veins of clear mesozonal origin associated with weakly to strongly pervasive quartz-sericite-pyrite-carbonate ± tourmaline alteration. Initial classification as a porphyry gold system is thus disproved, and alternate orogenic and reduced intrusion-related gold interpretations are presented.

Vein-related alteration is relatively consistent throughout the Quartz-eye Rhyolite, Welded Tuff, Agglomerate and Feldspar Porphyry members of the Rochester Formation, though it is better developed in the latter. In the Feldspar Porphyry, proximal alteration consists of a light green to greenish-gray, weakly to strongly pervasive quartz-sericite-pyrite-carbonate ± tourmaline assemblage. Tourmaline is typically only found in selvages adjacent to tourmaline-bearing veins. Proximal quartz-sericite-pyrite-carbonate-tourmaline alteration grades outward into an intermediate to distal quartz-hematite alteration assemblage, characterized by the presence of very fine-grained hematite “dust” that imparts a distinct red-brown coloration to groundmass and feldspar phenocrysts. Quartz-hematite alteration may grade further outward into a distal quartz-specularite assemblage, in which very-fine grained, platey specularite lends a dark gray coloration to

groundmass. Alteration in the overlying Agglomerate unit of the Rochester Formation is best observed in reactive greenstone clasts. It consists of a light green quartz-sericite-pyrite-carbonate ± fuchsite ± tourmaline assemblage, where similarly to proximal alteration zones in the Feldspar Porphyry, tourmaline occurs consistently outboard of tourmaline-bearing veins. Proximal alteration grades outward into a dark gray quartz-specularite ± hematite assemblage. Hydrothermal alteration of Welded Tuff and Feldspar Porphyry clasts is similar to that of their source units. Alteration effects are generally not present in groundmass or unreactive quartzite and carbonate clasts.

Proximal alteration in the remainder of the Rochester Formation and in the Limerick Formation is consistent with that observed in the Feldspar Porphyry and Agglomerate units, though intermediate to distal alteration varies considerably. In the Welded Tuff, proximal alteration consists of a light green to gray quartz-sericite-pyrite-carbonate ± tourmaline assemblage that occurs interstitial to silicified fiamme. At depth, proximal alteration may grade outward into a dark gray to purplish quartz-specularite ± hematite assemblage, though at shallow levels, it generally grades outward into relatively unaltered wallrock. In the Quartz-eye Rhyolite, proximal light green quartz-sericite-pyrite-carbonate alteration grades outward into a greenschist-facies sericite-carbonate assemblage. In the Limerick Formation, proximal light green quartz-sericite-pyrite-carbonate ± fuchsite ± tourmaline alteration crosscuts a distinct, greenschist-facies chlorite-carbonate-hematite ± epidote assemblage. Proximal alteration may grade outward into a hematite-rich zone, but most commonly does not.

Following characterization of alteration assemblages and zoning, major element compositions of representative samples from alteration zones in the Feldspar Porphyry were determined. Al_2O_3 generally decreases from unaltered to proximally altered samples. It is broadly paralleled by an increase in SiO_2 and is thus likely due to increasing secondary quartz in quartz-sericite-pyrite-carbonate alteration zones. Decreasing CaO from unaltered to proximally altered zones is likely due to an increasing presence of iron in carbonate. Increasing K_2O, at first counterintuitive due to the certain loss of K_2O during sericitization of K-feldspar, is likely due to the relatively high volumes of sericite introduced in anastomosing veinlets. BaO trends mimic those of K_2O and are likely related to the substitution of Ba for K in sericite.

Quartz vein textures at Spring Valley are indicative of formation at mesozonal depth under high pressure and are thus also inconsistent with a porphyry interpretation. Pre-ore ataxial and ore-stage crack-seal and non-directional quartz veins were identified. Ataxial veins are composed of distinctive fibrous quartz and are associated with moderately to strongly pervasive silicification. Many trend northwest, suggesting formation during NW/SE-directed crustal shortening. Crack-seal and non-directional quartz veins are associated with previously described quartz-sericite-carbonate-pyrite ± tourmaline alteration and may host sphalerite-galena-gold ± chalcopyrite ± tetrahedrite mineralization. Crack-seal veins are generally earlier and are composed of elongate-blocky quartz ± pyrite, with late carbonate and tourmaline that formed previous to the crack-seal process. Non-directional quartz veins are composed of granular quartz-carbonate ± pyrite ± tourmaline ± sphalerite ± galena ± chalcopyrite ± tetrahedrite ± gold

and record the first introduction of Pb, Zn and Au mineralization. Ore stage veins are primarily brittle features, with internal textures indicative of formation during extension, including relatively planar, matching vein walls, open-space filling quartz textures, growth of elongated grains perpendicular to vein walls, and evidence of vein-opening direction, such as inclusion bands in crack-seal veins.

Eight vein stages were recognized at Spring Valley: 1. Pre-ore ataxial veins associated with moderately to strongly pervasive silicification; 2. Early gray granular quartz-tourmaline ± pyrite veins; 3. Early ore-stage gray elongate-blocky to granular quartz-carbonate ± pyrite veins; 4. White to gray elongate-blocky quartz ± carbonate-pyrite veins; 5. Gray granular quartz-carbonate ± pyrite veins; 6. Gray granular quartz-tourmaline ± carbonate-pyrite veins; 7. White granular quartz-tourmaline ± carbonate-pyrite; 8. White granular quartz-carbonate-pyrite ± sphalerite ± galena ± chalcopyrite ± tetrahedrite ± gold. The cyclical transition between granular and crack-seal veins likely reflects fluctuations in pressure and changes in fluid chemistry throughout the evolution of the deposit. Fluctuations in temperature were not likely a factor. Analyses of 129 L_{H_2O}-V_{CO_2} and L_{H_2O}-L_{CO_2}- V_{CO_2} inclusions identified in 6 of 8 ore-stage quartz veins indicate that the minimum temperature of formation was consistent throughout vein formation and ranged from 210°C to 340°C. An applied pressure correction 120°C to 180°C brings the range of trapping temperatures to approximately 330°C to 520°C.

Gold mineralization is also inconsistent with classification as a porphyry system. It may occur in all ore-stage vein stages, particularly where proximal to later Au-bearing veins. It is primarily associated with pyrite, though it may occur without pyrite and/or

with later sphalerite and galena. In contrast to porphyry systems, sulfide content is generally less than 2%, and only trace amounts of copper sulfides—primarily chalcopyrite and tetrahedrite—are present. Ore mineralogy is much simpler than that of nearby deposits, with virtually no silver and volumetrically minor sulfide mineralization.

Ore mineralogy, alteration mineralogy and zoning, and vein textures are inconsistent with classification as a porphyry gold system. Two alternative interpretations are proposed: orogenic and reduced intrusion-related gold. Spring Valley shares many similarities with orogenic gold deposits, including the mineralogy and consistency of alteration assemblages and zoning, the mineralogy and simplicity of gold and associated sulfides, and crack-seal and non-directional vein textures indicative of formation under mesothermal conditions. Similarly to most orogenic gold deposits, mineralization occurs in greenschist-facies host rocks where it is clearly retrograde in origin. However, the geometry of extensional crack-seal and non-directions veins is dissimilar to that of extensional veins in established orogenic gold deposits, and a definitive structural setting cannot be established.

Reduced intrusion-related gold (RIRG) deposits share many of the above characteristics with orogenic gold deposits and the gold occurrence at Spring Valley. Several additional lines of evidence suggest Spring Valley is a reduced intrusion-related gold deposit: 1. Mineralization is spatially and possibly temporally associated with the Late Cretaceous Rocky Canyon granodiorite; 2. Mineralization is low grade and irregularly distributed; 3. Quartz vein geometries are more in line with those of proximal RIRG deposits; and 4. Metal zoning in the Humboldt Range is strikingly similar to metal

zoning in established RIRG districts. However, RIRG deposits are typically associated with more complex ore and alteration mineralogy, and no evidence of a genetic relationship between varying deposits in the Humboldt Range has been established. In addition, a broad, NS-trending zone of Au-bearing metamorphic quartz veins similar in geometry, morphology and orientation identified throughout northwestern Nevada suggests that vein formation occurred independently of Late Cretaceous magmatism (Cheong, 1999). In the absence of an age of mineralization, the style of gold mineralization at Spring Valley cannot be definitively established.

Acknowledgements

Foremost, I would like to thank Dr. Tommy Thompson and the Center for Research in Economic Geology for providing not only the opportunity to work on this project, but also a solid education and a patient and knowledgeable sounding board. And to Julie, thank you for all your help navigating the bureaucracy and paperwork, and most importantly, thank you for your support and encouragement.

I would also like to thank Paul Dobak and Barrick Gold for providing funding; the Spring Valley crew, John Watson, Larry Pancoast, Chuck Bratland, Orion George, Bill Sevores and Bob Morrell for their insight and support, and Connie, Deanna, Gray and Epi for making my time in Lovelock as comfortable as possible; and my colleagues at the Center for Research in Economic Geology for their shared insights and knowledge and the occasional distraction.

Most importantly, I would like to thank my family—my parents for their unwavering support and the plane tickets home when I couldn't take the cold anymore; my sisters and brother for their encouragement, and in Jac's and Katie's cases, pretending to be interested and letting me ramble about my work on road trips. (Wait—was that a steamboat?) And Jason, thank you for your support, your understanding, and for coming with me to Reno so that I could pursue my education.

Table of Contents

List of Figures

List of Tables

Introduction

The Spring Valley gold deposit is located on the eastern flank of the Humboldt Range in the Spring Valley district of Pershing County, Nevada (Fig. 1). It lies approximately twenty miles northeast of Lovelock and three miles north of the Rochester silver mine. Pyrite ± sphalerite-galena-Au mineralization occurs in small (1-40mm), discontinuous quartz ± tourmaline-carbonate veins associated with weak to strong quartz-sericite-pyrite-carbonate alteration. It is primarily hosted within a sequence of intercalated latite to rhyolite tuffs, rhyolite flows and sedimentary rocks of the Rochester Formation. Minor mineralization also occurs in the underlying Limerick Formation and crosscutting dikes of the Weaver Formation, which together with the Rochester Formation comprise the Permo-Triassic Koipato Group.

The cornerstone of this study focuses on petrographic descriptions of host rocks, precious and base metal mineralization and hydrothermal alteration, with the ultimate goal of defining mineralogy and textures, and establishing paragenesis. It is subdivided into four main areas of concentration:

1. Petrographic description of host rocks, precious and base-metal mineralization, and alteration assemblages;

2. Determination of the timing of gold mineralization relative to base metal mineralization, host rocks, and alteration;

3 Description of vein types and determination of vein paragenesis; and

4. Dating of host rocks

Figure 1: Aerial photograph of the Lovelock area, Pershing County, Nevada. The NS-trending in the center is the Humboldt Range. The location of Spring Valley is denoted with a red star. The inset to the right is an enhanced view of the area delineated by the red square.

Characterization of alteration, mineralization, and vein types primarily serves to aid in the classification of the deposit and the development of an integrated genetic model that can be utilized in exploration.

Mineralization at Spring Valley was initially classified as a porphyry gold system with an associated, mineralized diatreme complex (Neal and LeLacheur, 2010; LeLacheur et al., 2011). However, this interpretation was lacking in supporting, focused and contextual descriptions of alteration assemblages, mineralization, and vein types; by

the commencement of this thesis project, the porphyry classification had largely fallen out of favor. It was supplanted by an open-minded sense of confusion and lively discussion, with interpretation running the gamut from orogenic to intrusion-related to—at the height of perplexity over the presence of jasperoid-like alteration—epithermal. The identification of metamorphic textures of quartz veins during the course of this study, coupled with detailed description of alteration assemblages, gold associations and the reevaluation of their implications, confirms that Spring Valley is not a porphyry gold deposit, but is likely rather an orogenic or reduced intrusion-related -gold vein deposit related to an as-of-yet defined deformational event.

District History

Earliest mining activity in the Spring Valley district was centered on the Bonanza King gold deposit, located approximately two miles east-southeast of Spring Valley (Johnson, 1977). The Bonanza King, known then as the Lady Mary, was located in 1868 and mined continuously until 1885 and sporadically until 1910 (Johnson, 1977). Placer mining in district was first recorded in Spring Valley Canyon in 1875 and occurred in the canyons to the south from 1880 to 1890 (Johnson, 1977). Early placer mining was largely conducted by Chinese miners who sunk shafts into the alluvium and mined along its contact with bedrock, though at one point, the Spring Valley Gold Dredging Co. operated a dry-land dredge (Johnson, 1977). In total, placer deposits in the Spring Valley district produced an estimated $10 million, with the majority attributed to Spring Valley Canyon and American Canyon (Johnson, 1977). The Wabash mine, located along the base of the ridge to the south of Spring Valley, was mined from 1935 to 1938 (Johnson, 1977). In

three years, the Wabash produced 170 tons of ore, including nearly 7000 oz silver, over 650 lbs of copper and over 9,500 pounds of lead, but only 1 oz of gold (Johnson, 1977).

Modern exploration at Spring Valley commenced in 1996 and was conducted by Kennecott geologists intent on finding the source of the extensive placers deposits in the canyon to the east (Neal and LeLacheur, 2010; LeLacheur et al., 2011). The discovery hole was drilled by Echo Bay in 2001, following acquisition from Kennecott in 2000, and was drilled continuously until 2003 when the former exploration company became a subsidiary of Kinross Gold (Neal and LeLacheur, 2010; LeLacheur et al., 2011). The drilling program initiated by Echo Bay was continued after acquisition of the property by Midway Gold Corp until 2008 (Neal and LeLacheur, 2010; LeLacheur et al., 2011). Exploration is currently being conducted by Barrick Gold Exploration, Inc., under a joint venture agreement with Midway Gold (Neal and LeLacheur, 2010; LeLacheur et al., 2011).

Methods

Field work was completed during the summer of 2011. A total of 8 complete drill holes and three additional partial holes were logged with an emphasis on alteration mineralogy and zoning, ore mineralogy, and vein types and relationships. Due to the small number of complete holes in storage and current whole core assaying procedures, the selected holes were concentrated in the south end of the deposit, with the exception of SV11-513C, which was located to the north and was used to compare mineralization and alteration in the north end of the deposit with that of the south. Locations of holes and the general outline of the study area are shown in Figure 2. Structure was difficult to

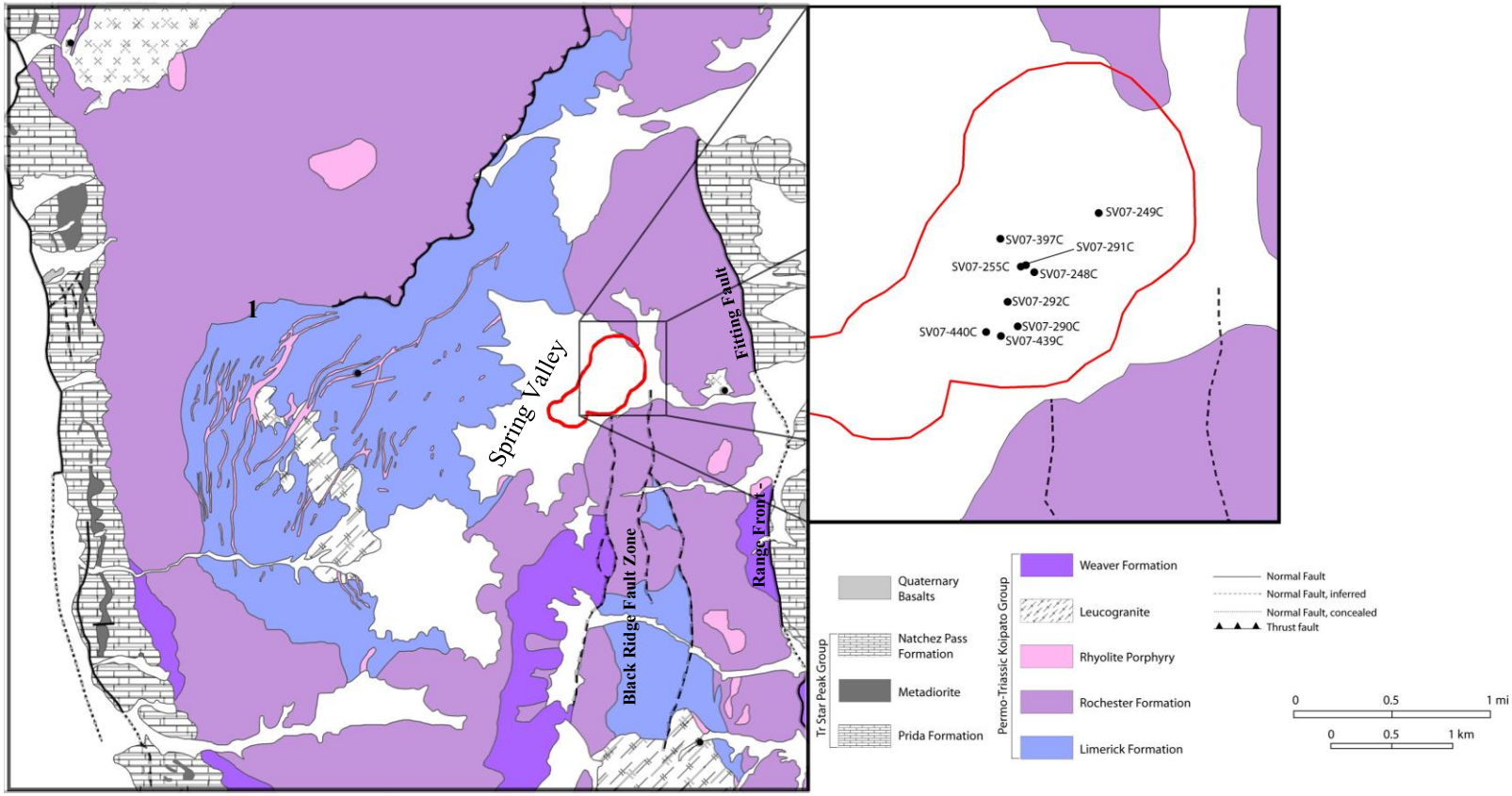

Figure 2: A. Simplified geologic map of Spring Valley and vicinity, modified from Wallace et al. (1969a). Numbers show locations of samples taken for U/Pb dating, described in Table 1. The red line delineates the $975/oz pit boundary from LeLacheur et al. (2011) and is used to show the approximate location of mineralization. B. Enlarged view of the Spring Valley project area and locations of drillholes logged during this study.

characterize in split core and of little importance to the study, and was thus largely ignored. The field season commenced with a lithology and alteration mapping project of a 2-3km^2 area to the north of Spring Valley. The purpose of the mapping project was to place the host rocks of the Koipato Group and the mineralized system into a broader regional context and to identify possible areas of economic interest.

Thin sections of fifty- samples and polished sections of eleven samples from core were made, and a detailed petrographic study commenced. Host rocks were described and lithology assignments were made. Ore-stage mineralization, vein types, and regional and hydrothermal alteration assemblages were identified and described. From this, a paragenetic sequence exploring the relationships between host rocks, gold and base metal mineralization, and hydrothermal alteration was derived. Billets and accompanying hand samples were stained with a mixtures of 1.5% HCl, 2g potassium ferricyanide and 2g alizarin red to determine carbonate composition and relation of carbonate composition to gold mineralization.

Following the characterization of alteration mineralogy and paragenetic relationships, ten samples from select alteration transects were sent to ALS Chemex for borate fusion analyses of trace element, metal, and major element geochemistry. The purpose of these analyses was to determine the geochemical associations of different alteration assemblages and to identify major and trace element changes from relatively unaltered to vein-distal altered to vein-proximal altered wallrock.

Fluid inclusion analyses commenced following the development of a paragenetic vein sequence and petrographic identification of fluid inclusion types. Six doubly-polished plates with seven ore-stage vein types were mapped and mounting epoxy was

dissolved in acetone. Homogenization temperatures were determined for 129 L_{H_2O}-L_{CO_2}-V_{CO_2} and L_{H_2O}-V_{CO_2} fluid inclusions. Heating runs were performed on a USGS-style gas-flow heating/freezing stage modified and produced by Fluid, Inc. Sample chips are placed beneath a calibrated thermocouple in a chamber with three glass plates above and three glass plates below. The chamber is then enclosed in a ceramic stage, through which hot air is channeled into the chamber through a glass tube. The heat source is controlled by a foot pedal, which, when depressed at fluid inclusion homogenization, turns the heat source off and fixes the homogenization temperature on a digital display connected to the thermocouple.

Geology of Spring Valley and the Humboldt Range

The Humboldt Range is a NS-trending anticlinorium composed of folded and uplifted Permo-Triassic through Jurassic volcanic and sedimentary rocks, intruded by Triassic through Cretaceous felsic to intermediate dikes, sills, plugs and stocks (Fig. 2) (Wallace et al., 1960; Silberling and Roberts, 1962; Vikre, 1977; Vikre, 1981; Skalbeck, 1985). It is bounded to the east by the Range Front/Fitting fault and to the west by an unnamed normal fault (Silberling and Wallace, 1967; Wallace et al., 1969a; Wallace et al., 1969b). Uplift of the range occurred during Miocene basin-and-range extension (Silberling and Wallace, 1967; Wallace et al., 1969a; Wallace et al., 1969b; Vikre, 1977; Skalbeck, 1985).

Spring Valley is the largest of several intermontane grabens that formed along the eastern flank of the Humboldt range during Miocene extension (Wallace et al., 1969a; Neal and LeLacheur, 2010). It is crosscut by a series of Permo-Triassic (?) through Cretaceous (?) normal faults and infilled by 50-650 feet of alluvium (Neal and LeLacheur, 2010; LeLacheur et al., 2011). The Rochester and Limerick formations of the Koipato Group form the basement of Spring Valley (Neal and LeLacheur, 2010; LaLacheur and Harris, 2011). They are crosscut by dikes and plugs ranging in age from Permo-Triassic through Cretaceous or Oligocene and in composition from rhyolite to quartz monzonite.

Lithology

The basement of the Humboldt Range is composed of interbedded volcanic flows, tuffs and volcaniclastic sedimentary rocks of the Permo-Triassic Koipato Group (Fig. 2) (Wallace et al., 1960; Silberling and Wallace, 1967; Wallace et al., 1969a; Wallace et al., 1969b). Koipato volcanism commenced during a period of incipient back-arc extension, largely concomitant with the emplacement of the Golconda allochthon (Vetz, 2011). At 248-254 Ma, it is among the earliest Cordilleran back-arc volcanic terranes in the Great Basin (Barth and Wooden, 2006), a fact that has led to some debate over its age relative to the emplacement of the Golconda allochthon. The angular unconformity at the contact between the Limerick Formation and the underlying, allochthonous Havallah Formation (Johnson, 1977), coupled with recent Sm/Nd and Rb/Sr isotopic data that suggests interaction with Paleoproterozoic crust, indicates that the Golconda allochthon was attached to the continent at the time of volcanism (Vetz, 2011) . However, numerous unconformities within the Koipato Group, most notably an apparent, local angular unconformity at the typically gradational contact between the Limerick and Rochester formations indicate that movement of the allochthon continued during volcanism (Vikre, 1977; Johnson, 1977; Tom Chadwick, pers. comm., 2011).

The oldest member of the Koipato Group is the Limerick Formation, dated by Vetz (2011) at 249.594 ± 0.081 to 249.371 ± 0.096 Ma. It consists of intercalated greenstone (andesite) flows, lithic to crystal tuffs, and volcaniclastic siltstone and is in excess of 6000 feet thick (Wallace et al., 1969a; Wallace et al., 1969b; Johnson, 1977; Vikre, 1977). It is exposed in the northern part of the range and generally lacks a defined

vertical sequence (Wallace et al., 1969a; Wallace et al., 1969b; Tom Chadwick, pers. comm., 2011).

The Limerick Formation is overlain by the intermediate to felsic Rochester Formation, determined by Vetz (2011) to be ~249.18 to ~248.97 Ma. The Rochester Formation consists of poorly to densely welded, rhyolite ash-flow tuffs and quartz latite to rhyolite flows, with minor, local tuffaceous sediments, fluvial siltstones and coarse-grained agglomerates (Wallace et al., 1969a; Wallace et al., 1969b; Johnson, 1977; Vikre, 1977). It is present throughout the Humboldt Range, though it is most abundant in the central and northern portions of the range and is in excess of 6000 feet in Rochester Canyon (Wallace et al., 1969a; Wallace et al., 1969b; Johnson, 1977; Vikre, 1977; Tom Chadwick, pers. comm., 2011). It is an important host to ore in the Rochester and Spring Valley districts, and in the Dun Glen district in the East Range (Johnson, 1977; Vikre, 1977).

The Rochester Formation is unconformably overlain by the silicic Weaver Formation (Silberling and Wallace, 1967; Wallace et al., 1969a; Wallace et al., 1969b; Johnson, 1977; Vikre, 1977). The Weaver Formation consists of tuffaceous and volcaniclastic sediments and rhyolite flows that can generally be distinguished from Rochester flows by an increase in quartz and phenocryst content (Vikre, 1977). In the Rochester district, basal Weaver consists predominantly of rhyolite flows, with arkosic siltstones, sandstones and conglomerates becoming more abundant upward in the sequence (Vikre, 1977). It is thickest in the south-central portion of the range, and thins considerably northward (Johnson, 1977; Vikre, 1977).

Back-arc extension continued and basin subsidence increased following the emplacement of the Golconda allochthon and the cessation of Koipato volcanism ~254 Ma (Dickinson, 2006; Vetz, 2011). The Star Peak Group, composed of interbedded shallow marine clastic and carbonate rocks of the Prida and Natchez Pass formations, was unconformably deposited over the Koipato Group during the mid-Triassic (Silberling and Roberts, 1962; Silberling and Wallace, 1969; Silberling and Nichols, 1982). The Star Peak Group is overlain by shallow marine to deltaic clastic to carbonate rocks of the Auld Land Syne Group (Silberling and Wallace, 1969; Burke and Silberling, 1974). In the north and central portions of the range, the Auld Lang Syne Group is represented by the mudstones and sandstones of the Grass Valley Formation (Silberling and Wallace, 1967; Wallace et al., 1969a; Burke and Silberling, 1973). To the south, the Grass Valley Formation is overlain by calcareous siltstone, limestone and carbonate of the Dun Glen Formation and a thick, undifferentiated Auld Lang Syne Group sequence of interbedded clastic and carbonate rocks (Wallace et al., 1969b).

Intrusive phases

The Leucogranite and Rhyolite Porphyry intrude lower Koipato and are believed to be the intrusive equivalent of the Weaver Formation (Figs.2- 3) (Wallace et al., 1960; Vikre, 1977). The Leucogranite forms a large plug in the central portion of the range east of Coeur Rochester and in the vicinity of Sage Hen Flat (Wallace et al., 1969a; Vikre, 1977). It is most easily accessed through South American and Troy canyons along the eastern flank of the range. It is also present in outcrop along the southern flank of Lone Mountain in eastern Limerick Canyon (Wallace et al., 1969a; Vikre, 1977). The

Leucogranite is light tan to white on fresh surface and weathers reddish tan. It is fine-to medium-grained with local aplitic facies (Vikre, 1977), and is composed of equigranular gray quartz, pink K-feldspar and white to tan plagioclase. Cupolas commonly contain small quartz-tourmaline veins with relatively abundant tourmaline and quartz in selvages (Vikre, 1977). Silicified portions that occur independently of tourmaline are commonly associated with small sulfide deposits, such as the quartz-sulfide-barite veins of the Pacific Matchless mine (Vikre, 1977). The Leucogranite is also commonly sericitized (Vikre, 1977).

The lower Koipato Group is also intruded by ~249 Ma Rhyolite Porphyry dikes, sills and plugs (Fig. 3) (Wallace et al., 1960; Vikre, 1977). Rhyolite Porphyry (RP) is light green to light gray and porphyritic, composed of 2-5% quartz, K-feldspar and plagioclase ± biotite phenocrysts in an aphanitic groundmass. A felsite border phase may occur locally (Tom Chadwick, pers. comm., 2011). It is compositionally similar to the overlying Weaver Formation and is believed to be the intrusive equivalent of Weaver rhyolite flows (Wallace et al., 1960; Vikre, 1977). Rhyolite Porphyry is present throughout the Humboldt Range. In the vicinity of Spring Valley, it occurs as dikes and sills to the north and west (Wallace et al., 1969a; Tom Chadwick, pers. comm., 2011). To the east of Spring Valley, small Rhyolite Porphyry plug caps the ridge above the Bonanza King (Wallace et al., 1969a). It occurs as dikes within Spring Valley that may host mineralization. Grade may increase in host rocks adjacent to Rhyolite Porphyry dikes.

Younger intrusives are intermediate in composition and formed during two separate periods of plutonism. The Rocky Canyon granodiorite stock is present in Rocky and Wright canyons on the northwestern flank of the range. It forms the prominent peaks

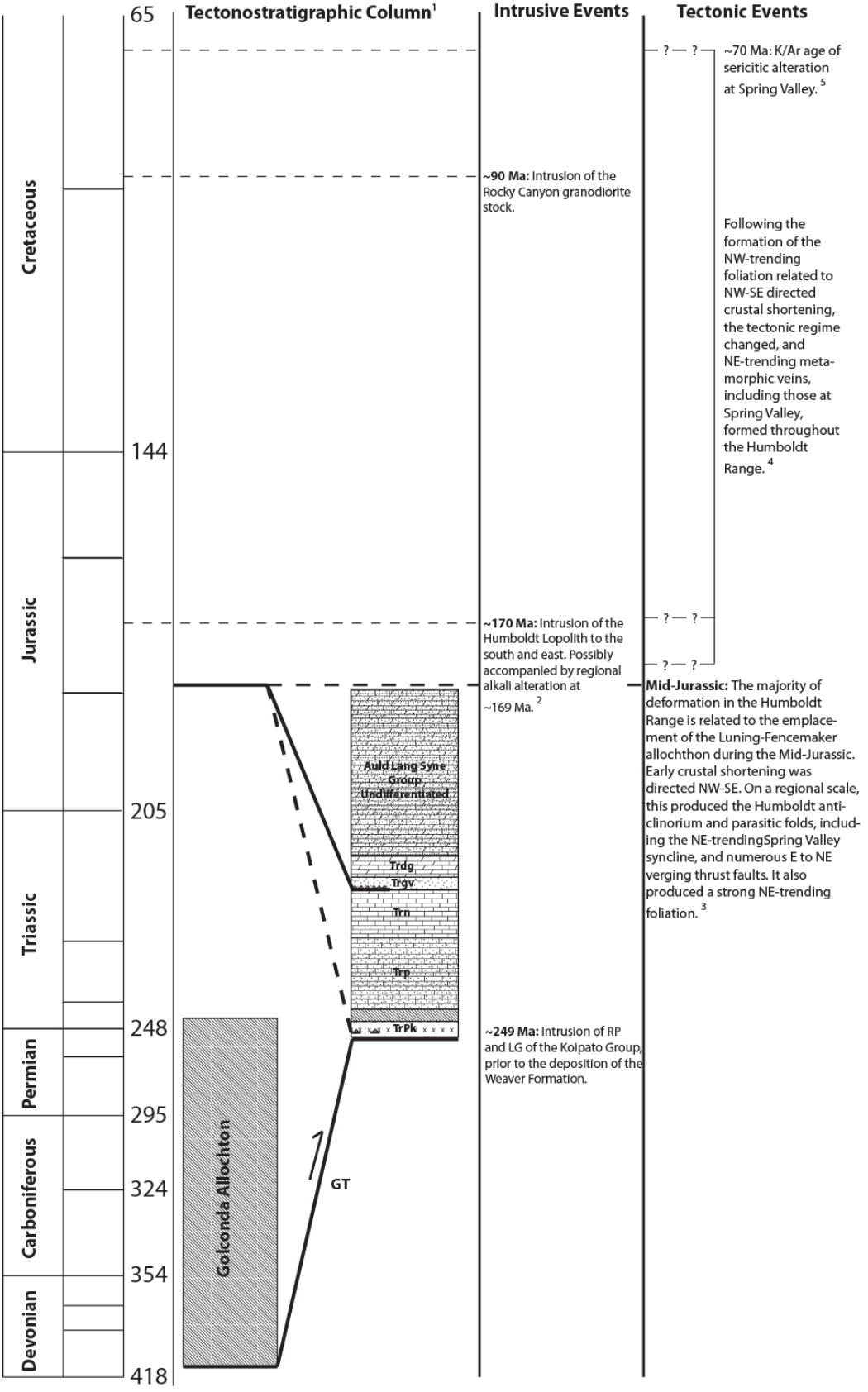
65
Tectonostratigraphic Column[1]
Intrusive Events
Tectonic Events
Cretaceous
Jurassic
Triassic
Permian
Carboniferous
Devonian
144
205
248
295
324
354
418
~70 Ma: K/Ar age of sericitic alteration at Spring Valley. [5]
~90 Ma: Intrusion of the Rocky Canyon granodiorite stock.
Following the formation of the NW-trending foliation related to NW-SE directed crustal shortening, the tectonic regime changed, and NE-trending meta-morphic veins, including those at Spring Valley, formed throughout the Humboldt Range. [4]
~170 Ma: Intrusion of the Humboldt Lopolith to the south and east. Possibly accompanied by regional alkali alteration at ~169 Ma. [2]
Mid-Jurassic: The majority of deformation in the Humboldt Range is related to the emplace-ment of the Luning-Fencemaker allochthon during the Mid-Jurassic. Early crustal shortening was directed NW-SE. On a regional scale, this produced the Humboldt anti-clinorium and parasitic folds, includ-ing the NE-trendingSpring Valley syncline, and numerous E to NE verging thrust faults. It also produced a strong NE-trending foliation. [3]
Auld Lang Syne Group, Undifferentiated
Trdg
Trgv
Trn
Trp
TrPk
~249 Ma: Intrusion of RP and LG of the Koipato Group, prior to the deposition of the Weaver Formation.
Golconda Allochton
GT

Figure 3 (previous page): Stratigraphic column of the Humboldt Range, showing corresponding intrusive and tectonic events, modeled after Cheong (1999).
References: 1: Wallace et al. (1966), Dickinson (2006); 2. Kistler and Speed (2000); Wallace et al. (1966), Cheong (1999); 4. Cheong (1999); 5. Chris Henry, pers. comm., 2011

observed from the west and highly weathered, rounded outcrops on slopes and canyon floors. It is fine- to medium-grained and equigranular, with local pegmatitic facies, and is composed of equigranular K-feldspar, plagioclase and quartz with abundant, strongly altered biotite.

A younger, porphyritic quartz diorite to diorite intrusive phase occurs as dikes and plugs within and adjacent to Spring Valley (Wallace et al., 1969a). A small plug composed of chloritized hornblende and biotite phenocrysts in a fine-grained feldspar- and chlorite-rich groundmass is present in outcrop in an arroyo to the north of Spring Valley canyon (Wallace et al., 1969a). Historically, porphyritic quartz diorite to diorite was believed to be related to the Rocky Canyon granodiorite, though an age of approximately 30Ma obtained from U/Pb dating of zircon grains suggests that it may be related to post-Laramide westward arc migration (see chapter 3; Wallace, et al., 1969a; Dickinson, 2006).

Host rocks at Spring Valley

Mineralization at Spring Valley is hosted within the Limerick and Rochester formations and in crosscutting Rhyolite Porphyry dikes of the Weaver Formation (Fig. 4) (Neal and LeLacheur, 2010; LeLacheur et al., 2011). Late Cretaceous hornblende porphyry dikes are present in the vicinity of the Wabash fault, and a small hornblende

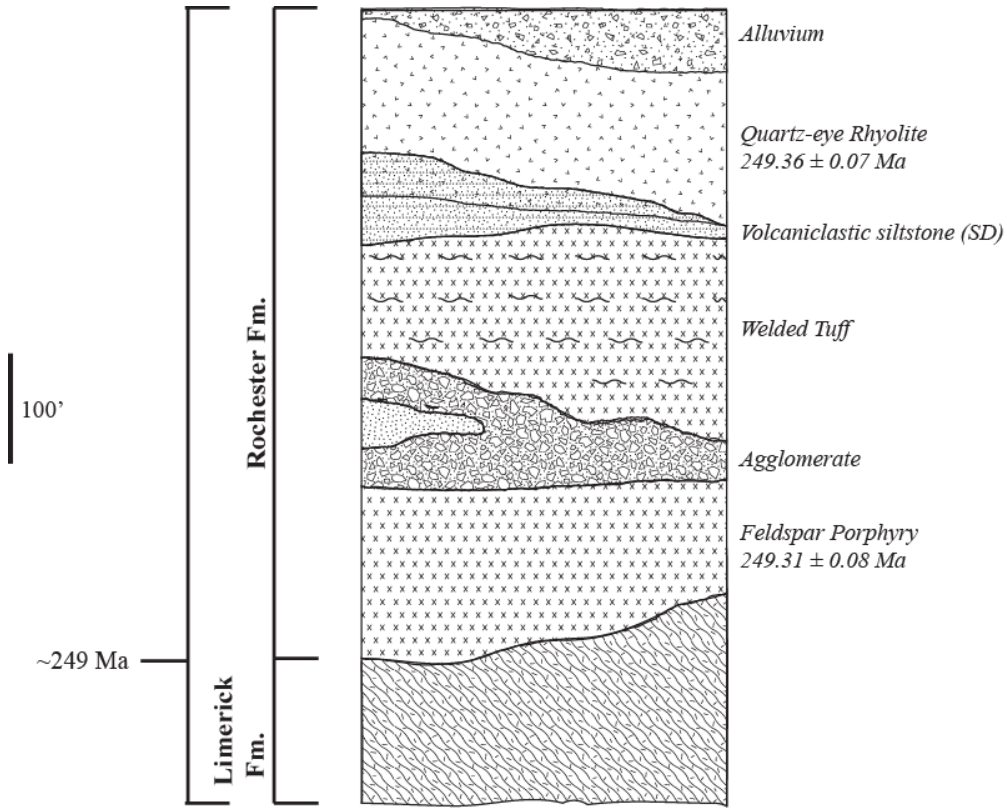

Figure 4: Tectonostratigraphic column of host rocks encountered within the study area.

porphyry plug is present in the western portion of Spring Valley (Tom Chadwick, pers. comm., 2011). Both are unmineralized, though grade may increase in adjacent wallrock.

Limerick Formation

In the vicinity of Spring Valley, the Limerick has no defined vertical sequence and consists primarily of weakly to moderately welded lithic tuffs and volcaniclastic siltstone, with subordinate greenstone and local cherty conglomerates (Tom Chadwick, pers. comm., 2011). Within the study area, the Limerick Formation consists of fine- to coarse-grained lithic tuffs interbedded with andesitic greenstone flows and local volcaniclastic siltstones. It is encountered at depths of 720 feet-1250 feet and has been

drilled to depths exceeding 1300 feet. Although it lacks a defined vertical sequence and sharp lateral changes between units are common, a thin lithic tuff interval is almost always present at the top of the formation. There is no discernible vertical sequence below the lithic tuff.

Lithic tuff is cognate to heterolithic and consists primarily of dark green to reddish greenstone clasts and black chert. Lithic clasts are coarse-sand to pebble-sized and are supported by a fine-grained, chloritic groundmass. Welding is not typically observed in core, but they are poorly to locally strongly welded in outcrop (Fig. 5) (Tom Chadwick, pers. comm., 2011). Lithic tuff commonly forms low-lying, resistant dark purplish gray ridges. Where strongly sericite-altered, it is typically medium to light green mottled red to purple. Local tuffaceous interbeds with lithic clasts suspended in a fine-grained matrix were mapped on the ridge to the north of Spring Valley, with thin air fall tuff interbeds. Irregular to rounded lithophysae, ranging in size from centimeters to 2-3 inches and infilled by quartz, are present locally (Fig. 6).

In core, the contact between lithic tuff and greenstone is commonly gradational and the two units may be difficult to distinguish, especially where greenstone lithic fragments predominate. Greenstone flows are composed of 5-10% chloritized biotite phenocrysts with lesser hornblende and pyroxene in an aphanitic, chlorite- and carbonate-rich groundmass. They are typically massive and exhibit no flow foliation. In outcrop, greenstone flows range from dark to light green where sericitized. They form continuous, resistant ledges 2-10 feet in height.

Volcaniclastic siltstone, commonly referred to in logs as greywacke, is much less common in core and is often difficult to distinguish from fine-grained lithic tuff. It rarely

Figure 5: Photograph of a moderately welded lithic tuff outcrop in the Limerick Formation near Gold Mountain, southeast of Spring Valley.

Figure 6: Photograph of an irregular lithophysal cavity infilled by microcrystalline quartz in a lithic tuff outcrop near Gold Mountain.

Figure 7: Photograph of densely spherulitic Feldspar Porphyry from drillhole SV11-513C. Note the abundance of feldspar phenocrysts.

crops out in the field and most commonly occurs as angular, orangish to greenish fragments in float (Tom Chadwick, pers. comm., 2011). It is composed primarily of silt-sized particles, though local coarse sand to pebble-sized lithic fragments are present. To the north of Spring Valley, volcaniclastic siltstone intervals localize small arroyos and saddles between more resistant lithic tuff and greenstone outcrops (Fig. 7).

Rochester Formation

Unlike the Limerick Formation, the Rochester sequence at Spring Valley is well defined and relatively consistent throughout the project area. It consists of a basal latite ash flow tuff, overlain by an agglomerate unit deposited during an eruptive hiatus, a densely welded quartz latite to rhyolite ash flow tuff, a discontinuous fluvial siltstone

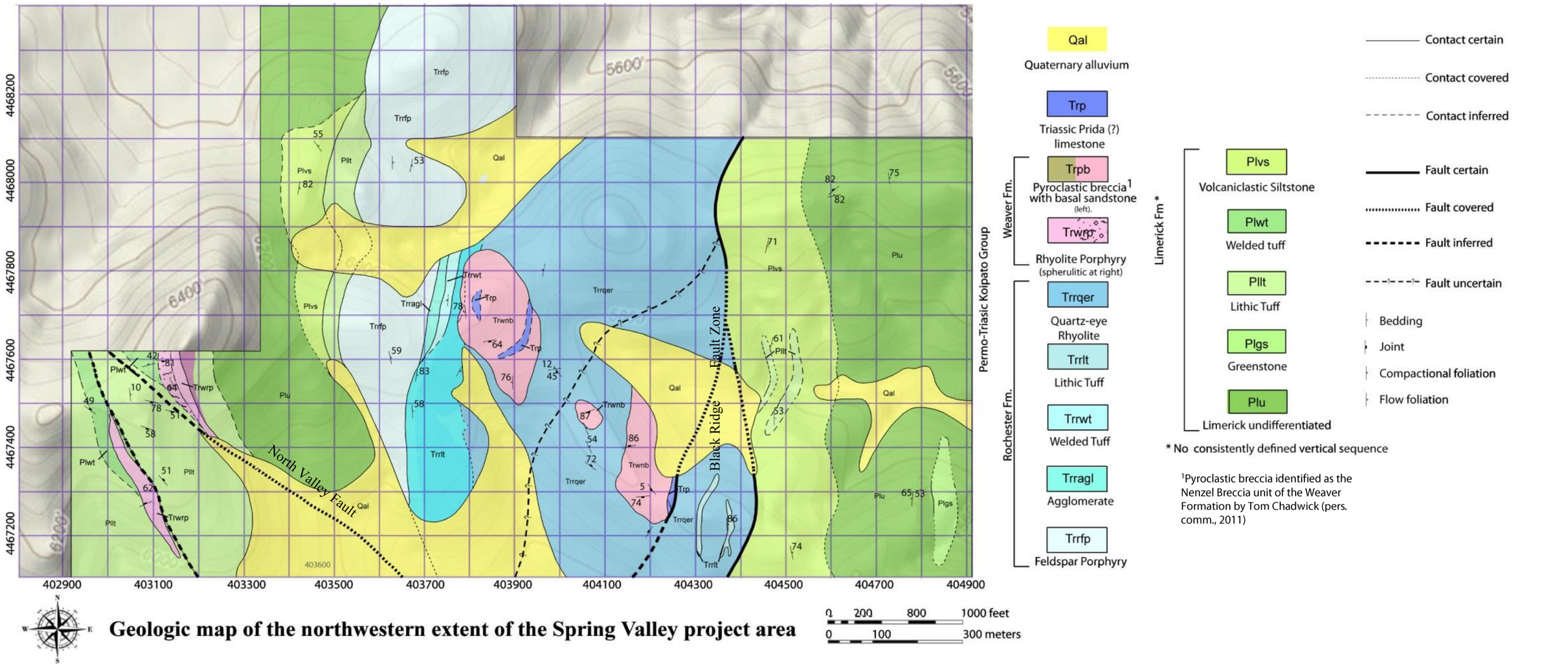

Figure 8: Geologic map of the northern extent of the Spring Valley project area modified from Chadwick (2011). Assignment of fault names and Weaver lithologies after Chadwick (2011).

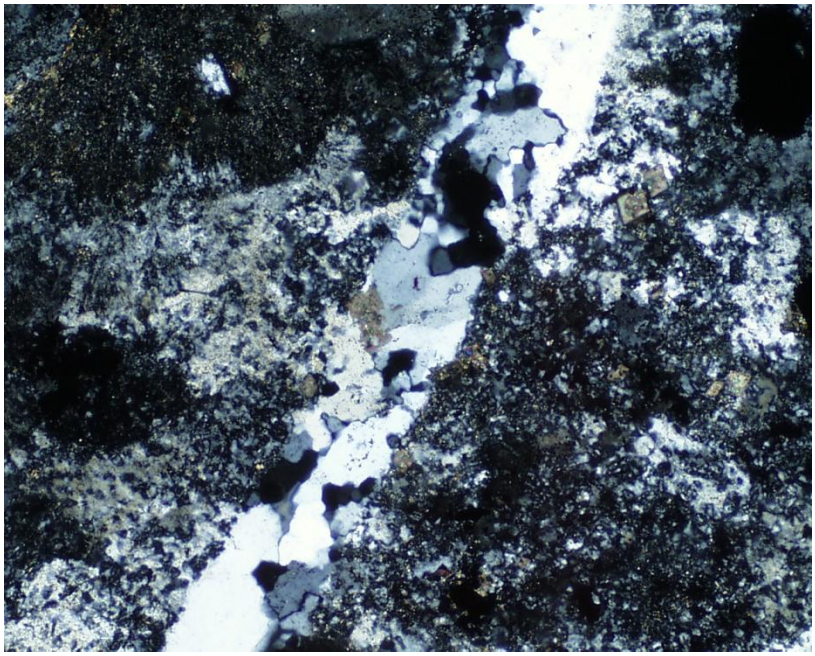

Figure 9: Photomicrograph of an early gray quartz vein (see vein section) crosscutting typical groundmass in the Feldspar Porphyry. Groundmass consists of intergrown quartz and K-feldspar with distinctly sutured grain boundaries indicative of recrystallization.5x, crossed nicols. FOV=1.70mm

unit, and an upper rhyolite flow package. The Rochester Formation generally becomes more differentiated and quartz-rich upward through the section.

Feldspar Porphyry

The Feldspar Porphyry is the lowermost member of the Spring Valley sequence of the Rochester Formation (Neal and LeLacheur, 2010; LeLacheur et al., 2011). It is a light gray to light green porphyritic and locally spherulitic quartz latite flow with phenocrysts of plagioclase, K-feldspar, biotite and rare quartz in a recrystallized, quartz- and K-feldspar-rich groundmass (Fig. 8). Plagioclase phenocrysts are typically 0.5-4mm and comprise 2-5%. They are albite in composition, with anorthite content ranging from An_{10} to An_{20}.They are commonly partially replaced by sericite, carbonate or quartz. In sample

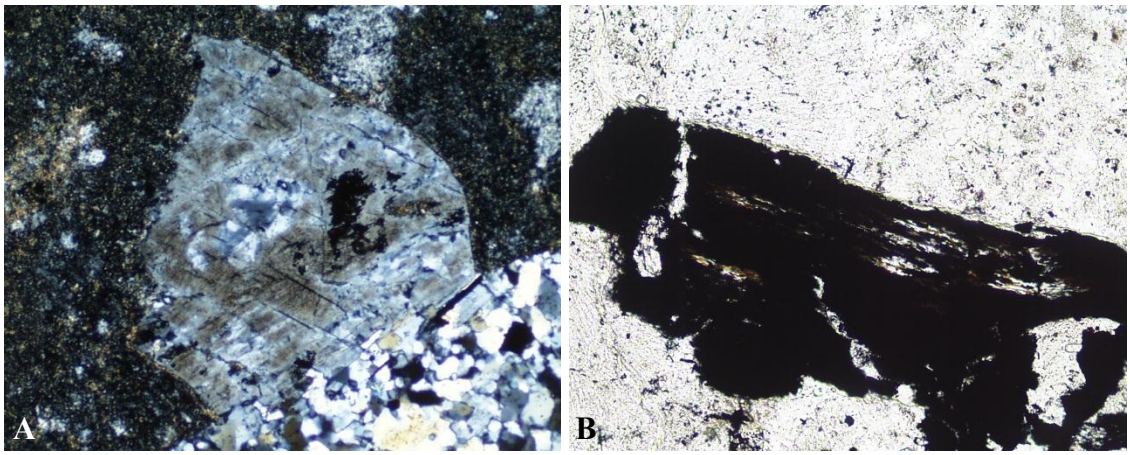

Figure 10: Photomicrographs of resorbed phenocrysts in the Feldspar Porphyry. Upon first glance, phenocrysts appear to be fragments. However, local, though poorly defined, sieve texture, and the lack of features supporting an ash flow tuff interpretation indicate that they are resorbed phenocrysts. A. Photomicrograph of a resorbed K-feldspar phenocryst adjacent to a granular quartz vein. 5x, crossed nicols. FOV= 4.4mm; B. Photomicrograph of a strongly hematite-leucoxene and sericite altered biotite phenocryst. Note the large embayment within the biotite phenocryst in the lower right and the irregular, resorbed grain boundary indicative of disequilibrium. 10x, crossed nicols. FOV= 0.85 mm.

1UP-044, several plagioclase phenocrysts are replaced by secondary K-feldspar, though this was not observed elsewhere. K-feldspar phenocrysts are typically 0.5-3mm and comprise 1-5%. They are commonly partially replaced by sericite, carbonate or quartz. Biotite is 0.25-0.5mm and typically only comprises 0.1-0.5%. It is completely replaced by sericite, with lesser leucoxene, pyrite, or magnetite. Fragmented accessory zircon is common. Apatite is rare.

Groundmass consists of intergrown K-feldspar and lesser quartz with distinctly sutured grain boundaries indicative of recrystallization (Fig. 9). Very fine-grained, granular quartz and K-feldspar may also be present. Spherulites are common and may comprise up to 50% of the groundmass. They are typically 0.25-1mm in diameter and

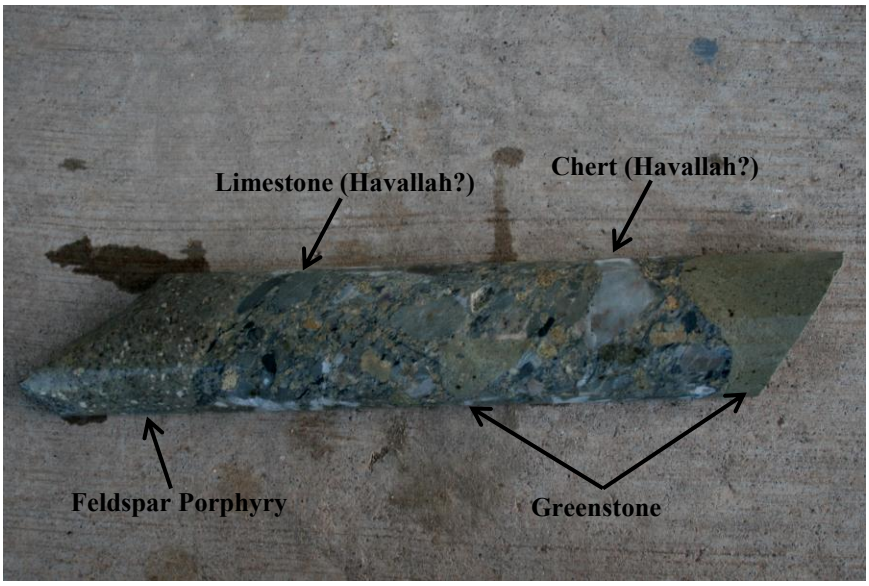

Figure 11: Photograph of a drillhole intercept of the Agglomerate unit. Pebble- to cobble-sized clasts of Feldspar Porphyry, greenstone, chert and limestone are supported by a poorly-sorted, coarse-grained sandy groundmass.

commonly nucleate on feldspar fragments. They are recrystallized to granular to sutured quartz and K-feldspar, though original, radiating appearance is preserved and observable in plane light.

In the south end of Spring Valley, the Feldspar Porphyry is commonly encountered at depths of 500-900 feet and is approximately120 to 560 feet thick. It is thickest to the west of the Limerick fault in holes SV08-397C and SV08-440C, where it is 420-560 feet thick, and thins to 120-300 feet to the east. It is present in outcrop within the mapping area on the ridge to the north of Spring Valley, where it forms massive cliffs 3-15 feet in height. It is tabular in geometry and consistent in spatial association to the underlying Limerick Formation and overlying units of the Rochester Formation.

Phenocrysts are typically resorbed, and commonly appear to be fragmented (Fig. 10). However, no features or structures typically associated with ash flow tuffs were

observed, with the exception of local spherulites. Local flow banding (Bill Sevores, pers. comm., June 2011) and autobrecciation suggest that it is a flow rather than a sill.

Agglomerate

A brief cessation of volcanic activity followed the deposition of the Feldspar Porphyry ash-flow tuff. Mass wasting of material from the footwall of the Black Ridge-East fault resulted in the deposition of the Agglomerate unit at Spring Valley (Tom Chadwick, pers. comm., 2011). The Agglomerate unit consists of pebble- to boulder-sized heterolithic clasts in a coarse-grained, sandy groundmass (Fig. 11). It is predominantly clast-supported, though local matrix-supported intervals are present. Clasts are poorly sorted, subrounded to subangular, and were derived from Koipato and earlier lithologies. Greenstone clasts derived from the Limerick Formation are the most common, followed by limestone and quartzite clasts possibly sourced from long-eroded Havallah formation. Fine-grained cobble to boulder-sized clasts of Feldspar Porphyry may be present. Sparse moderately to densely welded tuff clasts may have been derived from the Limerick Formation. Alternatively, there may be some overlap between the deposition of the Agglomerate and the overlying Welded Tuff.

Groundmass is predominantly composed of fine-grained, granular quartz with strongly pervasive interstitial Fe-bearing carbonate and weak to moderate sericite. It ranges in color from pale greenish gray to bright orange, dependent on the pervasiveness and degree of oxidation of the Fe-carbonate. Fine, acicular tourmaline is common, though minor and is usually associated with white, quartz-rich clasts. It is weakly to moderately pervasive in groundmass adjacent to tourmaline-bearing veins. Reactive greenstone,

Welded Tuff and Feldspar Porphyry clasts are typically strongly altered by hydrothermal fluids. Less reactive limestone clasts may be silicified or replaced by later Fe-bearing carbonate.

In the field, the Agglomerate forms distinctive, knobby outcrops that are strongly weathered to reddish brown. Clast composition may vary, but greenstone, limestone and quartzite clasts are relatively consistent. On the flanks of the ridge above the Bonanza King, to the east of Spring Valley, traditional Agglomerate is interbedded with purple to white tuffaceous sediment with sparse lithic clasts. In the south end of the resource area, the Agglomerate ranges in thickness from 22 feet to over 300 feet. It is thickest adjacent to the Limerick fault and thins westward and northward. The distribution of the Agglomerate to the north and east of Spring Valley suggests that multiple depocenters existed. A small lens of Agglomerate was mapped on the ridge to the north of Spring Valley, but it quickly pinches out under alluvium. To the east of Spring Valley, Tom Chadwick (pers. comm., 2011) mapped Agglomerate beds in contact with the Feldspar Porphyry and spatially associated with splays of the Black Ridge fault system. This suggests that the Black Ridge fault system actively controlled the deposition (Chadwick, pers. comm., 2011).

Welded Tuff

The Agglomerate is conformably overlain by the Welded Tuff member of the Rochester Formation (Neal and LeLacheur, 2010; LeLacheur et al., 2011). The Welded Tuff is a purplish-gray to greenish moderately to densely welded crystal ash-flow tuff. It is quartz latite to rhyolite in composition, with 1-2% K-feldspar, 1-2% plagioclase, and

trace to 0.5% biotite and quartz fragments in a recrystallized groundmass. Feldspar fragments are 1-2mm and are commonly replaced by weak sericite or weak to locally moderate carbonate. Biotite is rare, strongly altered, and is typically less than 0.5mm. Rounded to angular quartz fragments are more common in the Welded Tuff than in the Feldspar Porphyry, though they are still only minor. Sparse, cognate lithic fragments are present intermittently. Groundmass is composed of very fine- to medium-grained, K-feldspar intergrown with lesser quartz. Boundaries between coarser K-feldspar and quartz grains are sutured, indicating recrystallization. Rare, 0.5-1mm spherulites replaced by granular K-feldspar or quartz may be present. Small, irregular lithophysae rimmed by quartz or sericite are common, though minor.

The Welded Tuff is typically more densely welded than the lithic tuffs found in the Limerick Formation. Fiamme may have flattening ratios in excess of 10 (Tom Chadwick, pers. comm., 2011). They typically have dark purplish-gray to black rims or cores composed of fine-grained, granular quartz intergrown with minor sericite, red hematite nodules or specularite needles. Where black quartz rims fiamme, cores may be composed of light gray granular quartz. Adjacent to veins, fiamme are light grayish-green and composed of fine-grained, granular quartz with lesser sericite.

At its thickest in drillhole SV07-249 in the northern part of the study area, the Welded Tuff is approximately 241 feet thick. It thins southward to approximately 30 feet in the southernmost hole SV07-290C. North of Spring Valley, the Welded Tuff terminates against the Agglomerate (Fig. 7). To the south, it ranges considerably in thickness and aerial extent, and is likely equivalent to the welded tuff unit at Coeur Rochester (Tom Chadwick, pers. comm., 2011).

Volcaniclastic Siltstone (SD)

The Welded Tuff is overlain by a relatively thin, discontinuous volcaniclastic siltstone layer, referred to by site geologists as SD (Neal and LeLacheur, 2010; LeLacheur et al., 2011). SD is white to brown to greenish-gray, dependent on alteration mineralogy. It is fine-grained and composed predominantly of silt-sized volcaniclastic particles, with local muddy to tuffaceous facies (Chadwick, pers. comm., 2011). It may be poorly to well stratified, graded or cross-bedded (Chadwick, pers. comm., 2011). Argillic or sericitic alteration may be weak to moderate. Local, fine-grained euhedral tourmaline crystals may be disseminated throughout the groundmass, coloring the unit light to dark gray (Neal and LeLacheur, 2010).

In the study area, SD was only logged in hole SV07-292C. Texture was largely destroyed by moderately to strongly pervasive argillic alteration, with local QSP zones. SD is completely absent in holes SV08-397C, SV07-439C and SV08-440C. Elsewhere, SD intercepts in core were removed for metallurgical testing.

Quartz-eye Rhyolite

SD is conformably overlain and locally interbedded with the Quartz-eye Rhyolite (QER) (Neal and LeLacheur, 2010; LeLacheur et al., 2011). Quartz-eye Rhyolite is the youngest unit of the Rochester sequence at Spring Valley (Neal and LeLacheur, 2010; LeLacheur et al., 2011). It is light green and typically aphanitic, though sparsely porphyritic facies are present. Throughout much of the resource area, it can be subdivided into two units (Tom Chadwick, pers. comm., 2011). Upper QER is generally fine-grained, with only local quartz, feldspar or biotite phenocrysts. Lower QER is porphyritic

with up to 1-2% quartz eyes and less than 1% feldspar and biotite phenocrysts in an aphanitic, sparsely spherulitic groundmass. Quartz eyes are typically 1-2mm in width and are the defining characteristic of the unit. Feldspars phenocrysts are 2-3mm, while biotite is generally less than 1mm.

The Quartz-eye Rhyolite is intercalated with sparse, discontinuous cognate to heterolithic tuff lenses. Lithic tuffs are composed of sparse feldspar and quartz fragments, and coarse-sand to pebble-sized rhyolite and black chert fragments. In the study area, lithic tuff interbeds are most commonly found near the base of the unit above its contact with underlying SD or Welded Tuff. They are typically only a few feet in thickness. Local autobrecciated intervals characterized by cognate rhyolitic clasts in a sparsely porphyritic groundmass are common.

In the north end of the resource area, the Quartz-eye Rhyolite may be up to 700 feet thick (Fig. 7). It thins considerably in the study area to the south, where thickness ranges from 25-115 feet. In holes SV08-439 and SV08-440, it is absent entirely. It is aphanitic and relatively quartz- and spherulite-poor and is likely equivalent to Upper QER. It is typically fractured and strongly altered. Limonite consisting of hematite with lesser jarosite and goethite is weakly to strongly pervasive throughout, overprinting earlier quartz-sericite ± pyrite alteration and structurally-controlled argillic alteration.

In outcrop, the Quartz-eye Rhyolite is light green on fresh surface and may weather red to brown. It forms small, discrete and resistant outcrops along the flanks and tops of ridges that are typically only 2-5 feet in height. Banding consisting of alternating quartz- and sericite-rich layers may be present, though the unit generally lacks distinct flow foliation. It is intercalated with sparse, discontinuous cognate to heterolithic tuff

Figure 12: Photograph of an outcrop of a strongly spherulitic Rhyolite Porphyry dike that intrudes a NW-trending normal fault in the mapping area to the north of Spring Valley (See Fig. 7).

lenses, composed of sparse feldspar and quartz fragments, and coarse-sand to pebble-sized rhyolite and black chert fragments. On the ridge to the north of Spring Valley—particularly where it is present in outcrop in the south-central portion of the mapping area—fine-grained lithic tuffs appear very similar to aphanitic rhyolite flows and can only be distinguished by the presence of small chert fragments.

Weaver Formation

Rhyolite Porphyry dikes and sills, presumably the intrusive equivalent of Weaver rhyolite flows, crosscut lower Koipato lithologies within the Spring Valley project area (Fig. 12) (Wallace et al., 1960; Vikre, 1977). Composition and texture of the Rhyolite

Porphyry varies throughout the Humboldt Range (Vikre, 1977). Some facies are aphyric with only sparse phenocrysts of rounded quartz eyes, plagioclase, K-feldspar, and rarely biotite. Other faces are relatively crowded and porphyritic, with 1-3% feldspar phenocrysts, 1-2% quartz phenocrysts and local biotite in an aphanitic groundmass. Crowded porphyritic facies appear similar in hand specimen to the Feldspar Porphyry, which likely contributed to the initial intrusive interpretation of the latter. In addition, Rhyolite Porphyry dikes and sills may be weakly to strongly spherulitic, which suggests that they were deposited in a hypabyssal environment (Fig. 12).

Initially believed to be offshoots of the Feldspar Porphyry, Rhyolite Porphyry dikes encountered in core were heavily sampled and only a few examples remained in storage when this project began. Rhyolite Porphyry dikes encountered in core in the south end of Spring Valley are typically sparsely porphyritic, with phenocrysts of feldspar and rare quartz in an aphanitic and commonly flow-banded groundmass. It is typically light green to gray and occurs overwhelmingly in fault zones. Elsewhere in Spring Valley, grade is said to increase within the Limerick Formation adjacent to Rhyolite Porphyry dikes, though it is not clear if this is due to thermal or structural controls.

In outcrop, Rhyolite Porphyry dikes and sills are commonly light tan to light green on fresh surface and weather to a distinct pinkish-tan. They form resistant ledges or cliffs (particularly dikes), and where present, have vertical flow foliation in sharp contrast to foliations observed in surrounding country rock. They produce metasomatic aureoles ranging in width from a few meters to tens of meters, the compositions of which were described in the “Regional Alteration” section (also see Figs. 6 and 15).

An unusual, light gray to green spherulitic to banded porphyritic unit was encountered within the Limerick Formation in drill holes SV08-440C and SV08-397C. The banded unit, referred to as the banded porphyry, consists of 2-5% feldspar fragments in an aphanitic and weakly spherulitic groundmass. Bands are composed of dark gray to black quartz or reddish quartz with fine-grained hematite. With the exception of strong, through-going bands, it appears very similar to the Feldspar Porphyry. It has been reported by site geologists throughout the resource area, most commonly within the Limerick Formation near its contact with the Feldspar Porphyry (Bill Sevores, pers. comm., 2011; Larry Pancoast, pers. comm., 2011). In SV08-440C, the banded porphyry was encountered under approximately forty feet of Limerick greenstone and lithic tuff at 1127.5 feet (true depth is approximately 1110 feet). It extends to 1242.8 feet and has a thickness of approximately 113.5 feet.

The spherulitic spotted porphyry is compositionally similar to the banded porphyry, though it lacks through-going bands. It is light green mottled red-brown and moderately to strongly spherulitic. It has been reported throughout the resource area, almost always in association with the banded porphyry (Bill Sevores, pers. comm., 2011; Larry Pancoast, pers. comm., 2011). The banded porphyry was encountered in SV08-397C at a depth of 1463.7 feet (true calculated depth is approximately 1255 feet), beneath nearly 280 feet of Limerick greenstones and lithic tuffs. It extends to 1589.4 feet where it contacts the banded porphyry. It has a calculated thickness of approximately 108 feet. The banded porphyry extends to 1648 feet (true depth is approximately 1414 feet) and has a thickness of approximately 50 feet.

The banded porphyry and spotted porphyry are present in the northern end of the resource area (Fig. 7). They commonly occur together and at relatively shallow depths, near the contact with the Feldspar Porphyry. Banded and spotted porphyry intervals are too thick to be Rhyolite Porphyry dikes and are much thicker than Rhyolite Porphyry sills that crop out northwest of Spring Valley. Quartz latite crystal ash-flow tuffs were mapped by Vikre (1977) in the Rochester district, and it is possible that the banded porphyry and spotted porphyry are densely welded to spherulitic facies of Limerick crystal tuffs. Further petrographic work is needed to determine their origin.

Units similar to the banded porphyry and spotted porphyry were mapped within the Limerick Formation on a resistant knob north of Spring Valley. At the base of the knob, a strongly banded, porphyritic to fragmental unit with 1-3% feldspar overlies a moderately to densely welded lithic tuff. It grades into an overlying spherulitic unit of similar composition, with spherulites ranging in size from 1mm to 30mm. Spherulites gradually decrease and are largely absent in a porphyritic unit at the top of the knob. Here, steeply-dipping foliation trending N30-40°W and dipping 80-90°NE is dominant and indicates that the uppermost porphyritic unit is a Rhyolite Porphyry dike.

Intermediate dikes and plugs

Post-mineral, Hornblende Porphyry dikes and plugs intrude Koipato host rocks throughout Spring Valley, though none were encountered within the study area. They are typically light tan to gray and strongly altered (Tom Chadwick, pers. comm., 2011; Bill Sevores, pers. comm., 2011). They are composed of straw-yellow, pervasively sericitized hornblende phenocrysts in an aphanitic groundmass (Tom Chadwick, pers. comm.,

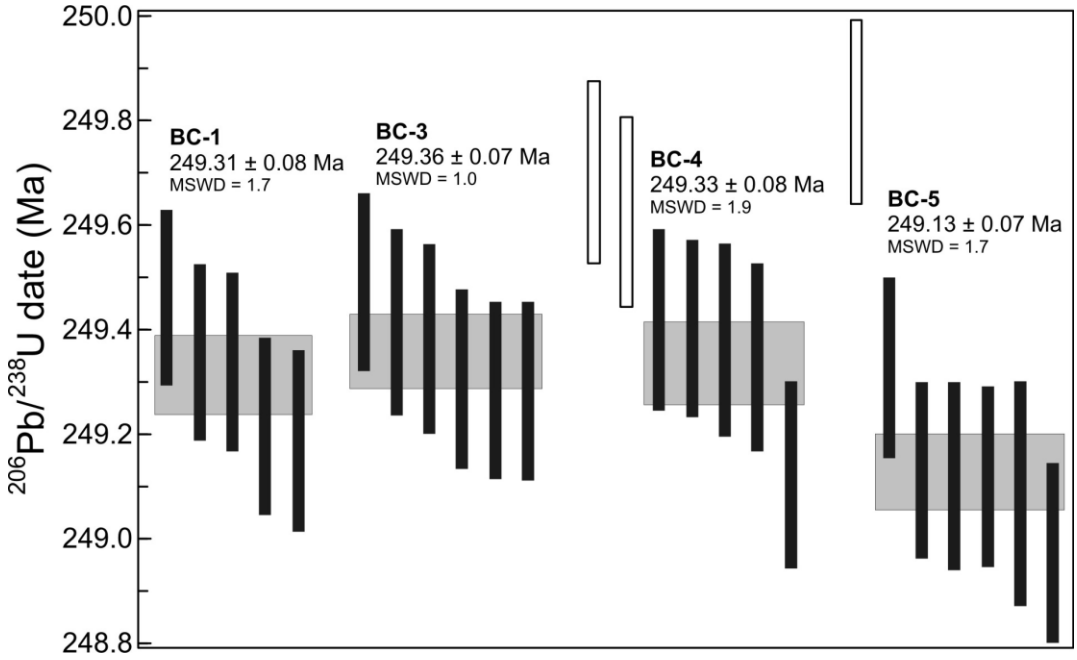

Figure 13: Ranked age plot of Permo-Triassic Koipato Group samples submitted for U-Pb CA-TIMS zircon dating. See Table 1 for sample descriptions, summary and locations.

2011). They are not mineralized, though grade may increase in the adjacent country rock (Bill Sevores, pers. comm., 2011).

Uranium-Lead dating of host rocks and intrusive phases

Uranium-Lead dating of zircon grains from the Feldspar Porphyry, Quartz-eye Rhyolite and Rhyolite Porphyry units was undertaken to constrain the relative timing of host rock eruption or emplacement, specifically the Feldspar Porphyry, which has been alternately interpreted as a large sill. Non-mineralized and relatively unaltered samples were selected from core and outcrop and were sent for mineral separation and CA-TIMS analyses by Jim Crowley at the Boise State University Isotope Geology Laboratory (Fig.

Table 1: Characteristics of samples submitted for U-Pb CA-TIMS dating. Numbers in parenthesis correspond to numbered locations in Figure 2.

Sample No.	Sample Description	Sample Location	Isotopic Date
BC-1	Quartz-eye Rhyolite	SV07-248C 173'-183'	249.36 ± 0.07 Ma
BC-3	Feldspar Porphyry	SV07-248C 766.5'-775'	249.31 ± 0.08 Ma
BC-4 (1)	Rhyolite Porphyry dike	399588E, 4465880N	249.33 ± 0.08
BC-5 (2)	Leucogranite	405127E, 4459908N	249.13 ± 0.07
BC-6 (3)	Rocky Canyon granodiorite	394936E, 4471226N	89.7 ± 1.1
BC-7 (4)	Canyon diorite to quartz diorite	405523E, 4465629N	32.072 ± 0.012

13; Table 1). The Welded Tuff did not contain sufficient zircon for analyses. Methods and raw data are presented in Appendix A.

Six zircon grains from the Feldspar Porphyry yielded an average date of 249.31 ± 0.08 Ma. Six zircon grains from the Quartz-eye Rhyolite yielded an average age of 249.36 ± 0.07 Ma, while a single zircon grain yielded a date of 254.81 ± 0.25 Ma. Though the results are too close to be conclusive, they are corroborated by additional direct evidence of the timing of the Feldspar Porphyry relative to the remainder of the Spring Valley Koipato sequence, such as the presence of Feldspar Porphyry clasts in the overlying Agglomerate, local autobrecciation indicative of flow, consistent distribution and spatial relationship to underlying and overlying units throughout the Spring Valley district, and the absence of thermal effects or "baking" in the overlying Agglomerate or in the underlying Limerick Formation.

CA-TIMS dating of zircon grains from the Leucogranite, Rhyolite Porphyry, Rocky Canyon Granodiorite and younger quartz diorite was conducted to determine the intrusive and thermal history of the Humboldt Range, the relative timing of Koipato

intrusives to host rocks at Spring Valley, and to identify possible causative intrusives that may be related to mineralization. Relatively unaltered samples and unmineralized samples were collected from outcrop (Fig. 2; Table 1). CA-TIMS analyses and mineral separations were conducted by Dr. Jim Crowley and the Boise State University Isotope Geology Laboratory.

The rhyolite porphyry sample is the older of the two Koipato phases submitted at 249.33 ± 0.08 Ma. At 249.13 ± 0.07 Ma, leucogranite is slightly younger, though field relationships suggest that emplacement of the two occurred largely synchronously. The Rocky Canyon granodiorite is the older of the two intermediate Cenozoic phases at 89.7 ± 1.1 Ma and is likely related to eastward migration of the arc during the Laramide (Dickinson, 2006). Conversely, the 32.072 ± 0.012 Ma quartz diorite is likely related to westward retreat of the magmatic arc following the Laramide (Dickinson, 2006).

Structural Setting

The Humboldt Range is an uplifted, NS-trending anticlinorium bounded to the east by the Range Front/Fitting fault and to the west by an unnamed normal fault (Fig. 2) (Silberling and Wallace, 1967; Wallace et al., 1969a; Wallace et al., 1969b). It is crosscut by a series of NW- and NS to NNE-trending normal faults of Permo-Triassic to Cenozoic (?) age and generally east to northeast-verging thrust faults of mid- to late-Jurassic age (Cheong, 1999; Neal and LeLacheur, 2010; LeLacheur et al., 2011). It has a long and complex structural history spanning hundreds of millions of years from the Paleozoic to the Cenozoic, characterized by earliest faults that controlled the distribution of the Permo-Triassic Koipato Group, local thrusts that formed concomitantly with late-stage

emplacement of the Golconda allochthon and Jurassic through Miocene folds, thrusts and normal faults that record continued and episodic compression and extension (Cheong, 1999; Neal and LeLacheur, 2010; LeLacheur et al., 2011).

The Black Ridge fault system is the most prominent structural feature in the south and central portions of the Humboldt Range (Silberling and Wallace, 1967; Wallace et al., 1969a; Wallace et al., 1969b). It generally trends NS to NNE and in the vicinity of Spring Valley is steeply dipping (Silberling and Wallace, 1967; Wallace et al., 1969a; Wallace et al., 1969b; Neal and LeLacheur, 2010). The Black Ridge Fault system extends northward from Black Ridge in the southernmost Buffalo Mountain quadrangle to the Moonlight Basin, approximately five kilometers north of Spring Valley (Silberling and Wallace, 1967; Wallace et al., 1969a; Wallace et al., 1969b; Tom Chadwick, pers. comm., 2011). Movement along the fault system is normal and initial subsidence occurred during the Permo-Triassic, concomitantly with the deposition of the Koipato Group, with further subsidence during Miocene extension (Neal and LeLacheur, 2010; Tom Chadwick, pers. comm., 2011).

Small thrusts and associated angular unconformities of probable Permo-Triassic age occur locally within the Koipato Group and reflect deposition during the waning stages of the emplacement of the Golconda allochthon. Larger thrusts, occurring both within the Koipato Group and later Triassic through Jurassic sedimentary units have been mapped primarily along the western flank of the range and are likely associated with the late Jurassic emplacement of the Luning-Fencemaker allochthon (Cheong, 1999; Wyld et al., 2003).

Deformational history

According to Cheong (1999), earliest deformation in the Humboldt Range is late-Jurassic in age and is associated with the emplacement of the Luning-Fencemaker allochthon. It is most pronounced in the western side of the range and decreases in intensity eastward (Silberling and Wallace, 1967; Wallace et al., 1969a; Wallace et al., 1969b; Cheong, 1999). Early deformation resulted in the formation of meso-scale, east-verging isoclinal folds and associated penetrative foliation that generally trends NS to NE (Cheong, 1999). Jurassic deformation related to the Luning-Fencemaker allochthon is crosscut by a younger deformational event that produced NE-trending metamorphic quartz veins throughout northwestern Nevada, though the age of this event is not known (Cheong, 1999).

Structural Setting of Spring Valley

The most prominent structural features at Spring Valley are steeply-dipping, NNE-trending dip-slip faults that are interpreted to be limbs of the Black Ridge fault (Neal and LeLacheur, 2010). The Black Ridge fault bisects the Humboldt Range, extending from Black Ridge to the south to as far north as the Moonlight Basin, up to five kilometers from Spring Valley (Silberling and Wallace, 1967; Wallace et al., 1969a; Wallace et al., 1969b; Chadwick, pers. comm., 2011). To the south of Spring Valley, the Black Ridge fault manifests as a broad, horse-tail zone consisting of multiple splays (Chadwick, pers. comm., 2011). These splays coalesce into two main limbs within Spring Valley, the central Limerick fault and the East fault (Chadwick, pers. comm., 2011). The Limerick fault trends NNE and dips 60-80°SE, steepening to the north. It is paralleled by

the 70-80°NW-trending East fault. The West fault parallels the Limerick and East faults and may be temporally related to the Black Ridge fault system. It trends NNE and dips 75°SW (Neal and LeLacheur, 2010).

The Agglomerate unit within the Rochester Formation thickens considerably adjacent to the Limerick fault system, which suggests it was active during deposition (Chadwick, pers. comm., 2011). Chadwick (pers. comm., June 2011) postulates that it was the eastern margin of one of likely several Koipato calderas, and that the Agglomerate unit formed by mass wasting of material from the caldera wall during an eruptive hiatus. It may also have simply been a normal fault related to incipient extension that controlled deposition of clastic material distal to the eruptive center. Within Spring Valley, the East fault limb juxtaposes the Limerick Formation and the Rochester Formation, and represents the eastern extent of the Rochester sequence in the resource area (Neal and LeLacheur, 2010). North of Spring Valley, the Black Ridge fault system drops the Limerick into contact with the Quartz-eye Rhyolite (Tom Chadwick, pers. comm., 2011).

NNE-trending faults are crosscut by a second set of faults that trend 280-290° (Neal and LeLacheur, 2010). The southernmost, the Pan American fault, dips 85°NE. It is paralleled by the 85°NE dipping Wabash fault and the SW dipping North Valley fault (Neal and LeLacheur, 2010). NW-trending faults post-date mineralization and alteration (Neal and LeLacheur, 2010), but their timing relative to later tectonic events is not known. The Wabash fault is intruded by Cretaceous (or Oligocene) hornblende porphyry dikes, which places a lower limit on the age of formation. Although they play a

significant role in localizing and controlling subsidence of the Spring Valley graben, they do not appear to be Miocene in age and predate basin-and-range extension.

Host rocks at Spring Valley are folded into a NE-trending, N-plunging syncline with local parasitic folds. The Spring Valley syncline is truncated to the west and to the east by the West and East faults, respectively, which juxtapose the Rochester and Limerick formations. It is asymmetrical, with dip along the western limb ranging from 70-75°, while dip along the eastern limb ranges from 25-30°. Folding likely occurred concomitantly with the NW/SE-directed emplacement of the Luning-Fencemaker allochthon during the late Jurassic, though some evidence, such as the distribution of sedimentary units within the Rochester Formation, suggests that folding occurred syn-deposition (Tom Chadwick, pers. comm., 2011).

Subsidence of the Spring Valley basin was accommodated along both NNE-trending and NW-trending structures during Miocene extension. The complex NNW-SSE and NE-SW directed extension at this unique and complex structural intersection effectively produced a bowl-shaped "double-graben" (Tom Chadwick, pers. comm., 2011).

Regional Alteration

In addition to hydrothermal alteration related to mineralization and centered on discrete loci, the Koipato Group has been subjected to at least one regional greenschist-facies alteration and recrystallization event that produced widespread sericitization and tourmalinization in the Rochester and Weaver formations and pervasive chlorite-carbonate-hematite and tourmaline alteration in the Limerick Formation (Vikre, 1977).

Greenschist-facies alteration and recrystallization in the Limerick and Rochester formations was historically believed to be related to the intrusion of the Leucogranite prior to the deposition of the Weaver Formation (Vikre, 1977; Tatlock, 1961). However, strong, NE-trending regional foliation consistent with NW/SE-directed crustal shortening, coupled with the development of local schistocity and more pervasive alteration along the western flank of the range, suggests that regional metamorphism may be related to the EW-directed emplacement of the Luning-Fencemaker allochthon that commenced in the mid-Jurassic (Silberling and Wallace, 1967; Wallace et al., 1969a; Wallace et al., 1969b; Cheong, 1999).

In the Limerick Formation, greenschist-facies alteration is characterized by a chlorite-epidote-calcite-albite ± pyrite or hematite assemblage (Vikre, 1977). At Spring Valley, chlorite is the most common alteration mineral in the Limerick Formation. It occurs after biotite and pyroxene phenocrysts, fragments and in groundmass. It also occurs lining fracture surfaces and in small veins, with or without calcite. Epidote is uncommon in the south end of Spring Valley, and only occurs rarely after biotite and in one hole, cementing a narrow breccia zone. Elsewhere, it is common after biotite and pyroxene phenocrysts and in groundmass (Vikre, 1977). Fine-grained secondary biotite is present locally and is similarly chloritized, though that may be a deuteric effect. Carbonate occurs primarily in irregular veins and veinlets. Rhombic carbonate is present disseminated throughout the groundmass.

Greenschist facies metamorphism in the Rochester Formation is more subtle. It consists primarily of sericite, quartz, and albite (Vikre, 1977) and due to the pervasiveness of alteration within the Koipato Group and similarities in mineralogy, it is

generally indistinguishable from vein-related hydrothermal alteration. Quartz and sericite are present in varying abundance throughout the silicic units of the Rochester Formation, and all plagioclase fragments and phenocrysts measured are albite in composition. Though albite may be related to the mineralizing event, its prevalence throughout mineralized and unmineralized intervals of the Koipato Group suggests that it is metamorphic in origin. At Spring Valley, intervals within the Feldspar Porphyry and Quartz-eye Rhyolite that contain moderate sericite and quartz, with trace local pyrite, are generally regarded as less altered and may represent true greenschist-facies alteration. Relatively unaltered Welded Tuff, consisting of fiamme replaced by dark gray to black quartz with weak to locally moderate interstitial sericite or hematite, occurs both within and outboard of the main resource area.

Greenschist facies metamorphism was accompanied by widespread recrystallization of the lower Koipato Group (Vikre, 1977; Chevillon, 2007). It is most apparent in the felsic tuffs and flows of the Rochester Formation. There, recrystallization of the groundmass produced medium- to coarse-grained, interlocking quartz and potassium feldspar with sutured grain boundaries. Spherulites were similarly replaced by granular to interlocking quartz or feldspar, though the original radiating appearance is preserved in plane light (Chevillon, 2007). This indicates that devitrification predates recrystallization.

Tourmalinization

Schorl-variety tourmaline is present throughout the Koipato Group, most commonly in the lower Rochester and Limerick formations. It occurs primarily as fine,

Figure 14: Photograph of fine-grained, schorl-variety tourmaline in the groundmass of a healed breccia in the Limerick greenstone. Greenstone clasts are altered to a quartz-sericite-pyrite assemblage.

acicular crystals and felty masses both within veins and adjoining selvages, disseminated along favorable horizons in sedimentary units (Neal and LeLacheur, 2010; LeLacheur et al., 2010), and cementing healed breccias (Fig. 14).

The distribution of tourmaline throughout the Koipato Group presents the strongest evidence for regional alteration during the Permo-Triassic. It is abundant in the apophyses of the Leucogranite, where it occurs in veins with quartz, and appears to increase adjacent to intrusive contacts (Vikre, 1977). It is largely absent in the Weaver Formation, which suggests that tourmalinization predates the commencement of Weaver volcanism (Vikre, 1977). However, tourmaline is also uncommon in the upper Rochester Quartz-eye Rhyolite, and thus the distribution of tourmaline may reflect thermal and spatial rather than temporal controls.

Tourmaline occurs in auriferous and barren quartz veins throughout the Limerick and Rochester formations in Spring Valley, though it is not known whether vein

tourmaline is related to the Leucogranite or if boron and other components were remobilized or introduced during a later hydrothermal or metamorphic event. At Lincoln Hill, boron-bearing dumortierite schist, most likely related to greenschist-facies metamorphism, crosscuts tourmaline-bearing veins, which indicates that remobilization of boron did occur in the Humboldt Range (Fairbanks, 1926; Jones, 1928; Wilson, 2010). In addition, quartz veins at Spring Valley have been observed crosscutting tourmaline-healed breccias in the Limerick Formation. Several generations of tourmaline-bearing veins, indicative of multiple tourmaline introduction events, have also been documented.

Tourmaline occurs adjacent to fault zones cementing healed tectonic breccias, particularly in the Limerick Formation and the Rochester Agglomerate unit (Fig. 14). In the Agglomerate, fine-grained, acicular tourmaline may occur disseminated throughout permeable silty to sandy groundmass and rarely after mafic-bearing clasts. In the fine-grained siltstone unit, tourmaline occurs as fine, euhedral needles present in distinct bands (Neal and LeLacheur, 2010; LeLacheur et al., 2011). Tourmaline is not broken or abraded, which, due to the presumed impermeability of the siltstone unit, suggests that it precipitated prior to lithification (Neal and LeLacheur, 2010). Alternatively, tourmaline in the siltstone unit may be metamorphic in origin (van Hinsberg et al., 2011).

K-feldspar

K-feldspar, predominantly orthoclase in composition, is abundant in felsic igneous units at Spring Valley. It is the dominant groundmass constituent in the Feldspar Porphyry, Welded Tuff and Quartz-eye Rhyolite units, where it occurs intergrown with lesser quartz, and is also the dominant fragment and phenocryst composition. In

groundmass, K-feldspar is typically fine- to coarse-grained and anhedral, with sutured grain boundaries indicative of recrystallization (Chevillon, 2007). Most spherulites are similarly composed and recrystallized (Chevillon, 2007).

Due to the pervasiveness of K-feldspar in the groundmass of felsic units, it was initially believed that it was secondary and related to the mineralizing event. K-feldspar rims on primary feldspar and finely disseminated secondary biotite were reported by Neal and LeLacheur (2010) and LeLacheur et al. (2011). However, petrographic analyses of felsic samples produced little evidence for potassic alteration. More notable than its occurrences were the lack of secondary K-feldspar replacing primary feldspar, the absence of secondary K-feldspar veinlets in altered zones, and the lack of complimentary potassic alteration in the Limerick Formation and in greenstone clasts in the Agglomerate. Further, K_2O concentrations in altered and relatively unaltered samples of Feldspar Porphyry are comparable to K_2O concentrations in Rochester and Weaver samples throughout the Humboldt, Stillwater and East ranges. Anhedral K-feldspar is present in groundmass in all alteration zones in the Feldspar Porphyry, Welded Tuff and Quartz-eye Rhyolite units, as well as in relatively unaltered Feldspar Porphyry, and shows no spatial relationship to mineralized veins. Previously reported potassic alteration may be present only locally or may be metamorphic in origin and unrelated to the mineralizing event.

A colorless, rhombic mineral believed to be adularia was observed in a granular quartz-tourmaline vein in sample 291C, though it was too fine-grained to accurately characterize. Additionally, Ross (2006) identified adularia in quartz-tourmaline and

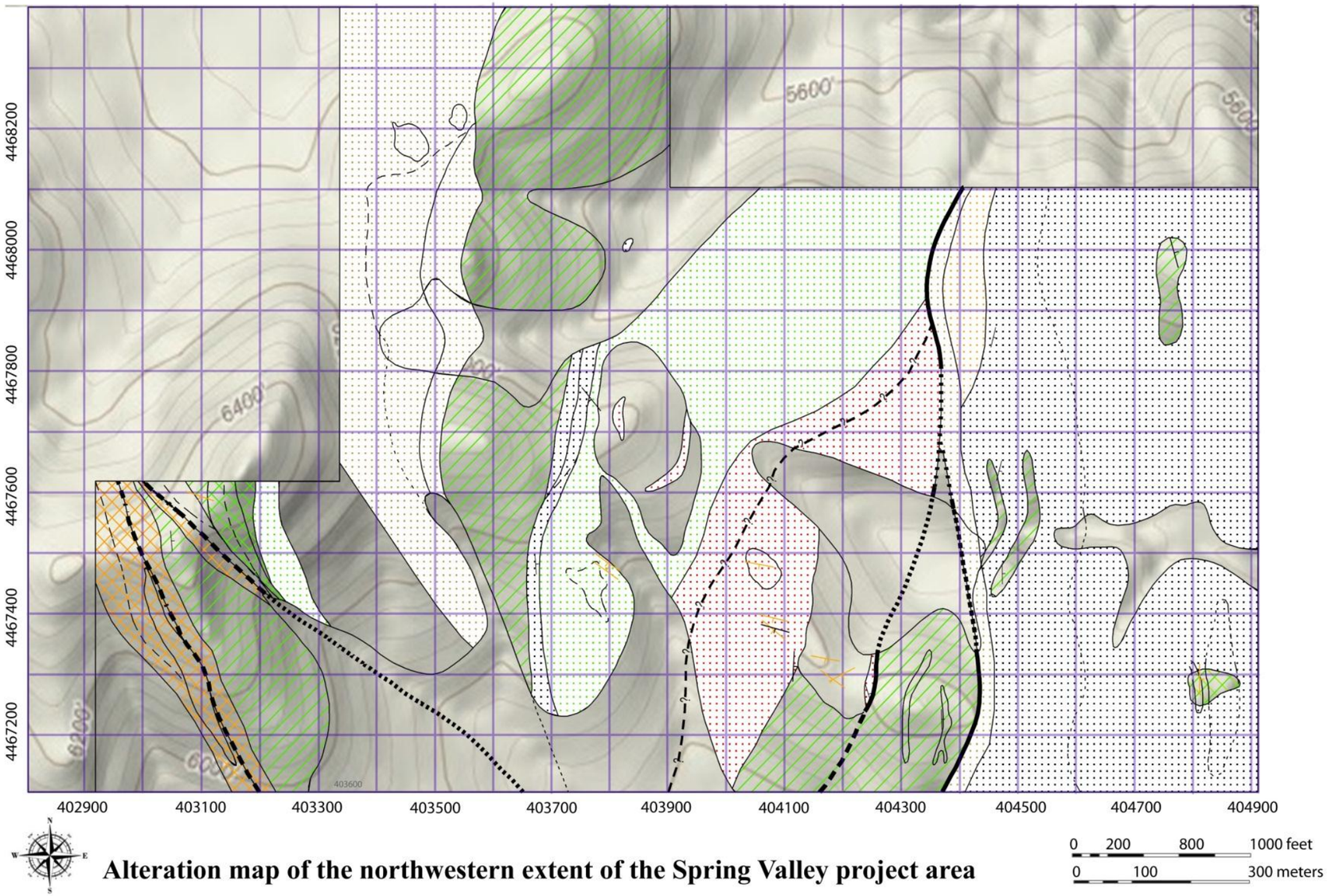

Figure 15: Alteration map of the northwest extent of the Spring Valley project area. See Fig. 7 for lithologic map.

Figure 16: Photograph of a jasperoid-cemented breccia adjacent to a fault zone in the mapping area to the north of the resource area.

quartz veins in two samples. The timing of adularia relative to mineralization and the type of vein in which it was observed are unknown.

Structurally-controlled alteration

Where well developed, alteration related to faulting consists of proximal quartz ± tourmaline, grading outward into an intermediate iron carbonate assemblage and a distal background greenschist or sericitic assemblage (Tom Chadwick, pers. comm., June 2011). Iron carbonate (likely an iron-bearing calcite due to low reaction with cold HCl) and tourmaline may or may not be present, though quartz almost always occurs (Tom Chadwick, pers. comm., June 2011) (Fig. 15). Increased limonite mineralization is also very common adjacent to fault zones, which may host discrete, discontinuous pockets of

Figure 17: Photograph of strongly pervasive and texturally destructive sericite-pyrite alteration adjacent to a white bull quartz vein in a volcaniclastic siltstone interval in the Limerick Formation. QSP alteration overprints a greenschist-facies chlorite-carbonate assemblage, though its relationship to structurally-controlled alteration is unknown. This photograph was taken in the mapping area to the north of Spring Valley.

jasperoid breccia or swirled and spotted Fe-oxide staining similar to spotted hornfelsing (Tom Chadwick, pers. comm., June 2011) (Fig. 16). In the southern portion of the claim block in American Canyon, a wide fault zone is marked by strongly pervasive white argillic alteration (Tom Chadwick, pers. comm., June 2011). The timing of fault movement relative to the intrusive history of the region may explain the different structurally-controlled alteration assemblages present.

In the Limerick Formation, structurally-controlled and hydrothermal alteration can be very pervasive and texturally destructive, commonly rendering it nearly impossible to determine rock type or formation (Tom Chadwick, pers. comm., June

2011). On the ridge to the north of Spring Valley, the splayed North Valley fault system localized strong silicification, grading outward into a greenschist-facies assemblage overprinted by minor orange iron carbonate (Fig. 15). Silicification is so pervasive in the area that it is difficult to discern spherulitic welded tuff horizons from spherulitic Rhyolite Porphyry dikes.

Quartz vein breccias and irregular masses of jasperoid breccia are also present in the North Valley fault zone, primarily within and adjacent to a relatively large Rhyolite Porphyry dike (Figs. 7, 15 and 16). The zone is further complicated by locally pervasive, light green vein-related quartz-sericite-pyrite alteration overprinting greenschist alteration (Fig. 17). Weakly to strongly pervasive quartz-sericite-pyrite alteration present elsewhere in the Limerick and Rochester formations is likely metamorphic in origin (Fig. 15). In the south end of Spring Valley, healed tourmaline breccias adjacent to fault zones are common within the Limerick Formation, commonly associated with increased argillic, sericitic and/or silicic alteration. They may be crosscut by later quartz veins, which suggest that some tourmaline predates mineralization.

In the Rochester Formation, fault zones are commonly associated with strong argillic and sericitic alteration, with or without pervasive silicification. Argillic alteration clearly crosscuts vein-related QSP alteration and commonly contains reduced pyrite, which suggests that is not supergene in origin and may have formed by collapse of the hydrothermal system or by retrograde metamorphism. Host rocks to the south of the main resource area and to the north of the thesis area in drill hole SV11-513C exhibit much stronger silicification.

Hydrothermal Alteration

Hydrothermal alteration is here defined as alteration related to both pre-ore and ore-stage quartz veins within the Spring Valley deposit. Ore-stage alteration post-dates an early greenschist-facies metamorphic event, though the timing of pre-ore alteration relative to metamorphism is unknown. Both vein density and stratigraphy appear to exert a strong control over the distribution and intensity of hydrothermal alteration. Zoning is best developed in the Feldspar Porphyry, though it is remarkably consistent between units, with the exception of the Quartz-eye Rhyolite. Proximal alteration consists of a sericite-pyrite ± quartz assemblage, grading outward into a later, distal hematite ± quartz (silica-hematite in LeLacheur et al. (2011) and Neal and LeLacheur (2010)) assemblage. Carbonate—both calcite and an iron-bearing phase—is ubiquitous, though it commonly clearly post-dates mineralization. Tourmaline may be present in groundmass adjacent to early or intermediate-stage tourmaline-bearing veins. Alteration assemblages and occurrences observed in the Limerick and Rochester formations are described by unit below.

Quartz-Eye Rhyolite

Vein-proximal alteration in the Quartz-eye Rhyolite and intercalated Lithic Tuff consists primarily of fine-grained sericite, with 0.1-1% fine-grained pyrite and minor carbonate. It grades outward seamlessly into a distal sericite ± carbonate assemblage, the only notable difference being the absence of pyrite. In both proximal and distal

assemblages, moderately to strongly pervasive sericite occurs primarily after groundmass K-feldspar and in a stockwork of microscopic veinlets that crosscut groundmass and form along grain boundaries. Weak to locally moderate sericite occurs after feldspar phenocrysts and fragments. It is pervasive after biotite, commonly occurring with Fe-oxides, pyrite or leucoxene. Pyrite is typically fine-grained, cubic and occurs disseminated throughout the wallrock. Carbonate is relatively minor and occurs after feldspars and intergrown with sericite.

Hydrothermal alteration in the Quartz-eye Rhyolite is overprinted by supergene Fe-oxide and clays. Limonite, primarily goethite, and lesser hematite are ubiquitous and weakly to strongly pervasive. They occur after biotite and pyrite and in small, stockwork veinlets, with or without earlier sericite. Clay, primarily kaolinite, is weakly to locally strongly pervasive and occurs after feldspar.

The Quartz-eye Rhyolite is the only unit in the resource area that does not contain a hematite-bearing assemblage distal to ore-stage veins. Rather, alteration is consistent throughout the entire interval, and hydrothermal alteration is generally indistinguishable from regional sericite alteration in both mineralogy and intensity. Alteration in the Quartz-eye Rhyolite is similar to that described by Vikre (1977) adjacent to silver-bearing quartz veins in the overlying Weaver Formation at Nenzel Hill.

Welded Tuff

Vein-proximal alteration in the Welded Tuff consists of a light green to gray, weak to locally pervasive sericite-pyrite assemblage (Fig. 18). Very fine- to fine-grained, feathery sericite occurs primarily in irregular veinlets that extend outward from the vein

Figure 18: Light greenish-gray quartz-sericite-pyrite-carbonate alteration adjacent to a white granular quartz vein in the Welded Tuff. Note gray quartz replacing fiamme and interstitial sericite. Core diameter is 2.5 inches.

and locally crosscut vein-distal alteration assemblages (Fig.19a). Weak to locally pervasive sericite also occurs after feldspar fragments and rarely biotite. Adjacent to the vein, sericite is moderately pervasive in groundmass, likely after K-feldspar (Fig. 19a). Carbonate is weak to moderate and occurs as scaly masses after feldspar fragments and as rhombic crystals disseminated throughout the groundmass (Fig. 19b). With the exception of fine quartz veinlets likely related to veining, there is no obvious increase in quartz. In hand specimen, sericite-pyrite altered Welded Tuff is light greenish-gray, with light gray to dark gray quartz after fiamme, dependent on the presence or absence of hematite.

Sericite-pyrite alteration typically grades outward into relatively unaltered wallrock, though a weakly to moderately developed purple to reddish hematitic zone may

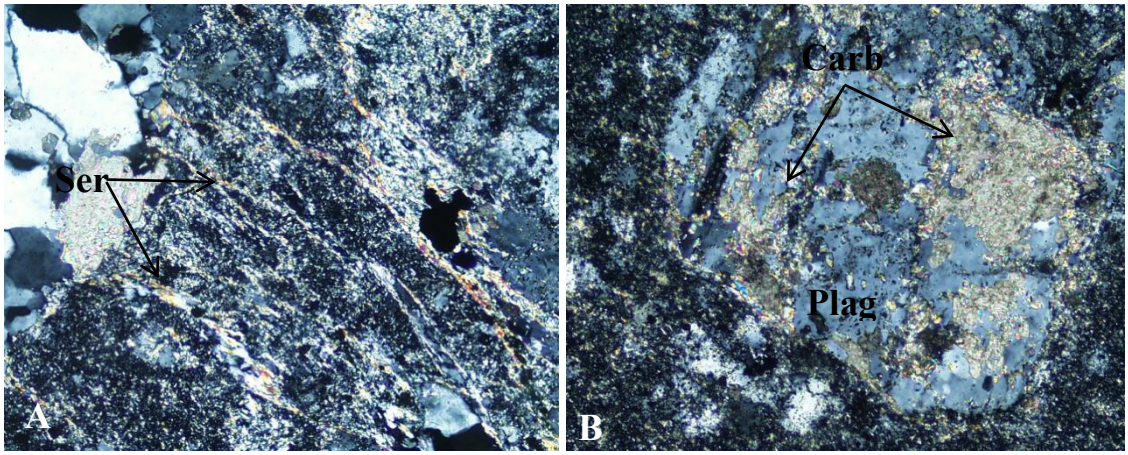

Figure 19: Photomicrographs illustrating alteration effects in the Welded Tuff. A. Sericite veinlets extending outward from a 1mm gray granular quartz-carbonate vein. Sericite is also present replacing groundmass K-feldspar. 10x, crossed nicols. FOV=0.85mm; B. Carbonate and minor sericite replacing a plagioclase fragment. 10x, crossed nicols. FOV=0.85mm.

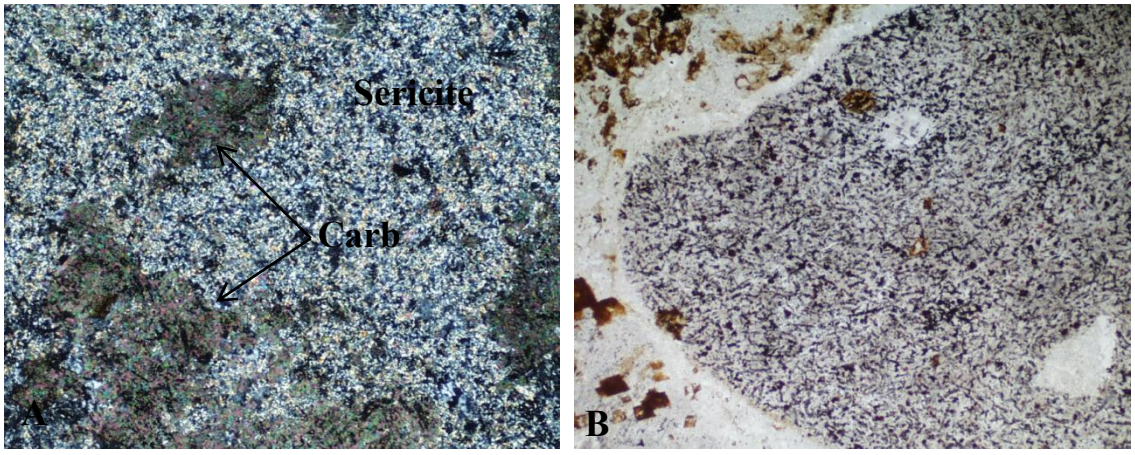

Figure 20: Photomicrographs illustrating alteration effects in the Agglomerate; A. Strongly pervasive sericite intergrown with carbonate in greenstone clast adjacent to quartz-tourmaline vein. Note minor, nodular to acicular hematite and specularite. 5x, crossed nicols. FOV=1.70mm; B. Vein-distal alteration of greenstone clast consisting of fine, nodular hematite and acicular specularite disseminated throughout a quartz-rich groundmass. Late granular quartz occurs in nodules. Note red to orange Fe-bearing carbonate in groundmass. 5x, crossed nicols. FOV=1.70mm

be present. It is characterized by very fine-grained granular hematite disseminated throughout groundmass and in silicified fiamme. Fine, acicular specular hematite may also be present, lending a purplish-black color to groundmass. Hematite alteration is best developed adjacent to areas of high vein density and at deeper levels. Unaltered or less altered Welded Tuff consists of weak to moderate sericite in veinlets, after feldspar fragments, and after K-feldspar fragments and groundmass. Fine- to medium-grained granular quartz, with sparse local microcrystalline quartz and local fine-grained K-feldspar, occurs after fiamme, and rarely after feldspar fragments. In less altered zones, fiamme are commonly dark gray to black, while interstitial groundmass is gray to locally light green.

Agglomerate

Hydrothermal alteration in the Agglomerate is best observed in reactive Welded Tuff, Feldspar Porphyry and greenstone clasts. Welded Tuff and Feldspar Porphyry clasts alter similarly to the source units from which they were derived. Alteration within greenstone clasts--which are far more common and are therefore a better indicator of alteration mineralogy and zoning--is strongly texturally destructive and primary mineralogy and textures are typically not preserved.

Proximal to veins, greenstone clasts are bright to pale green and altered to a moderately to strongly pervasive QSP-fuchsite (?) assemblage. Sericite is pervasive in groundmass of greenstone clasts and is commonly intergrown with aggregated to discrete, fine- to medium-grained quartz and anhedral carbonate (Fig. 20a). Hematite and specularite are present disseminated throughout, but in far lower concentrations than

distal black greenstone clasts (Fig. 20a). They are present with pyrite and appear to be a late-stage overprint formed distally to a later vein. Fine- to coarse-grained cubic pyrite may comprise up to 1% of the clast. The composition of groundmass proximal to quartz veins is largely similar to the composition of groundmass in distal alteration zones. It typically has slightly elevated sericite content, and near tourmaline-bearing veins, it may contain considerably more tourmaline. Two stages of carbonate are present in QSP-altered zones. The first is associated with vein alteration and occurs intergrown with sericite in greenstone clasts. A later, oxidized Fe-bearing phase crosscuts quartz veins and related alteration.

Distal from veins, greenstone clasts are dark gray to purplish-black and composed of granular quartz with abundant hematite, specularite and chlorite inclusions (Fig. 20b). Specularite occurs as very fine, randomly-oriented acicular crystals disseminated throughout the groundmass. Hematite occurs as very-fine, discrete granules or as acicular intergrowths with specularite. Rounded to irregular aggregates of relatively clean, fine- to medium-grained granular quartz may or may not be present. Groundmass in vein-distal zones is quartz-rich, with abundant late Fe-carbonate, weak sericite and sparse tourmaline. Granular to comb-textured subhedral quartz intergrown with sericite rims carbonate-filled vugs present adjacent to clasts and within groundmass.

Transition zones between quartz-hematite and QSP-carbonate alteration are deep reddish-purple to gray and are typically gradational, extending from 1 inch to several feet (Fig. 21). They are composed of relatively equal parts quartz-hematite and QSP-carbonate assemblages, though they are usually pyrite- and fuchsite-poor. Distribution is irregular, and adjacent clasts in transition zones may be variably altered.

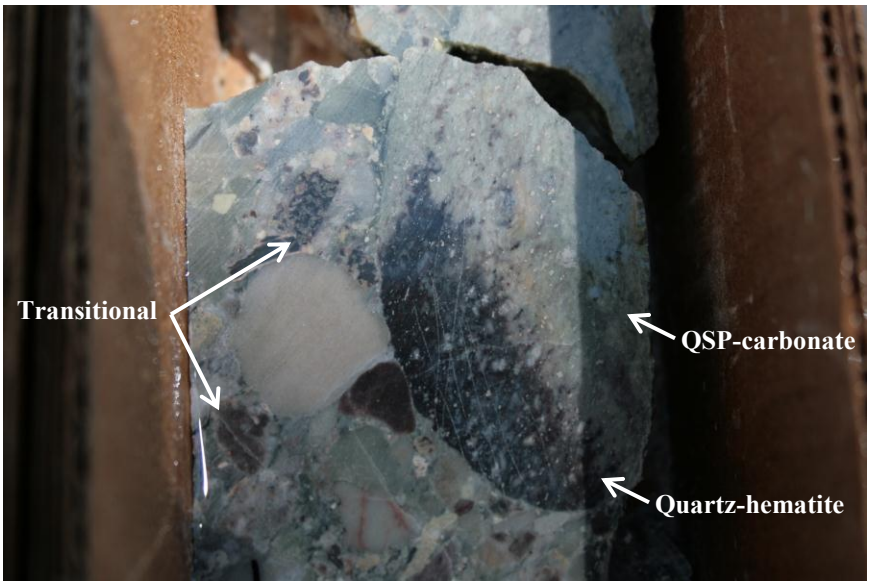

Figure 21: Photograph illustrating transitional alteration effects in the Agglomerate. Core diameter is 2.5 inches.

Tourmaline is much more abundant in the Agglomerate unit than in the overlying Welded Tuff or the underlying Feldspar Porphyry. In those units, it is almost exclusively associated with tourmaline-bearing veins. In the Agglomerate, however, tourmaline is present distal to veins in groundmass and in unusual, light gray siliceous clasts. In many tourmaline-bearing veins, tourmaline is actually a late constituent introduced to the vein through permeable groundmass.

Feldspar Porphyry

Alteration zoning in the Feldspar Porphyry is best developed in holes peripheral to the principal ore trends where vein density is lowest. It consists of vein-proximal quartz-sericite-pyrite-carbonate ± tourmaline, grading outward into a quartz-hematite zone, and then a quartz-specularite zone. QSP-carbonate is always present except where

Figure 22: Photograph of core exhibiting two stages of vein-proximal alteration in the Feldspar Porphyry. First, QSP-carbonate-tourmaline (black schorl variety) alteration occurs adjacent to an early gray granular quartz-pyrite-tourmaline vein. The quartz-pyrite-tourmaline vein and related selvage is crosscut by a later granular gray quartz-carbonate-pyrite vein with QSP-carbonate selvages (pale green).

it is overprinted by later quartz-hematite or quartz-specularite alteration. Quartz-hematite or quartz-specularite alteration may be absent entirely or, most commonly, they may be intergrown. Where a clear transition is observed, quartz-hematite alteration is always intermediate between QSP-carbonate and quartz-specularite zones. The contacts between alteration zones are typically transitional.

Vein-proximal alteration in the Feldspar Porphyry consists of a light greenish-gray, weak to pervasive quartz-sericite-pyrite-carbonate ± tourmaline assemblage (Fig. 22). In zones of high vein density, selvages are moderately to strongly pervasive and can extend several feet. Selvages related to individual veins range from 5-6mm to 1 foot and are weakly to moderately pervasive, dependent primarily on the size of the vein, and to a

lesser extent, vein mineralogy. QSP altered rock is light green, mottled gray with green to pale yellow sericite and gray to white quartz.

Fine- to very fine-grained sericite comprises between 10-20% of altered samples and primarily occurs in anastomosing veinlets that run perpendicular to oblique outward from the vein. Sericite veinlets are typically weakly to strongly pervasive in density and form along grain boundaries, rarely crosscutting grains (Fig. 23a). Adjacent to veins, fine-grained sericite is selectively pervasive after groundmass K-feldspar, decreasing in intensity outward (Fig. 23a-b). Relatively minor and weakly pervasive sericite also occurs after feldspar phenocrysts, where it primarily forms along grain boundaries, and twin and cleavage planes (Fig. 23a). It also occurs in and adjacent to fractures within feldspar phenocrysts and as acicular, radiating crystals intergrown with very fine-grained quartz after feldspar phenocrysts. Sericite, with associated leucoxene, kaolinite, pyrite or hematite, is selectively pervasive after biotite

Hydrothermal quartz is fine- to medium-grained and granular and primarily occurs in discrete irregular to rounded clusters. In addition to fine-grained quartz intergrown with sericite, fine- to medium-grained granular quartz may replace feldspar phenocrysts. It also occurs in fine, planar veinlets with or without carbonate crosscutting sericite veinlets. In transition zones, planar quartz veinlets crosscut irregular sericite veinlets. Hydrothermal quartz may comprise up to 10-20% of the sample.

Pyrite is predominantly subhedral to euhedral cubic, with lesser dodecahedron forms. It is fine- to locally coarse-grained, and occurs disseminated throughout the groundmass. Minor, fine- grained euhedral to anhedral pyrite also occurs with sericite

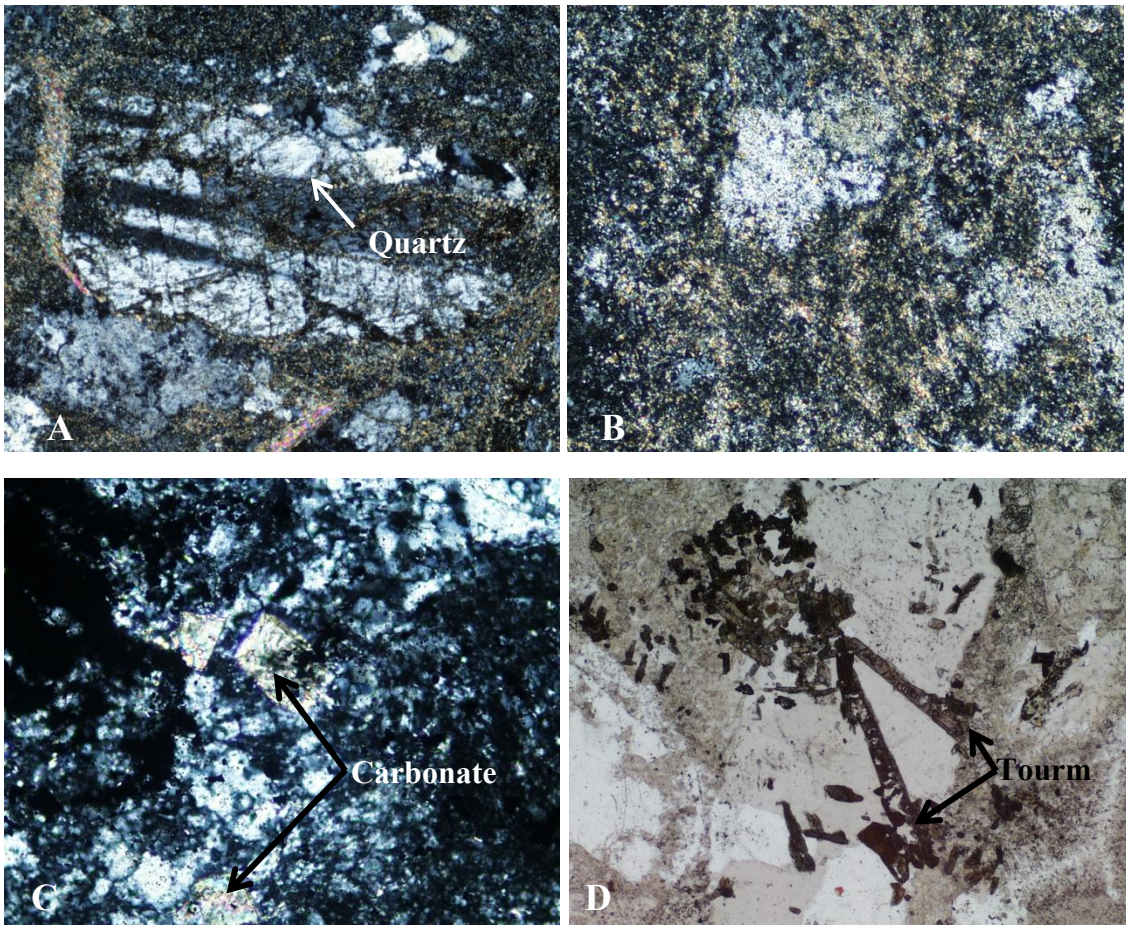

Figure 23: Photomicrographs of proximal alteration effects in the Feldspar Porphyry. A. Sericite rimming and replacing plagioclase phenocrysts along fracture surfaces. Fine-grained granular quartz replaces the feldspar phenocryst. 5x, crossed nicols. FOV=1.70mm; B. Selectively pervasive sericite after groundmass K-feldspar. Note sutured grain boundaries. 20x, crossed nicols. FOV=0.43mm; C. Euhedral carbonate replacing groundmass. 20x, crossed nicols. FOV=0.43mm; D. Fine-grained, subhedral tourmaline occurs in selvages adjacent to a tourmaline-bearing quartz vein. 10x, plane light. FOV=0.85mm.

after biotite. Pyrite typically comprises 0.5-1%, but it may be up to 3% locally. Up to 2% fine to coarse-grained, euhedral tourmaline occurs in QSP selvages adjacent to veins where tourmaline is an early to intermediate vein constituent (Figs. 22 and 23d). Though rare, chlorite may replace tourmaline.

Carbonate is ubiquitous and present in all alteration zones. It forms scaly masses after feldspar fragments and K-feldspar in groundmass. In several samples, rhombic carbonate crystals are present disseminated throughout the groundmass. It occurs in veinlets with quartz, and rarely in vugs. It is more pervasive adjacent to carbonate-bearing

veins. Both Fe-bearing carbonate and relatively pure calcite are present and are discussed in the following carbonate section.

Gold mineralization is most commonly associated with QSP alteration. Strongest alteration occurs in zones of high vein density and begins at variable depths ranging from 750 feet to 1200 feet. It may extend throughout the Feldspar Porphyry interval or it may extend only 200-300 feet.

QSP alteration grades outward into a red-brown quartz-hematite assemblage (silica-hematite after LeLacheur et al. (2011) and Neal and LeLacheur (2010)) (Fig. 24). Similarly to the QSP assemblage, quartz occurs as fine- to medium-grained quartz in discrete clusters. It also occurs in small, discontinuous veinlets, commonly with carbonate. In transition zones, quartz veinlets crosscut anastomosing sericite veinlets. Fine quartz veinlets also crosscut groundmass and fragments. Quartz is much less pervasive than in the QSP zone and comprises 5-10% of the sample volume. Hematite occurs as very fine nodules disseminated throughout the groundmass and in feldspar and

Figure 24: Photograph of the transition between proximal QSP-carbonate alteration (light green) and intermediate red-brown quartz-hematite alteration in the Feldspar Porphyry.

Figure 25: Photograph of dark gray quartz-specularite alteration of the Feldspar Porphyry.

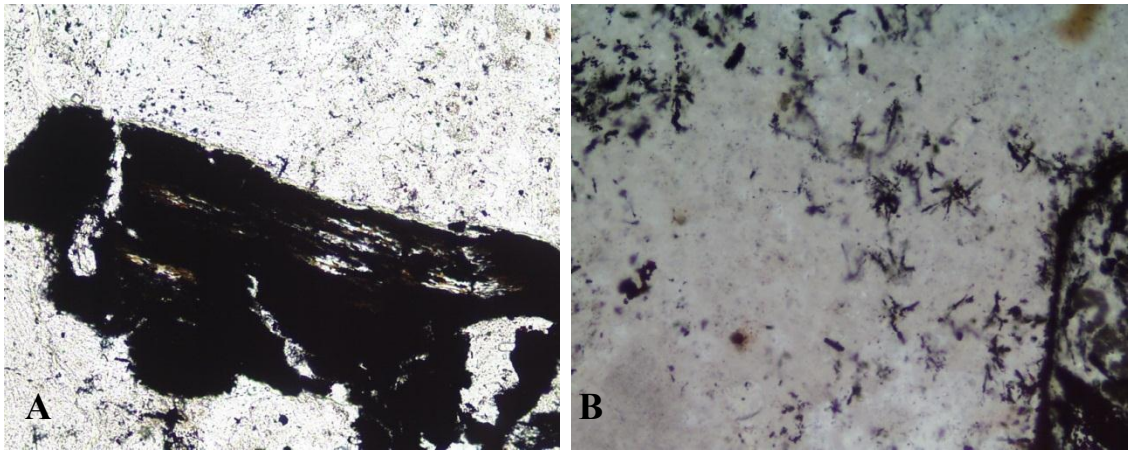

Figure 26: Photomicrographs depicting distal alteration effects in the Feldspar Porphyry; A. Very fine-grained hematite nodules disseminated throughout the groundmass. Note relict spherulitic texture. Biotite is replaced by a mixture of sericite, leucoxene, and hematite. 10x, plane light. FOV=0.85mm; B: Very fine-grained, acicular specularite intergrown with quartz. Specularite is intergrown with minor nodular hematite. 20x, plane light. FOV=0.43mm.

biotite phenocrysts, coloring the former a distinct salmon to red color (Figs. 24 and 26a). Carbonate, most commonly Fe-calcite or siderite/ankerite with lesser calcite, occurs after feldspar phenocrysts and K-feldspar in groundmass. It also occurs in veinlets with quartz. Weak to moderate sericite, similar in occurrence to sericite within QSP-carbonate alteration zones, is invariably present, though less abundant. In drillholes SV07-249C, SV07-255C, and SV07-291C, red-brown quartz-hematite alteration is related to weak to locally pervasive chlorite and may be analogous to weak propylitic alteration. Where present, chlorite occurs within groundmass and along fracture surfaces. Elsewhere, chlorite, though uncommon, is clearly associated with late-stage argillic alteration.

Gray to black quartz-specularite alteration occurs outboard of the red-brown quartz-hematite zone (Fig. 25). It is erratically distributed and commonly absent. It is

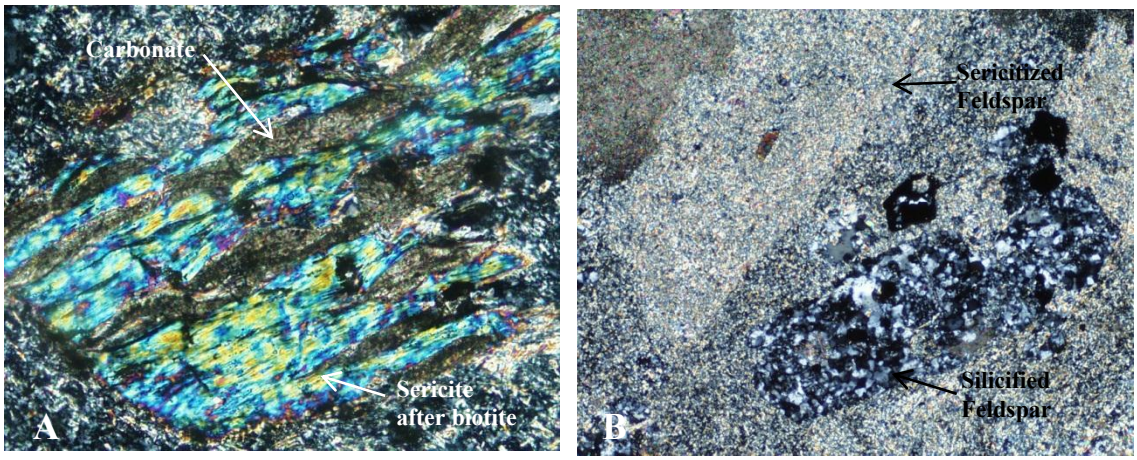

Figure 27: Photomicrographs illustrating proximal alteration in the Limerick Formation; A. Sericite, with lesser carbonate, leucoxene and fine-grained anhedral pyrite, replacing a biotite phenocryst in sample 1UP-035. 20x, crossed nicols. FOV=0.43mm; B. Strongly pervasive sericite in groundmass and after feldspar phenocryst (upper left). Fine-grained, granular quartz psuedomorphs a feldspar fragment. 5x, crossed nicols. FOV=1.70mm;

characterized by fine- to medium-grained granular quartz, intergrown with very fine- to fine-grained acicular to granular specularite (Fig. 26b). Specularite is commonly partially replaced by botryoidal hematite. Similarly to red-brown quartz-hematite alteration, quartz occurs in irregular clusters and in small, discontinuous veinlets with or without carbonate. Less commonly, fine- to medium-grained quartz occurs after feldspar fragments. Weak sericite commonly occurs in the quartz-specularite zone in groundmass and in irregular veinlets.

Limerick Formation

Vein selvages in greenstone and lithic tuff intervals in the Limerick Formation consist of strongly pervasive QSP ± fuchsite or tourmaline. Sericite is fine- to relatively coarse-grained and occurs after groundmass biotite and chlorite and after biotite

phenocrysts or fragments (Fig. 27a). Irregular sericite veinlets extend perpendicular to oblique outward from veins. Strongly pervasive sericite after feldspar fragments occurs adjacent to some veins (Fig. 27b). Moderately pervasive, very fine to fine-grained granular quartz is present in groundmass, while medium- to coarse-grained granular quartz occurs in irregular vugs and clusters. Fine- to medium-grained granular quartz is pervasive after feldspar fragments adjacent to veins (Fig. 27b). Pyrite is typically fine- to medium-grained and cubic. It comprises 0.1-1% of the sample, while sericite constitutes 15-25% and quartz comprises up to 30%. Fuchsite is rare, and occurs after biotite. Fine- to medium-grained euhedral tourmaline is present in selvages adjacent to tourmaline-bearing veins, disseminated throughout the groundmass or forming along clast boundaries in the lithic tuff.

At least two stages of carbonate are present. Early, anhedral scaly carbonate occurs disseminated throughout the groundmass and after biotite, and has a ragged appearance. It is likely related to greenschist-facies alteration, and it is crosscut by later sericite veinlets. A later carbonate phase, commonly associated with veining, occurs disseminated throughout the groundmass and in veinlets that crosscut early sericite. Vein-related alteration in the Limerick Formation is clearly retrograde relative to greenschist-facies alteration. Chlorite is present in pervasive QSP zones, though it is very minor. Chlorite content increases outward from the vein. QSP-fuchsite alteration most commonly grades outward into a greenschist facies chlorite-carbonate-hematite assemblage. Distal, vein-related hematite may be present, though it is difficult to separate from earlier hematite. QSP alteration is strongly texturally destructive and original mineralogy and textures are seldom preserved.

Carbonate

Both Fe-bearing carbonate and relatively pure calcite are present in all alteration zones and in all previously described host rocks. It is the second most abundant vein constituent after quartz and the third most abundant gangue mineral after quartz and sericite. The most common Fe-bearing carbonate phase reacts readily with HCl and is thus likely Fe-calcite. A less reactive carbonate phase is also present, and due to its reaction with potassium ferricyanide, it is likely ankeritic rather than sideritic. Fe-carbonate occurs in all vein types and in their selvages and appears to be more common in earlier veins than calcite. It is also present in relatively unaltered wallrock. There is no obvious correlation between Fe-bearing carbonate and gold mineralization.

At least two stages of calcite are present. Earliest calcite occurs in selvages and likely in veins and is commonly rimmed by later Fe-bearing phases. Later calcite occurs as massive open-space filling phase in some veins, and in two samples, it is bladed. The timing of late calcite relative to mineralization is uncertain.

Argillic Alteration

Late-stage, hypogene argillic alteration occurs primarily in and adjacent to fault zones. It is weakly to strongly pervasive, and it overprints earlier QSP-carbonate and quartz-hematite alteration assemblages. It comprises the groundmass of what is referred to as the Clay Matrix Breccia, narrow (<10 feet) to broad (>50 feet) zones of fault gauge with 20% to 80% clays and milled, cognate clasts. It is composed of interlayered clays with or without chlorite and fine-grained, disseminated pyrite. Quartz vein fragments

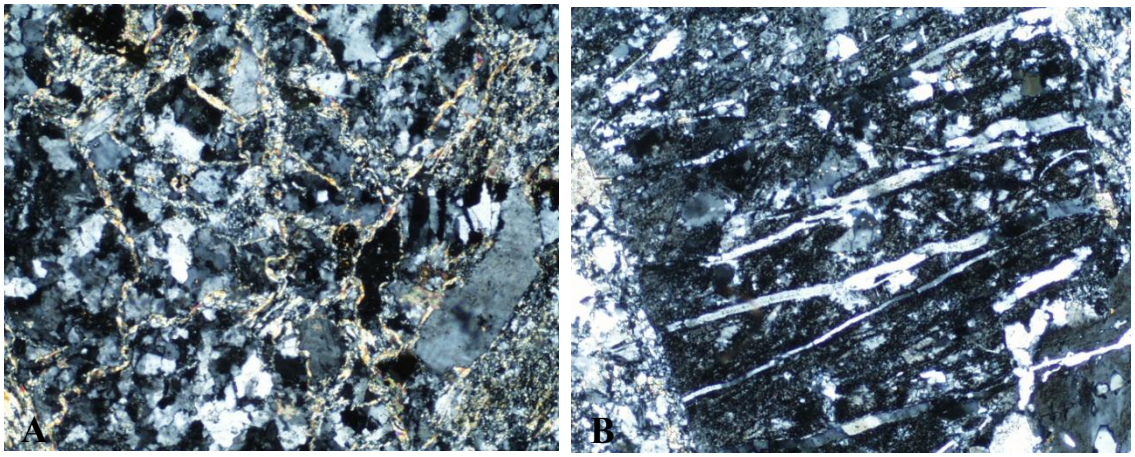

Figure 28: Photomicrographs of silicification associated with pre-ore veins. A. Strongly pervasive, fine- to medium-grained granular quartz in in wallrock adjacent to pre-ore veins. Later sericite forms in fractures around quartz grain boundaries. 5x, crossed nicols. FOV=1.70mm; B. Very fine, discontinuous quartz veins crosscutting a feldspar fragment outboard of a pre-ore vein. 5x, crossed nicols. FOV=1.70mm.

within the Clay Matrix Breccia indicate that argillic alteration postdates mineralization, though the presence of pyrite within argillic zones suggests that it is hypogene rather than supergene. Argillic alteration possibly formed following late-stage collapse of the hydrothermal system, or it may have formed during a separate event.

Pre-ore and Post-ore Alteration

Early, pre-ore ataxial quartz veins are associated with pervasive silicification. Fine- to medium-grained granular quartz is strongly pervasive in groundmass and after feldspar fragments (Fig. 28a). Fine-grained quartz also occurs in discontinuous, wispy veinlets that crosscut groundmass and wallrock fragments (Fig. 28b).

Ore-stage alteration is overprinted by later calcite and Fe-calcite alteration. It is pervasive in the Agglomerate unit, where it occurs in veins, clasts and groundmass and is

commonly stained bright orange by limonite or pink by hematite. Local white to pink calcite-cemented breccias are present and are likewise believed to post-date mineralization.

Alteration Geochemistry

Ten altered and relatively unaltered samples from the Feldspar Porphyry were analyzed for whole rock and trace element composition by combined lithium borate fusion and ICP-AES (Appendix B). Samples were chosen from each alteration zone, from proximal QSP-carbonate to distal quartz-hematite and quartz-specularite alteration, and from a relatively unaltered interval at the top of the Feldspar Porphyry section in drillhole SV07-248C. Analyses were conducted by ALS-Chemex at their assay lab in Sparks, Nevada.

Barium content of altered and relatively unaltered samples ranged from 695 ppm to 1530 ppm (Fig. 29). Typical barium-bearing minerals such as barite are not present, and barium likely occurs as a substitution for potassium in sericite. Potassium content is similarly elevated, ranging from approximately 2-6%, and likely reflects both K-feldspar in groundmass and subsequent sericitization. As mentioned previously, K_2O concentrations in the Feldspar Porphyry are comparable to that of other samples from the Rochester and Weaver formations within the Humboldt, East and Stillwater ranges.

SiO_2, MnO, MgO and P_2O_5 contents were irregular (Fig. 29). K_2O content in unaltered samples is generally lower than in quartz-hematite or QSP-carbonate altered samples (Fig. 29). This is likely due to increased sericite introduction adjacent to veins, though it may be indicative of multiple sericite events of differing composition (i.e.

earlier greenschist-facies sericite and later hydrothermal sericite). A decrease in Na_2O from unaltered to altered samples is also likely related to an increase in sericite after plagioclase. BaO trends mimic those of K_2O and are similarly likely related to sericite concentrations.

CaO content is variable, though it generally decreases towards the vein (Fig. 29). This likely reflects variable carbonate content and composition. In hematite-altered zones where CaO concentrations are on average the lowest, Fe-bearing carbonate is dominant. QSP-carbonate altered samples FP-2 and FP-3 have the lowest CaO concentrations and are similarly Fe-bearing carbonate dominant. Samples FP-8 and FP-9, which are also QSP-carbonate altered and have significantly higher CaO concentrations, were adjacent to calcite-bearing veins and thus had higher calcite content.

Fe_2O_3 generally increases towards the vein. This is due to increasing specularite, hematite, pyrite and Fe-carbonate concentrations, though interestingly, Fe_2O_3 concentrations are anomalously low in quartz-hematite altered samples. Overall, the Fe_2O_3 trend is the mirror opposite of the CaO trend.

Al_2O_3 concentrations are anomalously low in proximal QSP-carbonate altered zones. They are broadly correlative with increased SiO_2 concentrations and can likely be explained by increased quartz and carbonate after feldspar. However, petrographic study of other QSP-carbonate altered samples does not substantiate a general increase in quartz adjacent to veins, and increased quartz may only occur locally.

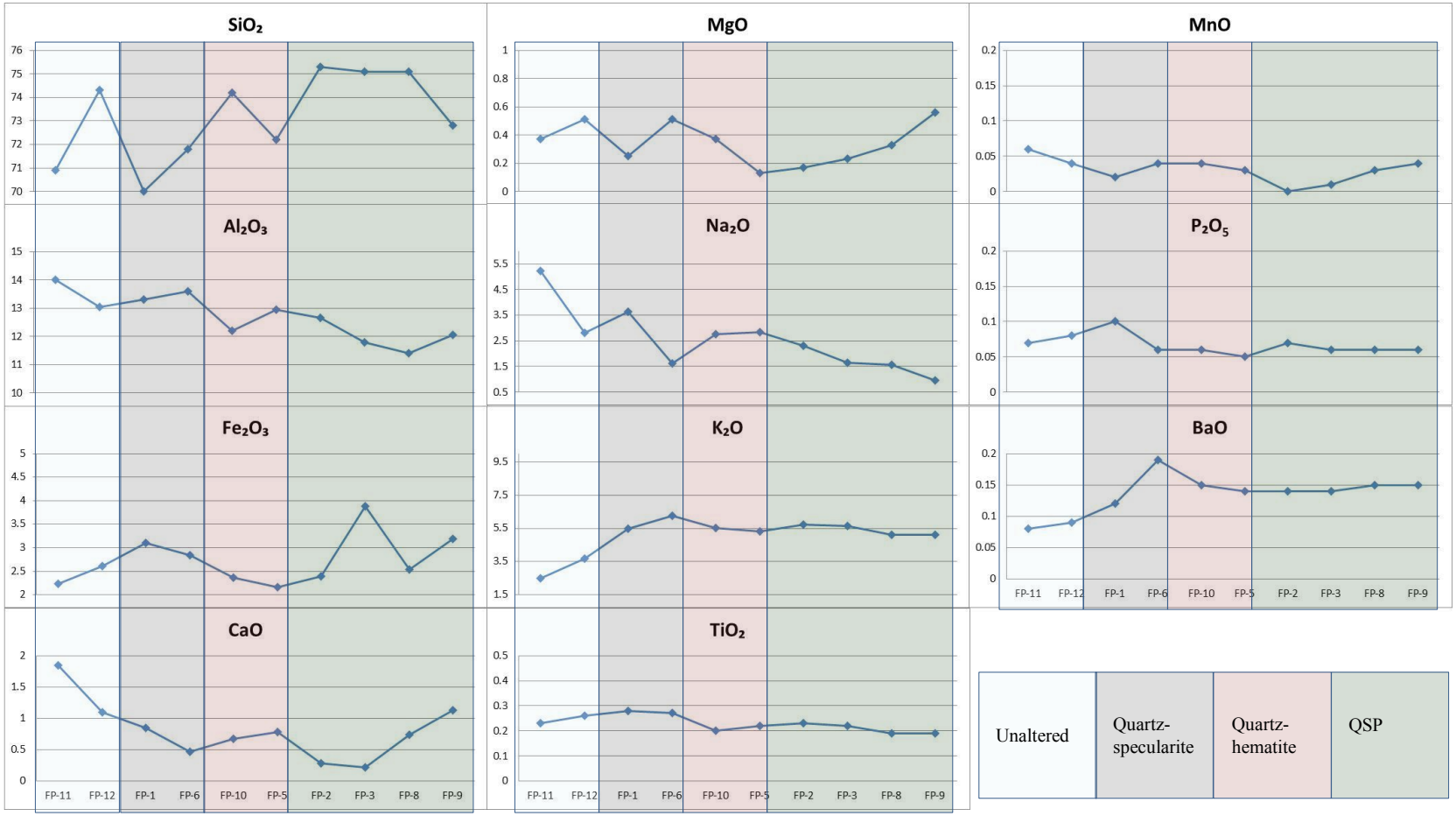

Figure 29: Scatter plots showing variations in major element composition of alteration zones in the Feldspar Porphyry. Samples exhibit increasing alteration and proximity to the vein from left to right. Note that samples are not corrected for density, as they are likely very close in density and results are easily verifiable through petrographic analysis.

Vein Mineralogy, Textures and Paragenesis

Gold-bearing veins at Spring Valley are dissimilar to classic porphyry-style A-type, B-type and D-type veins in morphology, mineralogy and alteration association. They have internal textures indicative of formation in a mesothermal environment and are likely metamorphic in origin. Three types of so-called metamorphic veins were identified at Spring Valley: 1. Ataxial displacement-controlled; 2. Face-controlled crack-seal; and 3. Non-directional. (Refer to the "Discussion of Metamorphic Vein Textures" section for general characteristics and genesis of metamorphic quartz veins).

Gold and base-metal mineralization at Spring Valley is hosted within crack-seal and granular quartz-carbonate veins that crosscut pre-ore ataxial quartz veins. In addition to quartz and carbonate, ore-stage veins commonly contain minor early sericite or early to late schorl-variety tourmaline. They are typically between 0.5mm and 50mm in width, though veins with up to 1.5 feet are present, most commonly in the Limerick Formation and Rochester Agglomerate. Veins are not laterally continuous, though observations on strike length are hindered by the lack of exposure and limited by the diameter of core.

Quartz-carbonate veins are most commonly oriented 42-74°, 60°S and 272°, 46°N (Neal and LeLacheur, 2010). They are oblique to the overall NNE trend of the orebody and are oblique to sub-parallel to the hinge of the Spring Valley anticline and to NE-trending faults (Neal and LeLacheur, 2010).This principal northeast orientation of gold-bearing metamorphic veins has been noted throughout the Humboldt, East, Pine Forest and Antelope ranges (Cheong, 1999). Regionally, such veins crosscut earlier late Jurassic

Figure 30: Photograph of a planar crack-seal quartz-pyrite vein (white) crosscut by an irregular gray quartz-tourmaline-pyrite vein in the Feldspar Porphyry. Further down hole, the white crack-seal vein is also crosscut by a 6-8mm planar gray quartz-pyrite-carbonate vein. Core is 2.5 inches in diameter.

foliation and are believed to be related to Late Cretaceous northeast- to southwest-directed crustal shortening (Cheong, 1999). At Spring Valley, vein orientations are likely controlled by the northeast-trending Black Ridge Fault system or the northeast-trending Spring Valley anticline.

Though ore-stage veins are clearly mesozonal in origin, they are primarily brittle features with internal textures indicative of formation during extension. First, they have relatively well-defined and matching vein walls. Second, they have quartz textures indicative of formation in open-space. In addition, elongated quartz within crack-seal veins forms perpendicular to slightly oblique to vein walls, indicating nearly perpendicular to slightly orthogonal extension. This is corroborated by the presence of bands of included wallrock in crack-seal veins that are parallel to vein margins and record opening direction.

While the margins of granular quartz veins are typically planar, irregular and branching veins of similar composition and timing occur locally, particularly in the Feldspar Porphyry. There, it is not uncommon for relatively planar veins to be crosscut by later stage veins with irregular margins (Fig. 30). This suggests some anisotropy in the rheology of the unit, through both space and time.

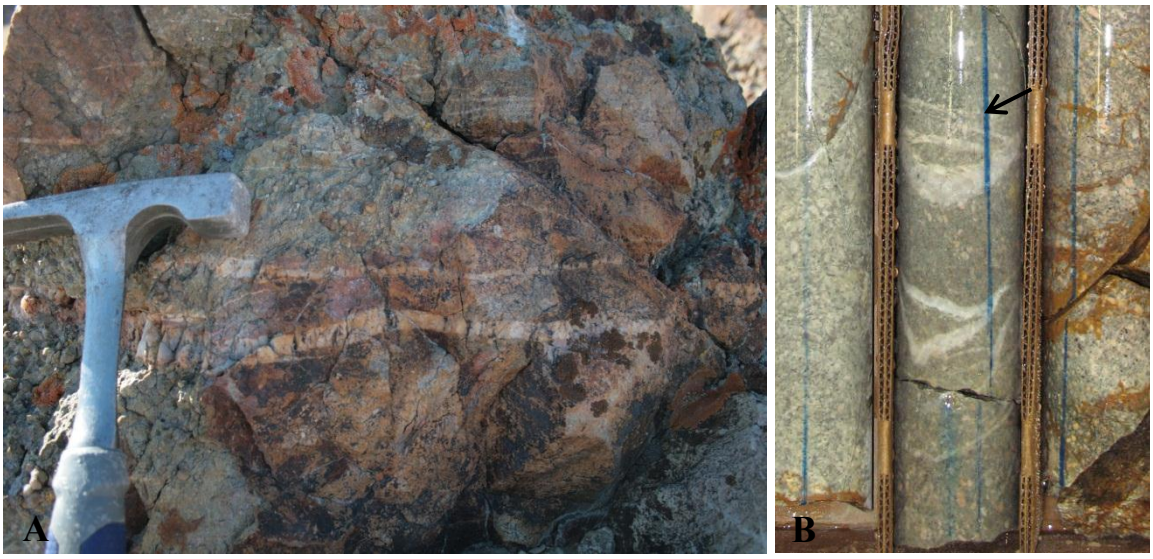

Figure 31: Photographs of sheeted ataxial veins in core and outcrop. A. Sheeted ataxial veins crosscut an outcrop of lithic tuff within the Limerick Formation in the mapping area to the north of Spring Valley. B. Sheeted ataxial veins (shown by the black arrow) crosscutting the Feldspar Porphyry in drillhole SV07-290C. Ataxial veins are crosscut by white granular quartz-carbonate veins.

Ataxial veins

The earliest veins in the Spring Valley deposit are white ataxial veins that predate gold mineralization. They are sigmoidal and commonly sheeted, occurring in groups of three or more (Fig. 31a-b). They are composed primarily of fibrous quartz with distinctly serrated grain boundaries, and lesser fibrous plagioclase and K-feldspar derived from the wallrock (Fig. 32a-b). Grain widths are relatively consistent across the vein, and where shear is evident, fibers near margins are perpendicular to vein walls (Fig. 32a and 32c). Parallel, discontinuous inclusion bands are present in some veins, which suggests a composite genesis with intermittent fracturing at the wallrock-vein interface and continued formation of ataxial quartz (Fig. 32d).

Ataxial veins are typically 3mm to 5mm in width and range in strike from 0.2 feet to 0.6 feet. At least two generations of these veins are present, with no textural or

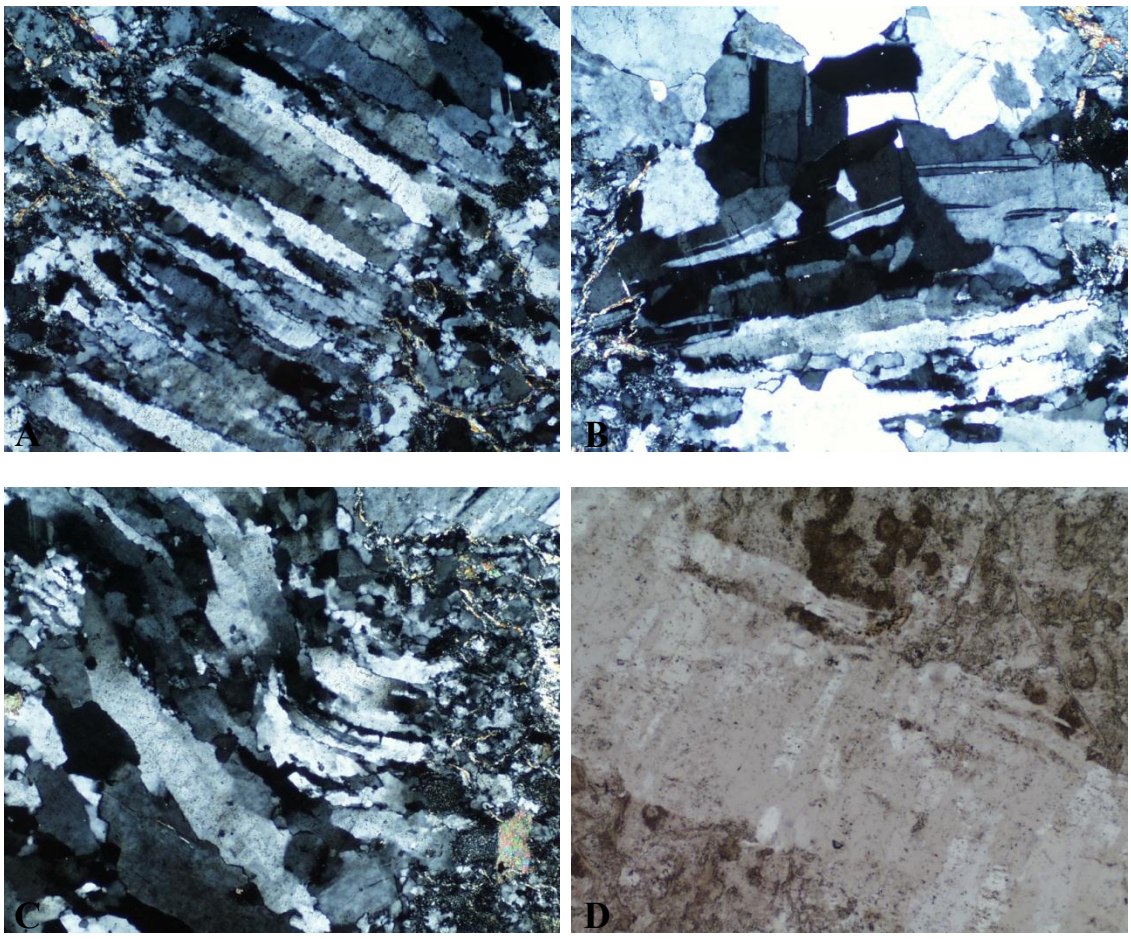

Figure 32: Photomicrographs depicting features common to ataxial veins at Spring Valley. A. Early, ataxial quartz vein. Quartz grain widths are fairly consistent and have characteristic serrated grain margins. 5x, crossed nicols. FOV=1.70mm; B. Wallrock plagioclase fragment incorporated into ataxial quartz vein. 5x, crossed nicols. FOV=1.70mm; C. Photomicrograph of am ataxial quartz vein showing accommodation of shear in the center of the vein. At vein margins, quartz fibers are perpendicular to the wall. 5x, crossed nicols. FOV=1.70mm; D. Wallrock inclusion bands in an ataxial quartz vein formed when vein-stage fracturing occurred at the vein-wallrock interface and ataxial quartz growth continued at the inclusion surface. 5x, plane light. FOV=1.70mm

mineralogical distinctions between them. They are not confined by depth or host rock, though they are most common in the Feldspar Porphyry and Agglomerate units. On the ridge to the north of Spring Valley, en echelon veins are present in upper Rochester rhyolite flows, where they are crosscut by 1-2mm gray quartz veins.

In hand sample, ataxial veins appear to crosscut alteration zones, producing no selvages. However, in thin section, it is apparent that they are associated with pervasive silicification, commonly obscured by later ore-stage alteration assemblages. In addition to locally derived quartz, plagioclase and K-feldspar, they may contain late, interstitial carbonate. In sample 1UP-051, cleavage planes of interstitial calcite are deformed, typically oblique to the trend of elongate-quartz growth. This suggests that deformation continued after carbonate formation.

Ataxial veins identified in the mapping area to the north of Spring Valley trend northwest. In addition, it was established that some ataxial veins measured by site geologists in oriented core similarly trend northwest. Ataxial veins may thus comprise the subset of quartz veins that trend northwest, most prominently 272°, throughout Spring Valley.

Crack-seal veins

White ataxial veins are crosscut by elongate-blocky to granular gray quartz veins (Fig. 33). The two vein types appear similarly in hand sample and can typically only be distinguished petrographically. Crack-seal veins are composed of elongate-blocky quartz with or without late tourmaline, carbonate, sericite or sulfides. Quartz grains have varying widths across the vein and characteristic serrated grain boundaries (Fig. 34a).

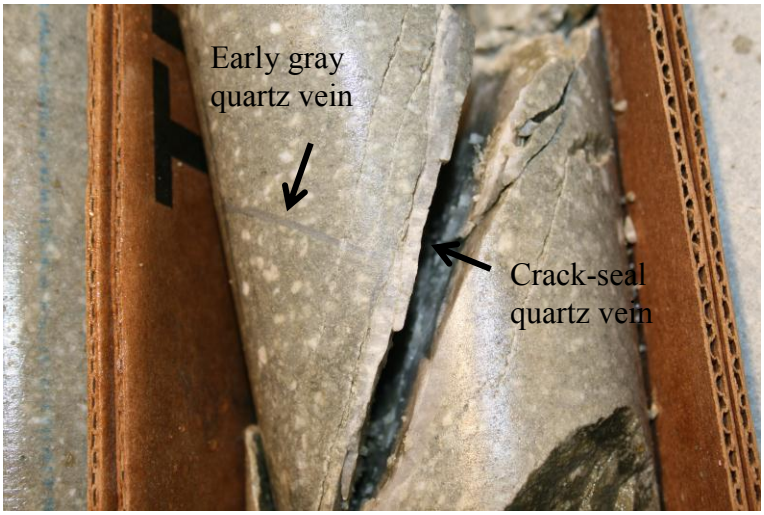

Figure 33: Photograph of a white crack-seal quartz vein crosscutting an early gray granular quartz vein in drillhole SV11-513C. Note faint, perpendicular lineations in in the crack-seal vein that delineate elongate-blocky quartz grain boundaries.

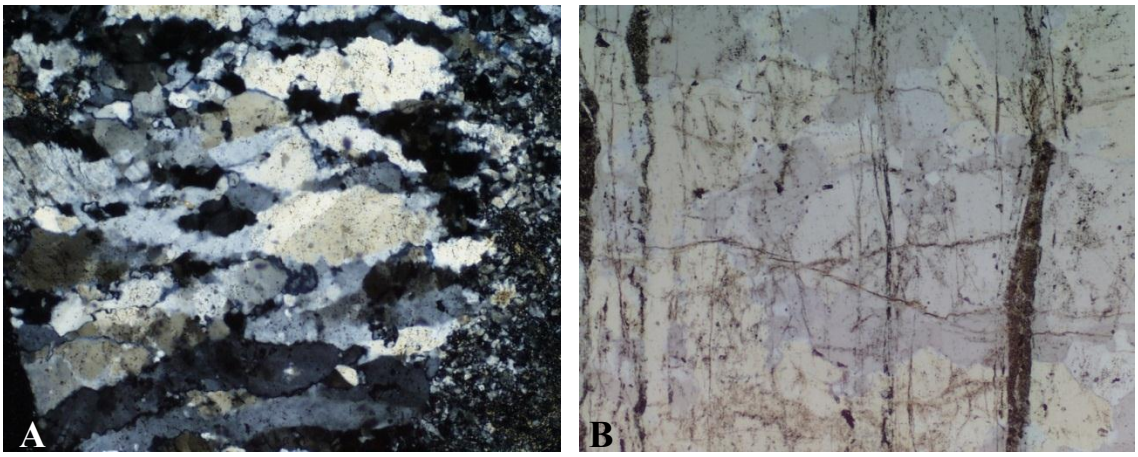

Figure 34: Photomicrographs illustrating features common to crack-seal veins at Spring Valley. A. Elongate-blocky quartz grains with varying widths and "radiator fin" textured grain boundaries. Note fine-grained, granular quartz that likely formed by recrystallization of elongate-blocky quartz along grain boundaries. 5x, crossed nicols. FOV=1.70mm. B. Discontinuous wallrock inclusion bands in a quartz-pyrite-sphalerite-galena vein. 5x, crossed nicols. FOV=1.70mm.

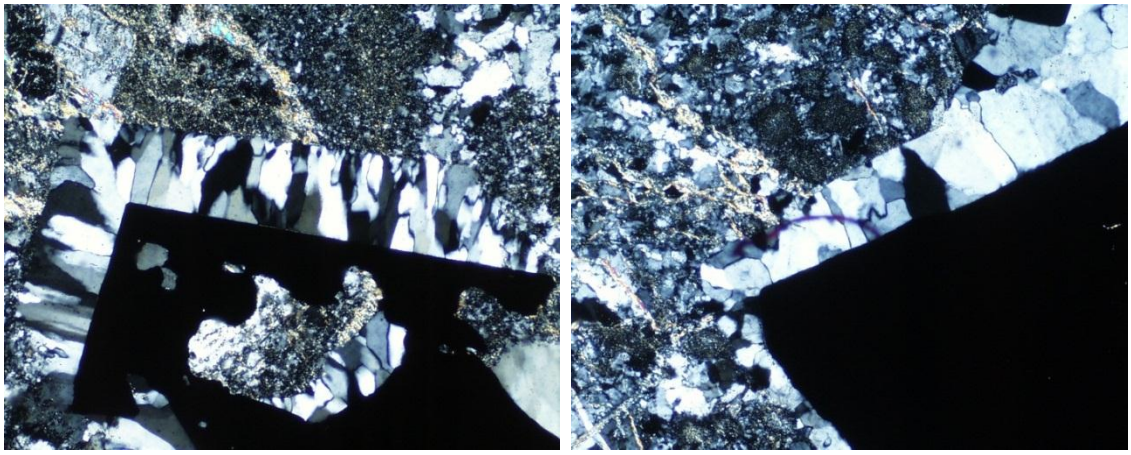

Figure 35: Photomicrographs of fibrous to elongate-blocky quartz infill associated with displacement of early pyrite. In both cases, pyrite was pulled away from the wallrock during granular quartz vein opening and the resulting void was infilled by quartz. 5x, crossed nicols. FOV=1.70mm

They are bisected by discontinuous to continuous inclusion bands that record cracking on a micron- to millimeter-scale (Fig. 34b). Crack-seal veins at Spring Valley do not exhibit banded or ribbon textures characteristic of other crack-seal veins in metamorphic deposits in northwestern Nevada. Very fine-to medium-grained quartz formed by recrystallization along grain boundaries occurs locally (Drury and Urai, 1990).

Crack-seal quartz veins are white to gray and are typically 3mm to 10mm in width. Unlike early ataxial veins, they are difficult to recognize in hand sample. They were observed in the Welded Tuff and Feldspar Porphyry units and the Limerick Formation, though due to their indistinct megascopic appearance, they may be much more common. They are associated with quartz-sericite-pyrite alteration and may host late pyrite, sphalerite or galena commonly associated with gold mineralization. In addition, they almost always contain interstitial carbonate, typically Fe-calcite that did not form by crack-seal mechanisms.

An early pyrite stage is associated with crack-seal quartz veins (Fig. 35). It is typically fine- to coarse-grained, subhedral to cubic, and occurs both within veins and selvages. Within veins, early pyrite may be strongly fractured or crushed, which suggests that it formed prior to or during crack-seal processes. In several samples, wallrock pyrite was incorporated into the vein and subsequently crushed and fractured as the crack-seal process propagated.

Wallrock pyrite may also be incorporated into later granular quartz veins, though it is typically not deformed. Open-space created when pyrite is incorporated into a later vein and pulled away from the wallrock may be infilled by granular to elongate-blocky or "fibrous" quartz (Fig. 35a-b). Such quartz infill resembles pressure shadows that may have formed during ductile shearing and metamorphism. However, planar margins, fracturing of adjacent pyrite and the lack of rotation of pyrite grains indicates they are distinct features associated with brittle deformation (Fig. 35a-b). Quartz infill is thus more analogous to a crack-seal vein.

Non-directional quartz veins

The majority of quartz veins at Spring Valley are composed of fine- to coarse-grained, granular (non-directional) to subhedral quartz with or without intermediate to late euhedral quartz. Several crosscutting generations are present, with gray quartz veins generally being earlier than white quartz veins. Weak zoning is evidence, with gray quartz veins typically occurring at greater depths than white quartz veins, though both are present throughout the resource area. Granular quartz veins range in width from 2mm to 2 feet, though most are between 2mm and 40mm. Strike lengths are generally greater

Figure 36: Photograph of a banded quartz-tourmaline fault-fill vein from drillhole SV07-292C. Note slickenlines on bottom face.

than the core diameter and some veins that run parallel to the core axis are up to 2 feet in length. Granular quartz may exhibit weak undulose extinction and minor recrystallization along grain boundaries, though deformation is local. Granular quartz veins are associated with weak to strongly pervasive QSP-carbonate alteration. Six stages of granular quartz veins were identified at Spring Valley. They record the evolution of mineralization fluids from relatively primitive, pre-gold quartz-pyrite-carbonate veins, through ore stage quartz-tourmaline veins and quartz-base metal veins. Non-directional quartz is also commonly referred to as blocky quartz (Bons, 2000; Faleiros, 2007), bull quartz (Cheong, 1999) or granular quartz. Hereafter, it is referred to granular quartz in discussion of vein composition, and non-directional quartz in discussion of vein formation.

Figure 37: Photograph of a banded and brecciated white quartz vein from a prospect to the north of Spring Valley. Brecciated quartz along vein walls suggests initial vein formation while the fault was active. The vein was then reopened, and banded quartz was precipitated.

Fault-fill veins

Though small, extensional quartz-carbonate veins are the dominant vein-type at Spring Valley, fault-fill veins are present locally. Fault-fill veins are identified primarily by the presence of distinct banding and slickenlines (Fig. 36) (Robert and Poulsen, 2001). They are typically 5 cm to 15 cm in width, and are composed of 2 cm to 5 cm bands of massive quartz, interlayered with thin, 0.5-2mm felty tourmaline bands. The paragenetic relationship between fault-fill and extensional veins is unclear.

On the ridge to the north a Spring Valley, a small prospect pit explores a 1 foot to 2 foot white quartz vein within a northwest-trending Rhyolite Porphyry dike in or adjacent to the North Valley fault zone (Figs. 4 and 37). The vein is composed of massive white quartz and strongly oxidized hematite bands and has strongly brecciated margins, indicative of multiple stages of vein formation.

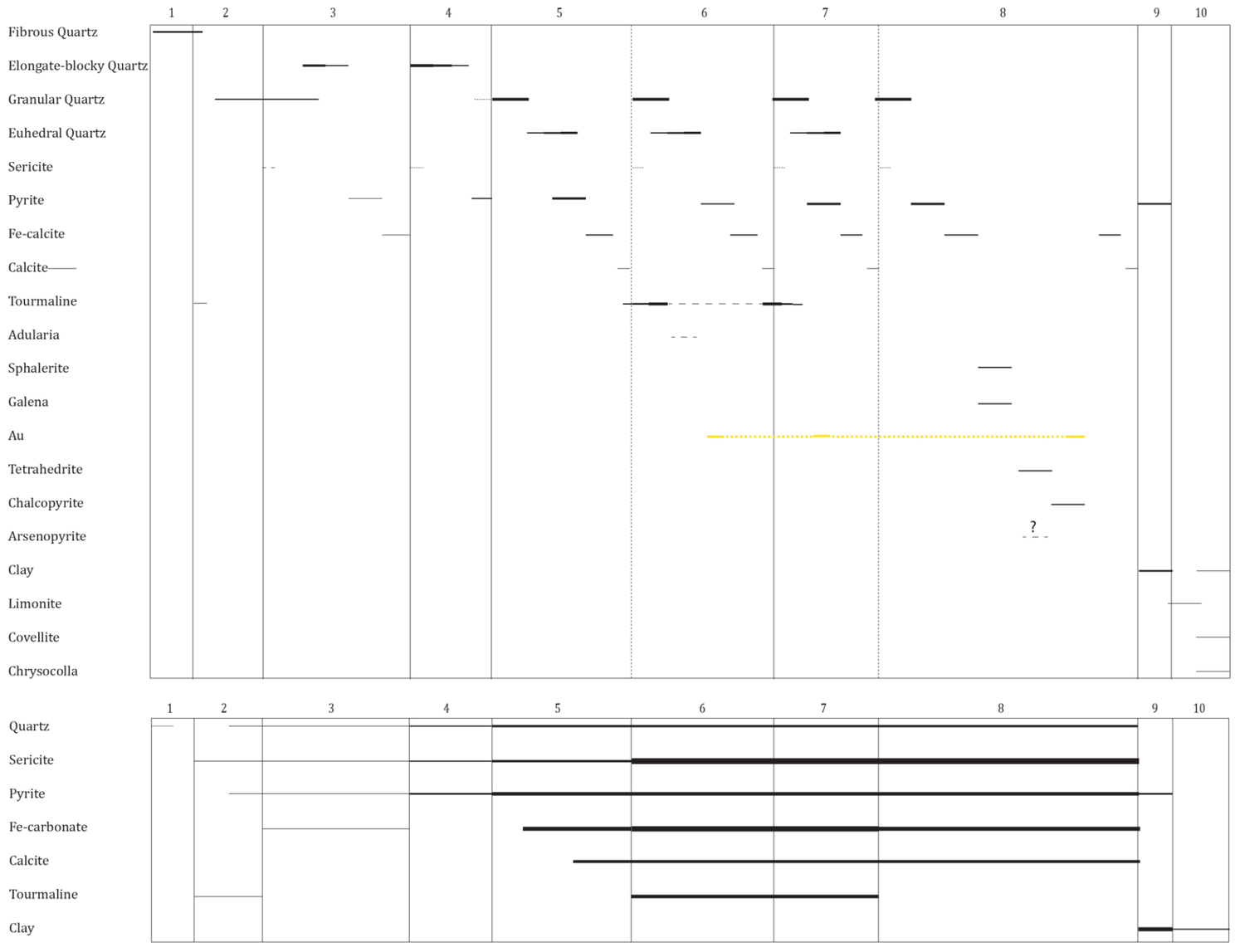

Figure 38: Paragenesis of pre-ore through ore-stage veins and associated alteration selvages at Spring Valley. The thickness of bars represents relative abundance. Refer to text for descriptions of vein stages 1-8. Post-ore argillic alteration occurred during stage 9. Supergene weathering occurred during stage 10.

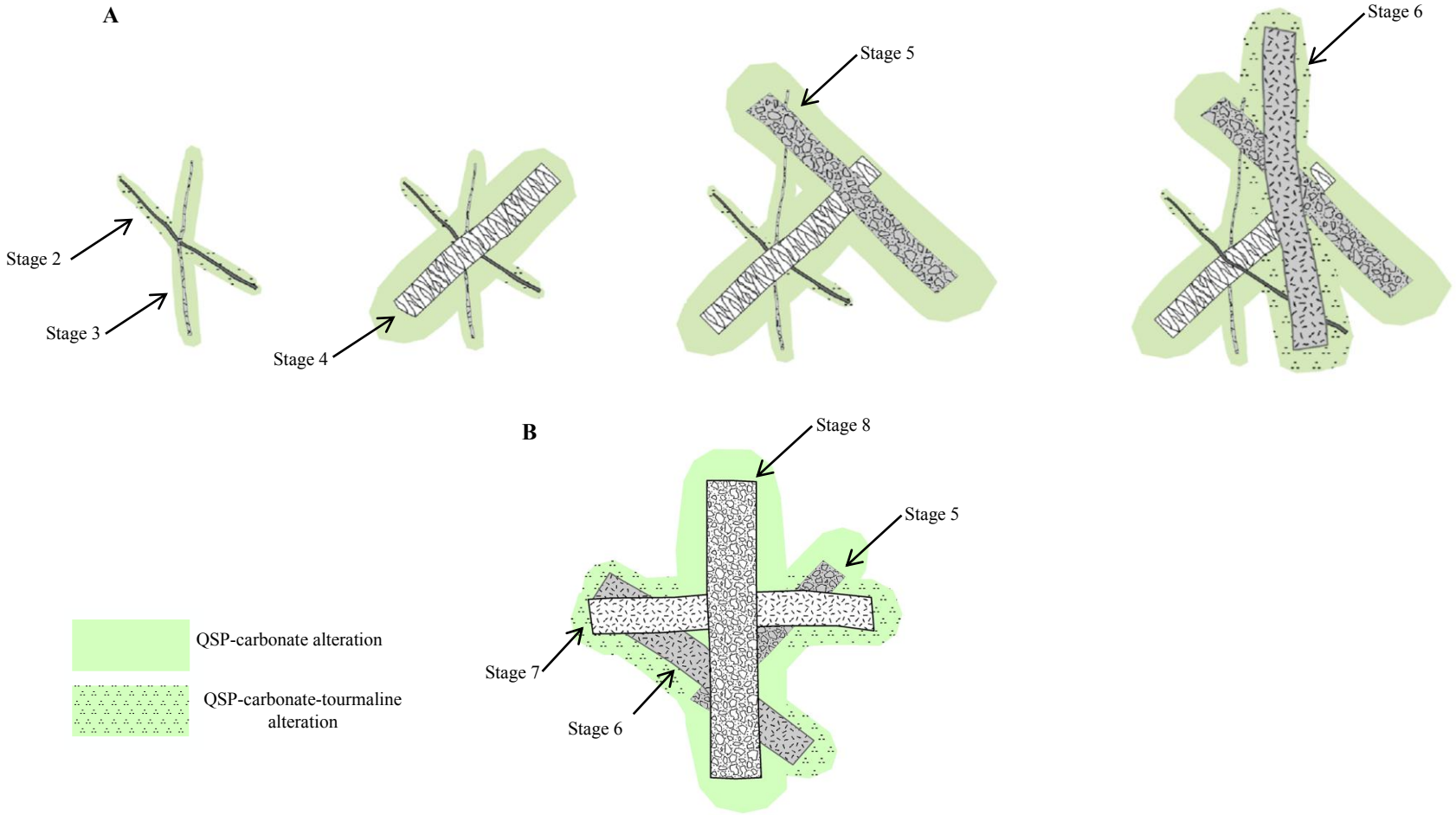

Figure 39: Illustrations depicting the paragenesis of ore-stage veins and associated selvages. A. Stages 2-6; B. Stages 6-8. Note the presence of tourmaline in selvages adjacent to tourmaline veins. Refer to text and Figure 38 for descriptions of vein stages.

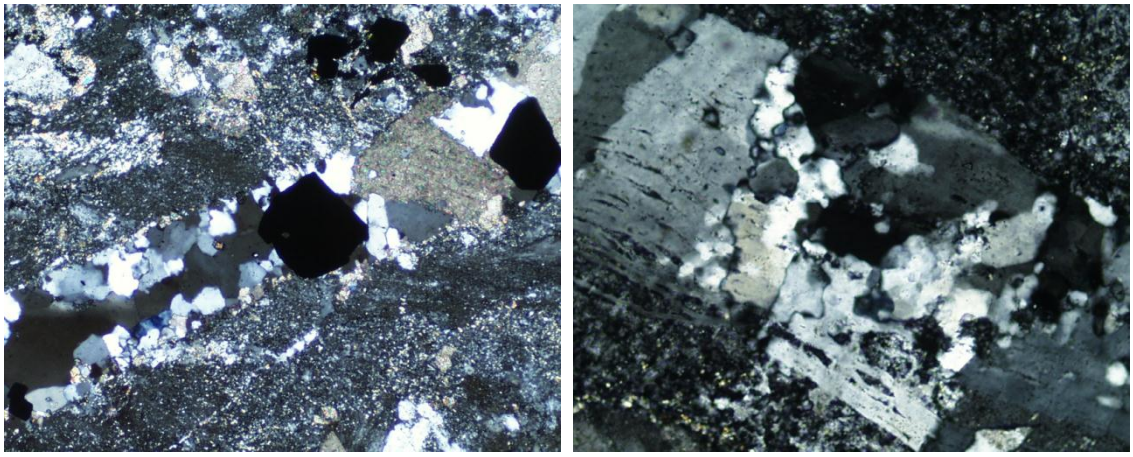

Figure 40: Photomicrographs of early ore-stage gray quartz veins. A. Early gray granular quartz-pyrite-carbonate vein in the Feldspar Porphyry. 5x, crossed nicols. FOV = 1.70 mm; B. Early gray elongate-blocky crack-seal vein in Feldspar Porphyry with numerous, discontinuous wallrock inclusions and local recrystallization to fine-grained granular quartz along grain boundaries. 5x, crossed nicols. FOV = 1.70 mm.

Vein Paragenesis

Stages 1-3

Stage 1 veins at Spring Valley are pre-ore ataxial veins. They are crosscut by small, discontinuous granular gray quartz veins, the earliest ore-stage veins at Spring Valley (Figs. 37-38; stages 2 and 3). Early gray quartz veins are typically hairline to 1.5mm in width, and while smaller, earlier veins are generally discontinuous and wispy, later and thicker veins have relatively planar walls and may be over a foot in strike length. They are the most common vein type in the south end of the Spring Valley deposit and occur in all host rocks, with similar relationships and geometries.

Stage 2 quartz veins at Spring Valley are composed of fine- to medium-grained granular quartz intergrown with relatively abundant, very fine-grained tourmaline, commonly lending a black color in hand sample. They are crosscut by stage 3 gray

granular to elongate-blocky quartz veins. The majority of stage 3 quartz veins are composed of fine- to medium-grained, granular to subhedral quartz, with later carbonate and/or pyrite. They may contain an early fine-grained quartz phase lining vein walls, infilled by later, coarser quartz, or they may be homogeneous in grain size. They are associated with very weak quartz-sericite-pyrite-carbonate alteration, and may host pyrite, sphalerite or galena, but typically only where spatially associated with later, base metal-bearing veins. Some of the earliest veins appear to be replacement rather than open-space filling, with highly irregular vein margins and increasing widths at intersections. Replacement veins are relatively minor.

Early gray granular quartz veins are crosscut by early gray crack-seal veins, though locally, the former crosscuts the latter (Figs. 37 and 39b; stage 3). The overlapping paragenetic relationship between early granular and early crack-seal veins reflects pressure fluctuations that favored the formation of one over the other. Regardless of texture, similarities in composition and overlap in paragenesis warrant the inclusion of both into a single stage.

Stages 4-6

Early gray granular and crack-seal veins are crosscut by later, crack-seal veins, described in the previous section (Figs. 37-38; stage 4). The primary distinction between earlier and later crack-seal veins is that the latter are generally wider and more

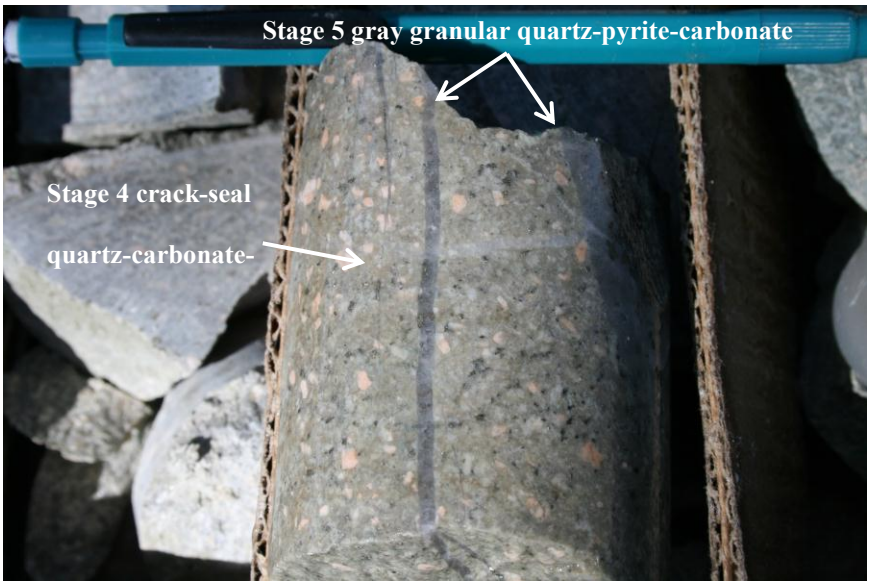

Figure 41: Photograph of a two subparallel gray granular quartz-carbonate-pyrite veins crosscutting a white crack-seal vein.

continuous, with relatively well-defined vein margins. The difference in the size of the vein manifests as a clear distinction in the morphology of elongate-blocky quartz, as quartz in later crack-seal veins had more time and space to grow (compare Figs. 33a and 39b).

Following the cessation of wide-spread crack-seal vein forming processes, two stages of gray granular quartz veins formed. The earliest of these are gray granular quartz veins with late interstitial carbonate ± euhedral to anhedral pyrite (Figs. 38- 40; stage 5). Fine- to medium-grained granular to subhedral quartz commonly discontinuously to continuously lines veins walls (Fig. 41a). Veins are infilled by intergrown fine- to very coarse grained granular to euhedral quartz (Fig. 41a). Late euhedral quartz may occur in carbonate-filled vugs, though it is uncommon (Fig. 41b). Carbonate is typically granular to scaly and comprises less than 10% of the vein. Veins in which carbonate comprises a much larger portion or veins in which carbonate is euhedral or bladed do occur, though

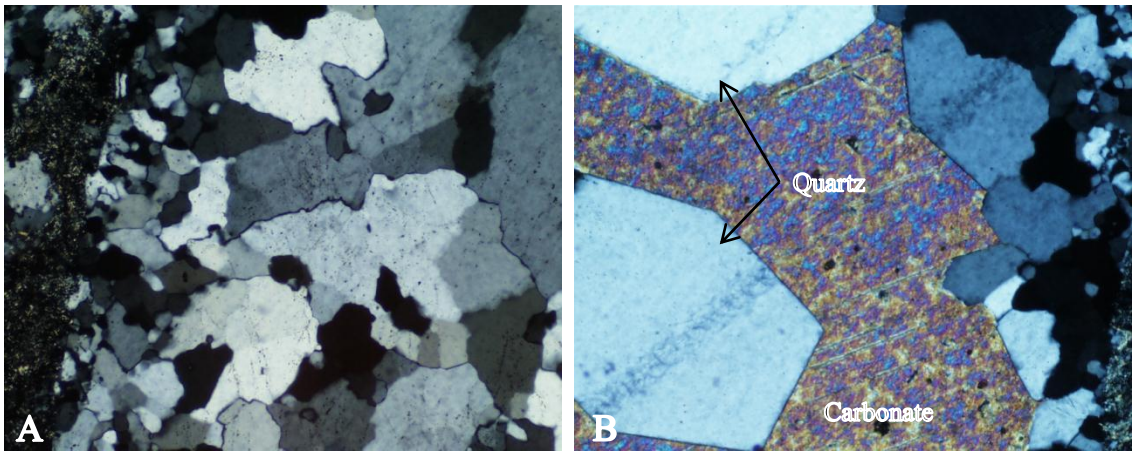

Figure 42: Photomicrographs of features common to gray granular quartz-carbonate-pyrite veins: A. Early fine-grained granular quartz lining the walls of a quartz-carbonate-pyrite vein in sample 1UP-062. Granular quartz generally coarsens inward from margins. 5x, crossed nicols. FOV=1.70mm; B. Late euhedral quartz and interstitial carbonate growing in a vug in a quartz-carbonate vein. Sample 1UP-062 5x, crossed nicols. FOV=1.70mm.

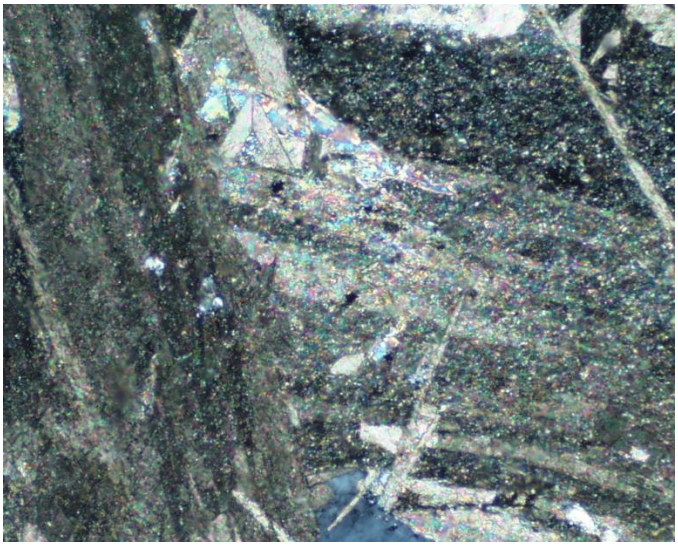

Figure 43: Photomicrograph of bladed carbonate in a gray granular quartz-carbonate vein. Bladed carbonate is indicative of boiling of ore-forming solutions, though it is uncommon at Spring Valley. 5x, crossed nicols. FOV=1.70mm.

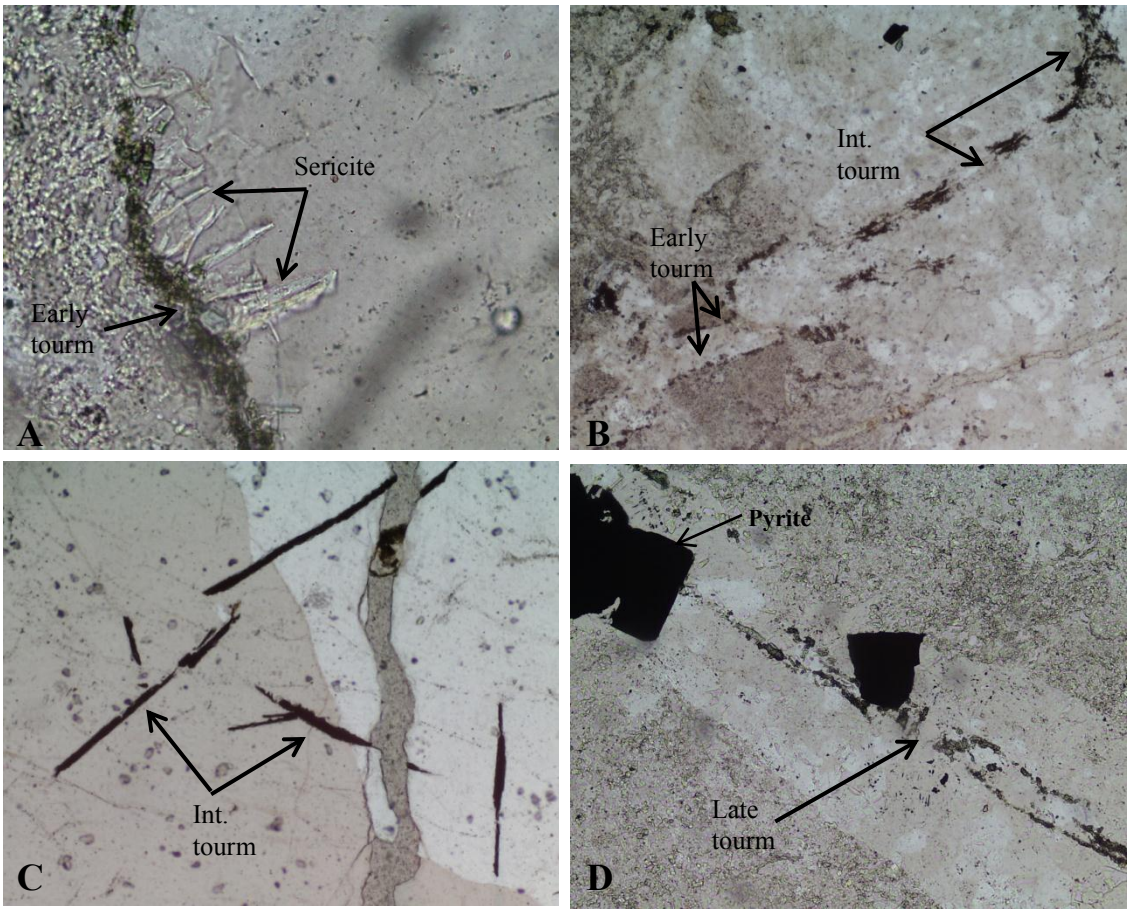

Figure 44: Photomicrographs illustrating tourmaline occurrences in quartz-carbonate-tourmaline veins: A. Early lineated to acicular tourmaline lining vein walls, and intermediate-stage tourmaline intergrown with early to late quartz. 5x, plane light. FOV=1.70mm; B. Early tourmaline in "feeder vein" injecting quartz and tourmaline into the larger vein. Intermediate-stage tourmaline in the larger vein forms between quartz phases. 5x, plane light. FOV=1.70mm; C. Intermediate-stage, strongly altered tourmaline intergrown with coarse-grained quartz. Quartz vein is crosscut by a late carbonate vein. 10x, plane light. FOV=0.85mm; D. Late tourmaline in a granular gray quartz-carbonate-pyrite vein near its intersection with a granular gray quartz-carbonate-tourmaline-(pyrite-sphalerite-galena) vein. 5x, crossed nicols. FOV=1.70mm.

they are minor (Fig. 42). In addition, minor early or late sericite or late chalcedony may be present. Early sericite occurs as fine, discrete crystals growing outward from vein walls. Later sericite, with or without chalcedony, may be present in fractures around quartz grains or intergrown with carbonate.

Quartz-carbonate ± pyrite veins are crosscut by several generations of tourmaline-bearing veins (Figs. 37-38; stage 6). Earliest tourmaline-bearing gray quartz veins are composed of granular quartz with or without carbonate, pyrite or sericite, and late tourmaline either intergrown with late quartz phases or as lineated crystals that crosscut quartz (Fig. 44d). In many cases, the earliest tourmaline-bearing veins are stage 3 or stage 5 gray quartz ± carbonate, sericite or pyrite veins with late tourmaline introduced at intersections with other tourmaline-bearing veins or within fractures crosscutting quartz (Fig. 44b and 44d). Late tourmaline may also be present in crack-seal veins, where it occurs in in open spaces between quartz grains or in reopened fractures with granular quartz.

Granular quartz-late tourmaline veins are crosscut by quartz veins with early tourmaline (Fig. 44a). Early tourmaline occurs as either lineated, vein-lining masses composed of very fine euhedral to granular crystals or as fine to relatively coarse-grained discrete euhedral crystals that grow outward from vein walls. It is commonly intergrown with early, fine- to medium-grained granular to subhedral quartz or early sericite. Late, interstitial carbonate is common, though it is not always present. Fine- to coarse-grained subhedral to euhedral pyrite may or may not be present.

In many early tourmaline-bearing veins, tourmaline formation continued throughout the development of the vein. Intermediate-stage tourmaline most commonly

Figure 45: Photograph of a granular white quartz-tourmaline vein crosscutting the Agglomerate unit. An adjacent greenstone clast is altered to a QSP-carbonate assemblage. Groundmass (black) is tourmalinized. Sample is 2.5 inches in diameter.

occurs as discrete, fine- to coarse-grained euhedral crystals intergrown with early to late quartz (Fig. 44c). It may also occur as fine, lineated euhedral to granular crystals that precipitate between quartz phases. Quartz veins with intermediate tourmaline are mineralogically similar to other tourmaline-bearing vein types. They may contain late interstitial carbonate or pyrite, or early to late sericite.

Stages 7-8

Gray quartz veins are crosscut by a series of white granular quartz veins (Figs. 37-38; stages 7-8). White quartz veins range in width from 2mm to 40mm. They are present in all host rocks and are more common than gray quartz veins at shallow depths. The earliest of the white quartz vein stages consists of white and white to gray granular quartz-tourmaline veins with or without carbonate, pyrite, or sericite (Fig. 45; stage 7).

Figure 46: Photograph of a white quartz vein crosscutting a series of parallel, branching gray quartz-pyrite-tourmaline veins in a core intercept of the Feldspar Porphyry.

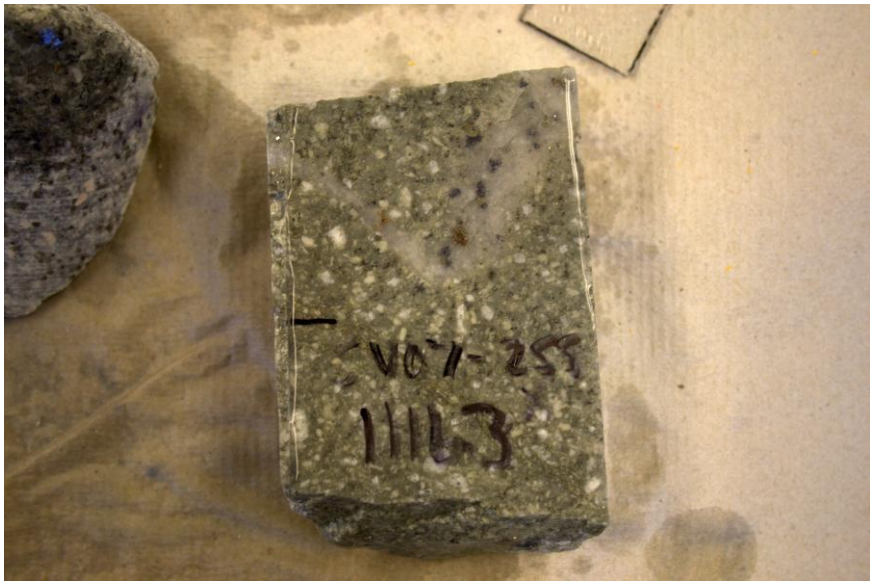

Figure 47: Photograph of a late granular white quartz-carbonate-pyrite-sphalerite-galena vein in QSP-carbonate altered Feldspar Porphyry. Core sample is 2.5 inches in diameter

This is interpreted as a continuation of the earlier gray quartz-tourmaline phase, and thus white quartz-tourmaline veins are likely earliest. White to gray quartz- tourmaline veins may also contain early to late sericite, intermediate to late pyrite or late interstitial carbonate.

They are crosscut by white quartz-carbonate veins with or without sericite, pyrite or late-stage sphalerite, galena, tetrahedrite or chalcopyrite (Figs. 37-38 and 46-47; stage 8). Latest stage 8 white quartz veins are typically thicker, more continuous and may contain relatively abundant sphalerite and galena. They may be over two feet in length and commonly taper to 2-4mm.

Carbonate composition

Both calcite and Fe-bearing calcite are present in ore-stage quartz veins. Fe-bearing calcite is the most common and volumetrically abundant. Its occurrence is not associated with a particular vein stage, and it has been identified in stage 3 through stage 8 quartz veins. It is also present in selvages of both calcite-dominant and Fe-bearing calcite-dominant veins, and in intermediate to distal alteration zones. Fe-calcite is typically granular to massive, and bladed phases have not been identified.

Calcite has similarly been identified all ore-stage quartz veins, though it is far less abundant and most commonly associated with stages 5-8. Where present with Fe-calcite, it is paragenetically late. Calcite is most commonly granular to massive, though in sample 248C-1043.1, calcite is bladed.

Composite veins

Composite veins, consisting of both elongate-blocky and granular quartz, occur throughout the resource area. In the majority of composite vein samples, elongate-blocky quartz formed prior to granular quartz. Latest very fine- to fine-grained granular quartz may replace elongate-blocky quartz along grain boundaries. In some composite vein samples, earlier fine- to medium-grained quartz lines vein walls and elongate-blocky quartz fills interstices. Such veins are interpreted as early granular quartz veins (stage 2 or 3) that reopened during crack-seal vein forming processes.

Post-ore carbonate veins

Ore-stage veins are crosscut by narrow, discontinuous calcite veins of unknown origin. They are most common in the Agglomerate unit and the Limerick Formation, though they were also observed in the Welded Tuff and Feldspar Porphyry. In the Rochester Formation, carbonate veins are 2mm to 5mm in width and have irregular, though typically matching, vein walls. In the agglomerate, they are typically irregular, with matching vein walls Carbonate veins become more irregular at depth, occurring in the Limerick Formation as irregular, branching and discontinuous “sweat-outs.” Post-ore carbonate veins may be genetically related to post-ore, hematite-stained calcite-matrix breccias common in the Agglomerate and Feldspar Porphyry.

Table 2: Summary of vein types and characteristics

Stage	Vein type	Quartz form	Th	Gangue mineralogy	Ore mineralogy	Comments
1	Ataxial	Fibrous	--	Quartz, rarely contains late, ore-stage carbonate	None	Pre-ore; associated with moderate to strongly pervasive silicification
2	Early granular quartz-tourmaline	Granular		Quartz, tourmaline and carbonate	?	Rare; tourmaline occurs in selvages
3	Early gray quartz	Granular	290-310°C	Quartz ± sericite-early tourmaline-late carbonate	May contain late sphalerite and galena; typically not associated with gold mineralization.	
3	Early crack-seal	Elongate-blocky	--	Quartz ± late carbonate-rare, late tourmaline	May contain late base metal sulfides, though not typically associated with mineralization	May be crosscut by early granular quartz veins, which suggests a cyclical relationship between crack-seal and granular quartz precipitation.
4	Crack-seal	Elongate-blocky	280-300°C	Quartz ± late carbonate-rare late tourmaline	Commonly contain sphalerite, galena and gold mineralization along margins opposite quartz growth.	White to gray; contain parallel inclusion bands
5	Gray granular quartz	Granular to subhedral; late euhedral.	270-290°C	Quartz-carbonate ± early sericite-late carbonate	Commonly contain pyrite; may contain sphalerite and galena, particularly where temporally associated with later base metal veins; may host late gold mineralization	Clear to slightly cloudy gray

Stage	Vein type	Quartz form	Th	Gangue mineralogy	Ore mineralogy	Comments
6	Gray quartz-tourmaline	Granular to subhedral; late euhedral in vugs.	280-300°C	Quartz-carbonate-early to late tourmaline ± early sericite	Commonly associated with gold mineralization may contain late base metal sulfides or early to late pyrite.	
7	White quartz-tourmaline	Granular to subhedral; late euhedral in vugs	270-290°C	Quartz-carbonate-early to late tourmaline ± early sericite	Commonly associated with gold mineralization; may contain late base metal sulfides or early to late py rite.	Continuation of earlier gray quartz-tourmaline vein stage; primary difference is milky white to graying white quartz with increased fluid inclusion abundance.
8	White quartz-carbonate ± base metal sulfides	Granular to subhedral; late euhedral in vugs.	280-300°C	Quartz-carbonate-early sericite	Record introduction of base metal sulfides sphalerite, galena, chalcopyrite, tetrahedrite and arsenopyrite. Sulfides may occur in early veins, most commonly where proximal to white quartz-carbonate-sulfide vein zones; gold mineralization is strongly associated with base metal sulfides.	High fluid inclusion abundance,

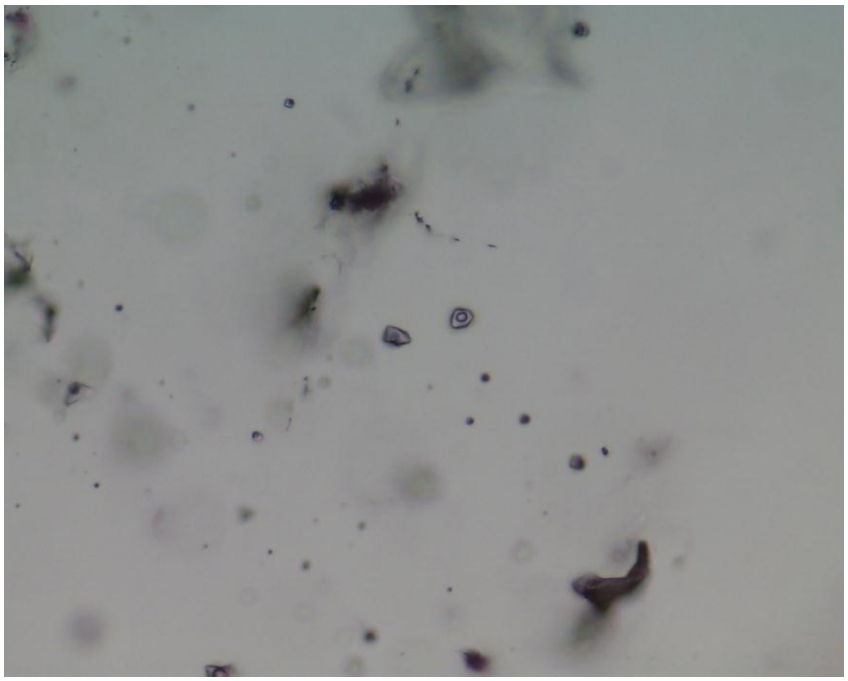

Figure 48: Photomicrograph of L_{H20} -V_{CO_2} fluid inclusions in a granular quartz grain in a white to gray quartz-tourmaline-pyrite-carbonate vein. 40x, plane light. FOV = 0.21mm.

Fluid Inclusion Analysis

Homogenization temperatures of 129 fluid inclusions from seven ore stage vein types were analyzed (Table 4; Fig. 50). Analyses were conducted on a modified USGS gas-flow ceramic heating and cooling stage. The purpose of the study was to determine if mineralogical changes between vein types were accompanied by significant changes in temperature and to establish the minimum temperature of formation of the system. Pre-ore ataxial and earliest tourmaline-bearing veins did not contain sufficient fluid inclusions and were omitted from analyses.

All inclusions were hosted within vein quartz. No freezing runs were conducted, though basic fluid inclusion petrography identified predominant liquid-dominant, L_{H2O}-V_{CO2} inclusions and lesser liquid-dominant, L_{H2O}- L_{CO2}-V_{CO2} inclusions (Figs. 48-49).

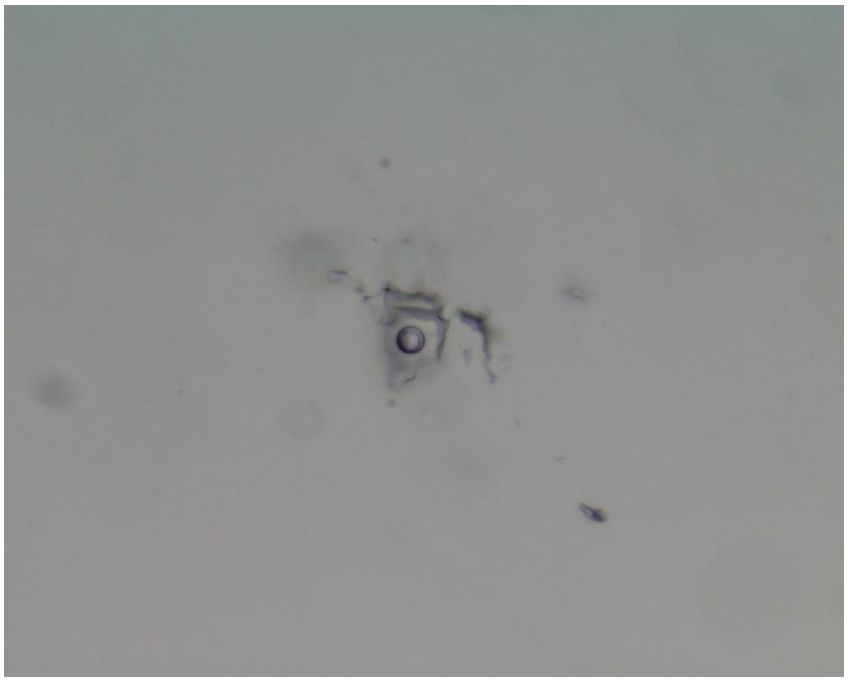

Figure 49: Photomicrograph of an irregular L_{H20}-L_{CO2}-V_{CO2} fluid inclusion in a subhedral quartz grain in a white to gray quartz-carbonate-tourmaline-pyrite vein the Feldspar Porphyry. 40x, plane light. FOV= 0.21mm.

L_{H2O}-V_{H2O} inclusions with a distinct and well defined meniscus may also be present, though confirmation of their composition would require further analyses. Regardless of composition, fluid inclusions typically ranged in size from 10µ to 50µ and were composed of 10% to 20% vapor. Liquid/vapor ratios throughout all samples were not generally widely variable, though rare vapor-dominant inclusions were present. All three fluid inclusion types are present in analyzed vein types, and homogenization temperatures of all inclusion types were comparable.

In all, six samples containing seven vein types were analyzed. All were from reasonable comparable depths in the Feldspar Porphyry, with the exception of sample 2OM-3, which was from the Agglomerate unit and contained a granular white quartz-

base metal vein. No notable differences in homogenization temperatures of fluid inclusions from the seven vein types were observed. Subtle changes were present, though such differences may be rectified by a larger sample size. The homogenization temperatures of fluid inclusions in analyzed veins ranged from approximately 210°C to 340°C, though the majority homogenized between ~260°C and ~320°C.

It should be noted that these values reflect the minimum temperature of formation, and a pressure correction would be necessary to ascertain the true temperature of formation. Lithostatic pressure at the time of vein formation can be reasonably estimated based on vein textures, gangue mineralogy, and comparison to similar systems. Vein textures and the brittle nature of vein opening, coupled with alteration products such as sericite and carbonate, suggest that Spring Valley formed within the lower range of mesothermal depths, between 5km and 10km and at corresponding pressures between approximately 1.5 kbar and 2.5 kbar (Goldfarb et al., 2005). This is further substantiated through geologic reconstruction that indicates that the basal Feldspar Porphyry was likely covered by at least 19,000 feet of material at the time of mineralization, 5-6 km with corresponding pressure of 1.2-1.5 kbar, in addition to the overburden of the Luning-Fencemaker allochthon (Johnson, 1977). Further, the absence of daughter products in fluid inclusions and the composition of fluids in similar systems suggest that fluids were likely low salinity, between 1-5 wt.% NaCl (Goldfarb et al., 2005). Thus, a pressure correction applied to low salinity L_{H2O}-V_{CO2} fluid inclusions could range from approximately 120°C to 180°C, and trapping temperatures would generally range from 330°C to 520°C (Potter, 1977).

Fluctuations in pressure likely controlled the transition from crack-seal to granular quartz vein formation, and pressure corrections may not be equally applicable to granular and crack-seal veins. Similarities in gangue and alteration mineralogy suggest that both likely formed at depths between 5 km and 10 km and that pressure fluctuations may have been negligible. Regardless, granular veins likely formed at lower pressures and would thus require a lower pressure correction than rack-seal veins.

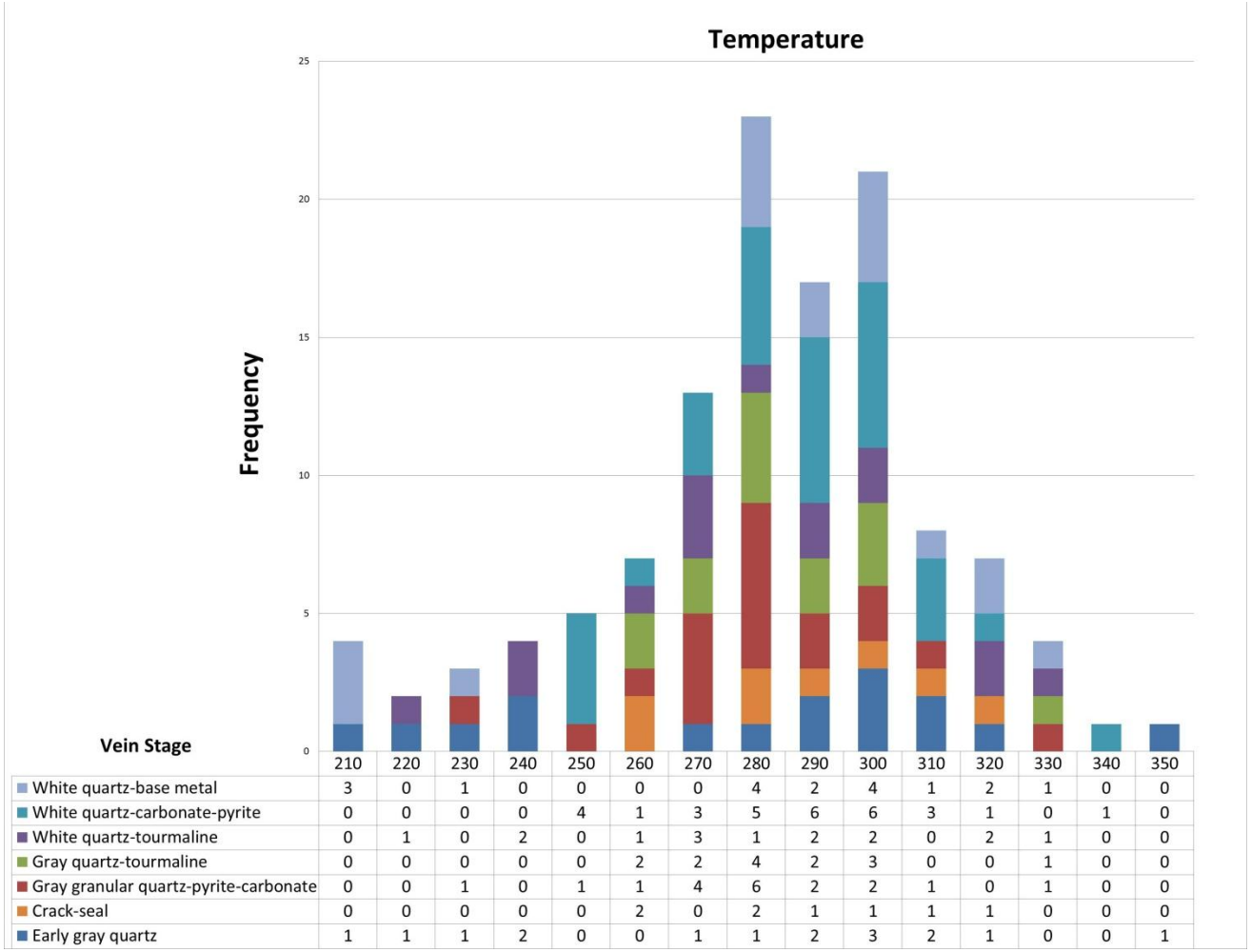

Vein Stage	210	220	230	240	250	260	270	280	290	300	310	320	330	340	350
White quartz-base metal	3	0	1	0	0	0	0	4	2	4	1	2	1	0	0
White quartz-carbonate-pyrite	0	0	0	0	4	1	3	5	6	6	3	1	0	1	0
White quartz-tourmaline	0	1	0	2	0	1	3	1	2	2	0	2	1	0	0
Gray quartz-tourmaline	0	0	0	0	0	2	2	4	2	3	0	0	1	0	0
Gray granular quartz-pyrite-carbonate	0	0	1	0	1	1	4	6	2	2	1	0	1	0	0
Crack-seal	0	0	0	0	0	2	0	2	1	1	1	1	0	0	0
Early gray quartz	1	1	1	2	0	0	1	1	2	3	2	1	0	0	1

Figure 50: Histogram showing the frequency of homogenization temperatures by vein type. Fluid inclusions generally homogenized between 260-320°C.

Table 3: Descriptions and locations of samples selected for fluid inclusion analyses

Sample No.	Location	Vein Stage	Vein Types	Th
2OM-001	SV07-255C 1120.5'	4	Crack-seal quartz	260°C to 320°C
2OM-002	SV07-397C 979.3'	3	Early gray quartz	210°C to 350°C
		5	Gray granular quartz-carbonate-pyrite	240°C to 330°C
2OM-003	SV07-255C 721.5'	8	White quartz-carbonate-pyrite-sphalerite-galena	200°C to 330°C
2OM-004	SV07-397C 977.9'	6	Gray quartz-tourmaline-pyrite-(sphalerite-galena)	260°C to 330°C
2OM-005	SV07-290C 849.1'	8	White quartz-carbonate-pyrite	250°C to 320°C
2OM-006	SV07-248C 1057.3'	3	Early gray quartz	220°C to 320°C
		7	White quartz-carbonate-tourmaline	250°C to 325°C
		8	White quartz-carbonate	250°C to 310°C

Gold and Base Metal Mineralization

Gold and base metal mineralization at Spring Valley occurs in four, NS-trending lobes that are oblique to principal vein orientations, but are parallel to subparallel to NNE-trending structures and the Spring Valley anticline (Neal and LeLacheur, 2010). Mineralization can occur in all ore-stage vein types and in all units of the Limerick and Rochester formations. It is most commonly associated with late, granular quartz veins, though it can occur in elongate-blocky veins. The Feldspar Porphyry is the most favorable host, followed by the Welded Tuff and Agglomerate. The Limerick Formation and the Quartz-eye Rhyolite are generally poor hosts, though local ore-grade intervals have been intercepted.

Relatively coarse, free gold occurs in quartz veins either filling fractures between quartz grains (Fig. 53a) or replacing earlier pyrite, sphalerite or galena (Fig. 53b). It may also occur disseminated throughout adjoining selvages, typically associated with wallrock pyrite (Ross, 2006), or along fracture surfaces (LeLacheur et al., 2011). Mineralization occurs in four NNE-trending lobes that are oblique to principal vein orientations but roughly parallel the Black Ridge fault system (Neal and LeLacheur, 2010). It is not clear at present what controls this distribution. Paragenetic relationships between gold and base metal sulfides and vein associations suggest that gold was introduced in three punctuated phases: the first during gray to white quartz-tourmaline vein formation; the second during white quartz-tourmaline vein formation; and the third during white quartz-pyrite-sphalerite-galena vein formation (Fig. 51). However, it is possible that gold was

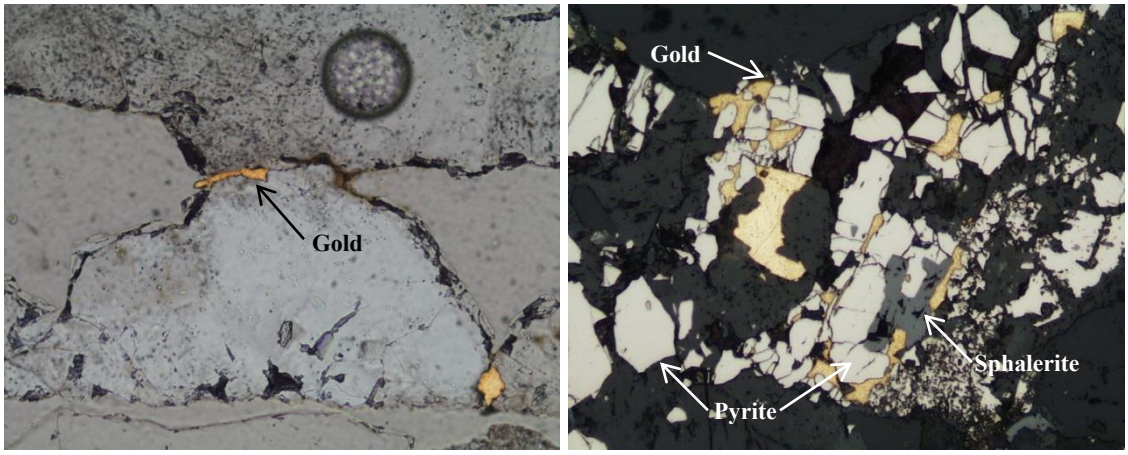

Figure 51: Reflected light photomicrographs illustrating gold occurrences. A. Gold forming in fracture between quartz grains in a white granular quartz-carbonate vein. 10x, plane light. FOV=0.85mm. B. Gold replacing pyrite along fractures and rimming sphalerite. Mineralization is hosted with a white crack-seal vein, and pyrite was fractured during the crack-seal process. 10x, reflected plane light FOV=0.85mm.

introduced during a single, continuous phase and that it was redistributed during subsequent uplift and shearing (Goldfarb et al., 2005).

Euhedral, cubic to dodecahedral pyrite is the most common sulfide at Spring Valley. It occurs in QSP-altered wallrock, though it typically only constitutes 0.5-2% of the total volume. In veins, pyrite is fine- to medium-grained and most commonly euhedral to subhedral, though anhedral pyrite does locally occur interstitial to quartz grains. Euhedral to subhedral pyrite is common in granular quartz veins, while subhedral pyrite is more common in elongate-blocky quartz veins. Euhedral to subhedral pyrite typically predates carbonate and may form syn- or post-quartz (Fig. 52). Anhedral pyrite post-dates quartz, though its temporal relationship with late carbonate could not be definitively established (Fig. 52).

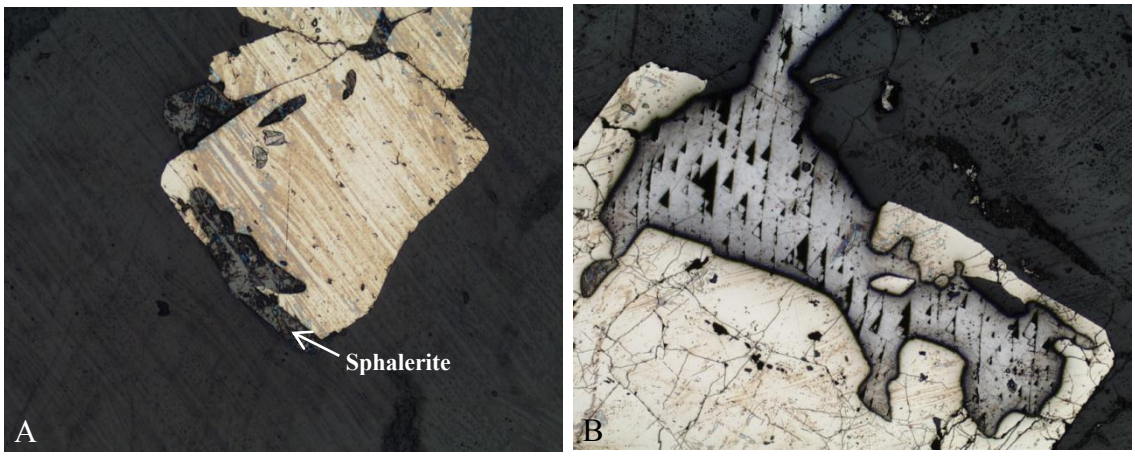

Figure 52: Reflected light photomicrographs of sulfide relationships; A. Sphalerite replacing subhedral pyrite. 5x, plane reflected light. FOV=1.70mm; B. Anhedral galena replacing cubic pyrite along grain boundary. 5x, plane reflected light. FOV=1.70mm.

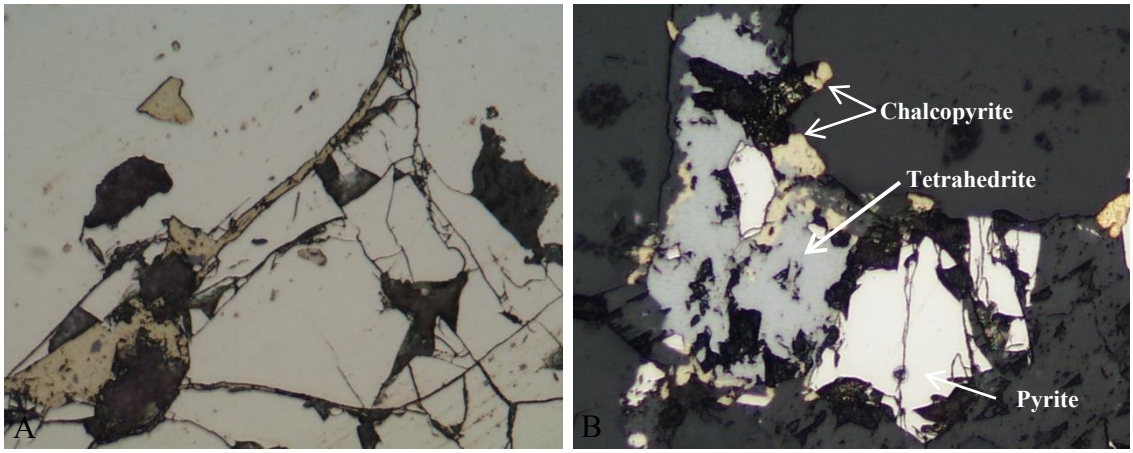

Figure 53: Reflected light photomicrographs of chalcopyrite relationships. A. Chalcopyrite filling fractures within a pyrite grain. 20x, reflected plane light. FOV=0.43mm; B. Late tetrahedrite and chalcopyrite replacing fractured pyrite grains. Chalcopyrite replaces tetrahedrite along grain boundaries. Pyrite was fractured during the crack-seal vein forming process. 20x, reflected plane light. FOV=0.43mm

Base metal sulfides galena, sphalerite, chalcopyrite and tetrahedrite almost exclusively occur within quartz veins and are uncommon relative to pyrite. They are typically associated with white granular quartz veins, but may occur in earlier veins, particularly where adjacent to later base metal veins. They typically comprise between 5% and 25% of the total vein volume and are always late, commonly occurring as anhedral growths on earlier subhedral to euhedral pyrite (Figs. 52 and 54a-b). Where visible gold is present with base metal sulfides, it is always paragenetically late (Fig. 52).

With the exception of pyrite, sphalerite and galena are the most common base metal sulfides present at Spring Valley. They are medium- to coarse-grained and typically occur in association with each other, though no definitive cross-cutting relationships were observed. They may occur with or without pyrite. Where they occur with pyrite, they are paragenetically late, commonly replacing pyrite along grain boundaries or fracture surfaces. Where present in crack-seal veins, sphalerite and galena are not deformed nor fractured, which suggests that they were precipitated following the cessation of crack-seal vein-forming processes. They also most commonly occur adjacent to margins in crack-seal veins where open space inherent of the crack-seal process would likely be present.

Chalcopyrite is associated with sphalerite or pyrite, though it is typically too fine to be seen in hand sample. Very fine-grained, anhedral chalcopyrite occurs as "chalcopyrite disease" in sphalerite and rimming or replacing pyrite, sphalerite, galena or tetrahedrite along fracture surfaces (Fig. 54a-b). Tetrahedrite is rare and was only observed in veins where sulfides constitute 20-40% of the vein. It is commonly associated with later chalcopyrite and is paragenetically later than pyrite (Fig. 54b),

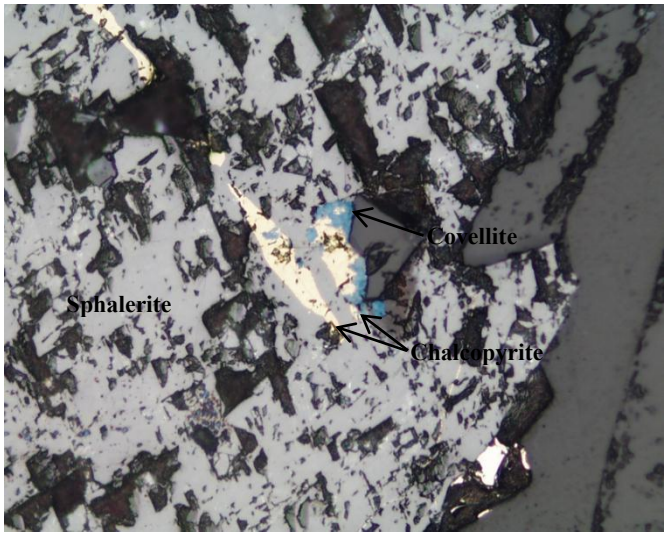

Figure 54: Reflected light photomicrograph of supergene covellite replacing chalcopyrite in a strongly oxidized white quartz-carbonate-base metal vein. Chalcopyrite occurs as "chalcopyrite disease" within a sphalerite grain. FOV=0.43mm

though its relationship to sphalerite and galena are unknown. Minor, anhedral arsenopyrite occurs locally after pyrite.

Highly fractured pyrite occurs locally in crack-seal veins. In sample 1UP-045, early, highly fractured and fragmented to moderately fractured subhedral pyrite is present in a composite crack-seal quartz vein within the Limerick Formation (Fig. 53b; Fig. 54a-b). Sphalerite, chalcopyrite and native gold fill fractures within pyrite and replace pyrite along fracture surfaces (Fig. 53b). Minor granular tetrahedrite locally crosscuts pyrite and is partially replaced by chalcopyrite (Fig. 54b). Sphalerite and galena are not deformed or fractured, which suggests that they post-date crack-seal vein formation and were precipitated in voids between quartz grains.

Late supergene weathering produced hematite and limonite, consisting of goethite and minor jarosite, after pyrite. Rare covellite and chrysocolla occur after chalcopyrite

(Fig. 55). Limonite distribution is structurally controlled and is most pervasive in the Quartz-eye Rhyolite and Agglomerate units, where it occurs after Fe-bearing carbonate. In highly fractured areas, oxidation may extend into the Feldspar Porphyry or Limerick Formation.

The Spring Valley deposit is unique in the Humboldt Range. Gold mineralization is characterized by the lack of a geochemical signature, with arsenic, lead and zinc only slightly elevated over base values (Neal and LeLacheur, 2010). In addition, sulfide mineralogy is much simpler than the nearby Bonanza King and Rochester deposits, with only pyrite, sphalerite and galena occurring consistently throughout. Spring Valley also hosts virtually no silver and only trace local copper mineralization.

Discussion

Ore mineralogy, alteration mineralogy and zoning, and vein textures defined in this study preclude classification of Spring Valley as a porphyry gold system. First, gold mineralization in porphyry systems is typically associated with pyrite and abundant copper sulfides, specifically chalcopyrite and bornite, while gold mineralization at Spring Valley is primarily associated only with pyrite and less commonly, sphalerite, galena and/or trace chalcopyrite. Secondly, alteration in porphyry gold systems is zoned outward from a central potassic assemblage characterized by K-feldspar, biotite and magnetite to a deuteric sericite ± chlorite ± pyrite event that may or may not be present. Paragenesis of alteration events are clearly recorded by changes in selvage and vein-filling assemblages for cross-cutting vein events. No evidence for an early potassic alteration event was found at Spring Valley, and alteration associated with different vein stages is remarkably consistent.

Vein textures at Spring Valley are also inconsistent with a porphyry gold interpretation as they present clear evidence that mineralization occurred at significant depths and pressures, well out of the 1-3 km range of most porphyry systems. This is further corroborated by the presence of liquid CO_2 in fluid inclusions that suggest they formed at relatively high pressure. Finally, the lack of high-salinity fluid inclusions indicates that mineralization did not form from the unmixed vapor and high-salinity brines that are characteristic of porphyry systems.

Mineralization, hydrothermal alteration and vein textures and mineralogy are consistent with the classification of orogenic gold deposits outlined by Groves et al. (1998), Groves et al. (2003), and Goldfarb et al. (2005) (Table 4). In addition to these characteristics, discussed in detail in the following section, several other key features are consistent with an orogenic classification. First, mineralization is hosted within greenschist-facies metavolcanic and metavolcaniclastic units. The relationship between orogenic gold deposits and greenschist-facies hosts has been well documented, though the implications of this observed association are not entirely understood (Goldfarb et al., 2005). Goldfarb et al. (2005) theorize that the volume of fluid released during the greenschist or amphibolite transition, the decreasing solubility of gold at greenschist temperatures, and the favorable brittle-ductile structural regime that overlies the greenschist transition zone all play an important role in developing orogenic systems in greenschist-facies host rocks.

Second, mineralization and alteration at Spring Valley post-dates greenschist-facies metamorphism. Sericite-carbonate-pyrite alteration in the Limerick Formation is clearly retrograde relative to greenschist-facies chlorite-carbonate assemblage. The same is likely true of the Rochester Formation, though the temporal relationship is obscured by similarities between hydrothermal and greenschist-facies alteration. Ore-stage crack-seal and granular quartz veins have well defined vein walls and formed under more brittle conditions than pre-ore ataxial veins. Late-stage sulfides sphalerite and galena show no

Table 4: Comparison of important characteristics of the Spring Valley deposit with other gold deposit styles.

	Spring Valley	Orogenic Gold [1]	Porphyry Gold [2,3]
Tectonic Setting	Mineralization occurs inboard of the Luning-Fencemaker allochthon in a greenschist-facies metamorphic belt. Age of mineralization is unknown, but likely post-dates emplacement and associated greenschist-facies metamorphism.	Second- and third-order structures adjacent to major crustal structures. Commonly form in low-grade metamorhpic belts in transpressional and compressional zones near major crustal boundaries.	Inboard of continental or island arc subduction zones. [2]
Host Rocks	Greenschist-facies metavolcanic and metavolcaniclastic units of the Koipato Group .	Commonly hosted in greenschist-facies metamorphic terranes	Quartz diorite to diorite intrusions[2] Some andesitic to dacitic (e.g., Maricunga Belt, northern Chile) [3]
Mineralization Style	Discontinuous, tabular veins and local stockworks and disseminations. Veins are likely extensional.	Most commonly in brittle-ductile to ductile shear and fault-fill veins, with lesser brittle extensional and stockwork veins and disseminations.	Stockworks[2]
Mineralization	Coarse, free gold associated with base metal sulfides pyrite, sphalerite and galena. Trace chalcopyrite and tetrahedrite	Pyrite/arsenopyrite/pyrrhotite-loellingite Base metal sulfides, such as sphalerite, galena, and rarely, molybdenite. Au-bearing tellurides and bismuthinides may be present in granitoid hosts.	Gold, pyrite, chacopyrite, bornite[3]
Alteration	Proximal QSP-carbonate ± tourmaline alteration, grading outward into quartz-hematite and/or quartz specularite alteration. Plagioclase is albite in composition, though the original composition of plagioclase and	Alteration in relatively shallow (5-10 km) deposits consists of carbonate phases of varying composition, alkali metasomatism that produces sericite, or less commonly K-feldspar or albite, and pyrite, pyrrhotite, arsenopyrite	Potassic alteration consisting of K-feldspar, biotite and/or oligoclase, with magnetite is common in the center of the intrusion. [2] In the Refugio District, gold mineralization is associated with chlorite, magnetite and al-

	the timing of albitization are unknown.	or oxidized Fe-bearing phases hematite or magnetite.	bite-bearing assemblages. Local QSP alteration associated with D-type veins may be present. [3] Hypogene intermediate argillic alteration is common. [2]
Gangue mineralogy	Quartz, carbonate and sericite predominate, with lesser tourmaline, and/or hematite/ specularite.	In shallow, felsic hosts: quartz, sericite, albite, chlorite, or tourmaline. Magnetite, hematite and anhydrite may be present.	Quartz, sericite, K-feldspar, biotite, magnetite[3]
Quartz textures	Non-directional, granular (bull) quartz; Elongate-blocky quartz formed by crack-seal processes.	Non-directional, granular (bull) quartz; Fibrous quartz in displacement-controlled syntaxial, ataxial and antitaxial veins. Elongate-blocky quartz formed by crack-seal processes.	Non-directional, granular quartz veins; saccaroidal quartz veins; comb-textured quartz at high levels. [3]

Table 5, cont'd:

	Spring Valley	**Low sulfidation epithermal [4]**	**High sulfidation epithermal [4]**
Tectonic Setting	Mineralization occurs inboard of the Luning-Fencemaker allochthon in a greenschist-facies metamorphic belt. Age of mineralization is unknown, but likely post-dates emplacement and associated greenschist-facies metamorphism.	Magmatic arc undergoing extension, leading to possible rifting	Magmatic arc undergoing weak extension; Rarely under compressional stress
Host Rocks	Greenschist-facies metavolcanic and meta-volcaniclastic units of the Koipato Group.	Commonly hosted in felsic and basaltic volcanics, but may also occur in sedimentary rocks.	Commonly in andesitic to dacitic volcanic Rocks

Mineralization Style	Discontinuous, tabular veins and local stockworks and disseminations. Veins are likely extensional.	Veins and disseminations	Stockwork veins, disseminations, veins and breccias.
Mineralization	Coarse, free gold associated with base metal sulfides pyrite, sphalerite and galena. Trace chalcopyrite and tetrahedrite	Gold associated with arsenopyrite, pyrite and/or pyrrhotite; base metal sulfides occur at depth. High level As, Sb and Hg-bearing minerals.	Gold associated with pyrite, enargite, covellite, digenite Orpiment and realgar may be present at shallow depths.
Alteration	Proximal QSP-carbonate ± tourmaline alteration, grading outward into quartz-hematite and/or quartz specularite alteration. Plagioclase is albite in composition, though the original composition of plagioclase and the timing of albitization are unknown.	Quartz-calcite-adularia-illite/sericite; Argillic alteration minerals such as kaolinite and smectite may be present outboard of the quartz-calcite-adularia zone. Advanced argillic alteration formed by condensation of acidic vapor may occur in the vadose zone.	Advanced argillic assemblage consisting of alunite, dickite, smectite, pyrophyllite and zunyite.
Gangue mineralogy	Quartz, carbonate and sericite predominate, with lesser tourmaline, and/or hematite/ specularite.	Quartz, calcite, adularia, illite/sericite, smectite, kaolinite.	Quartz, alunite, dickite, smectite, pyrophyllite, zunyite
Quartz textures	Non-directional, granular (bull) quartz; Elongate-blocky quartz formed by crack-seal processes.	Banded quartz-chalcedony veins; comb-textured quartz	Vuggy quartz Comb-textured euhedral quartz

[1]: Goldfarb et al., 2005; [2]: Sillitoe, 2008; [3]: Muntean and Einaudi, 2000; [4]: Simmons et al., 2005

deformation, and fracturing in earlier pyrite is clearly related to crack-seal vein opening. Further, granular quartz grains show only incipient, local recrystallization and minor, local subgrain rotation. Though more pronounced, recrystallization of elongate-blocky quartz in crack-seal veins is likewise only local. Recrystallization in all vein types is more likely related to uplift of the deposit rather than continued metamorphism (Goldfarb, 2005).

The retrograde nature of mineralization and alteration in orogenic deposits in greenstone belts is well known. Deposits tend to form during the later stages of an orogeny and typically post-date widespread metamorphism. As metamorphism and fluid evolution continue at greater depths, fluids flow into brittle-ductile structural regimes of already retrograde host rocks, where temperature and pressure are conducive to phase separation and gold precipitation (Goldfarb et al., 2005).

Discussion of Metamorphic Vein Textures

Ataxial, crack-seal and non-directional quartz vein textures identified at Spring Valley are likely metamorphic in origin. Metamorphic quartz veins can generally be classified as displacement-controlled, face-controlled or non-directional based on the growth mechanism and timing relative to vein opening, and grain texture and morphology (Fisher and Brantley, 1992; Vearncombe, 1993; Barker, 1998). Quartz—or other vein-filling minerals—in displacement-controlled veins precipitates as the vein or fracture opens (Fisher and Brantley, 1992; Barker, 1998). As a result, quartz grains do not compete for open space, and growth rates are isotropic (Fisher and Brantley, 1992).

Quartz grains are feathery to fibrous and elongated, with relatively constant width across the vein (Fisher and Brantley, 1992; Barker, 1998).

Displacement-controlled veins form under very specific conditions. First, fluid within the vein must retain sufficient pressure to keep the vein walls apart (Cox et al., 1986). Second, the rate of mineral growth must not exceed the rate of vein separation (Cox et al., 1986). If these conditions are not met, precipitating minerals may seal the vein (Cox et al., 1986). Third, fluids must be saturated in the precipitating mineral species throughout vein formation, or vein opening rates may exceed mineral growth rates and open space will be created (Cox et al., 1986).

Three types of displacement-controlled veins have been recognized (Fisher and Brantley, 1992; Vearncombe, 1993; Barker, 1998). Syntaxial veins form by growth that proceeds inward from both sides of a median plane, typically a fracture (Barker, 1998). Thus, the youngest phase is found at the center of the vein (Barker, 1998). Mineralogy of syntaxial veins is usually very similar to that of the wallrock, as significant overgrowth and incorporation of wallrock components may occur (Fisher and Brantley, 1992; Barker, 1998). When syntaxial veins are subjected to shear, it is accommodated near the center of the vein (Barker, 1998). As a result, feathery growths near margins are oriented perpendicular to the vein wall (Barker, 1998).

Antitaxial veins grow outward from the median plane towards the vein walls (Barker, 1998). Thus, youngest phases occur adjacent to the margins, and quartz grains show crystallographic continuity across the vein (Barker, 1988). Strain is accommodated near vein margins, and in veins that have been subjected to shear, quartz grains are

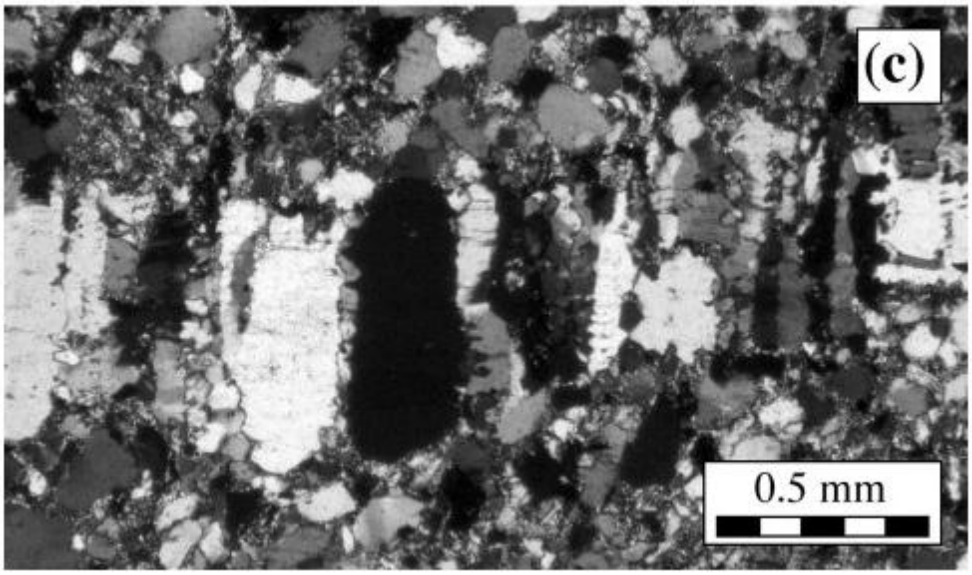

Figure 55: Photomicrograph of an Ataxial metamorphic quartz vein with fibrous to elongate quartz grains from Bons (2001). Note serrated grain boundaries.

oriented oblique to margins (Barker, 1998). Vein fill is not locally derived, and thus mineralogy of antitaxial veins is different from that of the wallrock (Barker, 1988).

Ataxial or stretching veins differ from syntaxial and antitaxial in that quartz growth propagates from multiple surfaces throughout vein formation rather than from vein margins or a single medial line (Passchier and Trouw, 1996; Bons, 2001). This occurs when small fractures open within the vein or the adjacent wallrock as the vein forms. Ataxial vein formation produces quartz grains with relatively constant widths, but with irregular, serrated grain boundaries (Fig. 30) (Passchier and Trouw, 1996). Similarly to syntaxial veins, wallrock material is commonly stretched and incorporated into the vein (Passchier and Trouw, 1996). Ataxial veins reflect increased brittle deformation relative to antitaxial and syntaxial veins. Pre-ore veins at Spring Valley were identified as

ataxial veins based primarily on the presence of fibrous quartz with serrated grain boundaries and the incorporation of wallrock material into the vein.

A second type of metamorphic quartz vein occurs at Spring Valley and forms by crack-seal mechanisms (Ramsay, 1980). Face-controlled crack-seal veins are brittle/ductile features that are common in low-grade metamorphic belts. They form at relatively high pressure at mesothermal depths where large open space cannot be supported, and even the smallest fractures are only supported when fluid pressure exceeds lithostatic pressure (Ramsay, 1980; Vearncombe, 1993). Therefore, vein growth is an incremental process, occurring on a small scale relative to the final width of the vein (Ramsay, 1980). The crack-seal process is initiated by fault rupture as fluid pressure approaches lithostatic pressure (Ramsay, 1980). Fluid flow is enhanced by newly-formed fractures, which seal as minerals precipitate (Ramsay, 1980). Fluid pressure again increases until it approaches lithostatic pressure, rupture occurs, and veins are cracked open (Ramsay, 1980). Quartz growth recommences in the newly opened space, and the cycle continues (Ramsay, 1980).

The crack-seal mechanism and associated anisotropic growth rate forms very distinctive textures and vein morphologies. Anisotropic growth produces serrated or radiator-fin grain boundaries (Cox et al., 1986; Fisher and Brantley, 1992; Barker, 1998). When cut perpendicular to the elongated axis, serrated, elongated quartz grains appear very similar to recrystallized granular quartz with significant subgrain rotation. If vein cracking occurs at the vein-wallrock interface, then wallrock inclusion bands may be incorporated into the vein (Ramsay, 1980; Cox et al., 1986; Fisher and Brantley, 1992). These inclusion bands parallel vein margins and record episodic vein cracking (Ramsay,

1980). Thus, they can be used to determine crack width and the number of vein opening events (Ramsay, 1980; Fisher and Brantley, 1992). In face-controlled metamorphic veins, the median line consists of a central inclusion band that recorded initial cracking (Barker, 1998).

A third type of metamorphic quartz vein, the non-directional quartz vein, is composed of granular to subhedral quartz with no obvious growth direction (Vearncombe, 1993). Non-directional quartz veins do not generally grow by crack-seal processes, though reopening of the vein and associated incorporation and inclusion of wall rock may occur at margins (Vearncombe, 1993). These appear similar to granular veins in other tectonic settings, and are not necessarily indicative of metamorphism, but rather formation at sub-epithermal depths.

Evaluation of Veins at Spring Valley in an Orogenic Context

Though gold-bearing veins at Spring Valley are clearly metamorphic in origin, they are primarily brittle features and differ from the brittle-ductile to ductile fault-fill and shear veins that characterize the majority of orogenic gold deposits (Robert and Poulsen, 2001; Goldfarb, 2005). Internal features of the majority of ore-stage quartz-carbonate veins are consistent with the description of oblique-extensional veins summarized in Robert and Poulsen (2001). Such veins have well-defined, matching, and relatively planar vein walls, and granular and crack-seal quartz textures (Robert and Poulsen, 2001). In contrast to fault fill veins in which quartz fibers grow at a low angle to vein walls, elongate-blocky quartz in veins at Spring Valley forms at a high angle to the vein wall, recording nearly perpendicular to slightly oblique extension. Widespread

lamination and slip surfaces along vein margins characteristic of fault fill veins are not present, and evidence of formation in an active shear zone—such as foliations and deformation of elongate-blocky quartz grains typical of extensional vein arrays and fault-fill veins—have not been observed. Further, oblique-extensional veins may form perpendicular or oblique to fold hinges, and veins at Spring Valley do, in fact, trend oblique to the NS-trending Spring Valley anticline.

Though discussion of vein geometry is limited by exposure in core, local stockwork and sheeted and/or discrete tabular veins are present, and ore-stage veins do not appear to be sigmoidal. Initial observations of vein geometry thus lend credence to an oblique-extensional interpretation. However, extensional veins in orogenic systems are typically subhorizontal to horizontal, while veins at Spring Valley are relatively steeply dipping. Though it is possible that the system was tilted following mineralization, the Spring Valley anticline, which formed prior to mineralization, does not appear to be overturned, and host rocks within the study area are relatively flat-lying. Also lacking is the identification of larger fault-fill and/or shear zones or veins that are believed to be genetically related to extensional veins in many orogenic deposits (e.g. Robert and Brown, 1986) (Robert and Poulsen, 2001). The nearby Bonanza King, which Campbell (1939) described as having similar alteration (sericite-carbonate), gangue mineralogy (notably tourmaline), and ore mineralogy (gold-pyrite-galena-sphalerite-tetrahedrite with apparently supergene argentite-stephanite-native Ag) to Spring Valley, is an attractive possibility. However, little information on the structural setting of the Bonanza King vein is available, and though brecciation and late quartz-sulfide-tourmaline introduction in

crosscutting fractures indicate that it did form during active faulting, the kinematics of said faulting are unknown. The possibility for brecciation and deformation under brittle shear after Hodgson (1989) is still present and may explain a similarly brecciated and laminated vein occupying a steeply dipping normal fault to the north of Spring Valley (see Fig. 7 and the "Fault-fill veins" section above).

At present exposure and understanding of vein geometry and regional tectonic setting, evaluation of the seemingly atypical vein occurrence at Spring Valley is at best speculative. Internal features and hand sample-scale morphology are consistent with the classification of oblique-extensional veins after Robert and Poulsen (2001) and extensional veins after Hodgson (1989). Deposit and district-scale features and morphology are inconclusive. Ultimately, prominent NS and NW-trending faults that were active prior to and following mineralization and the NS-trending Spring Valley anticline likely exert a strong control over the geometry and location of veins at Spring Valley.

Genetic implications of quartz vein textures

Cyclical shifts between non-directional and crack-seal vein-filling processes were accompanied by inherent shifts in the magnitude of quartz nucleation rates relative to quartz growth rates (Vearncombe, 1993). Such changes in nucleation- and growth-rates are related to changes in the prevailing conditions of the system at the time of vein formation (Vearncombe, 1993). Where steady-stage conditions exist, growth rates are typically greater and crack-seal veins form (Vearncombe, 1993). However, where conditions change suddenly, greater nucleation rates are favored and non-directional

quartz forms (Vearncombe, 1993). Changes that propel nucleation rates may be complex and varied, but they generally include changes in temperature, fluid chemistry or pressure (Vearncombe, 1993). In the absence of reliable pressure estimates, changes in pressure cannot be definitively established. However, there are several lines of indirect evidence that suggest vein formation and possibly gold precipitation were controlled by pressure fluctuations (Loucks and Mavrogenes, 1999).

Early gray granular quartz veins may have formed following a sudden decrease in pressure prior to the initiation of large-scale crack-seal vein formation. Due to the complex structural setting of Spring Valley and evidence of movement along structures both before and after mineralization, decreasing lithostatic pressure due to fault rupture is likely. Metamorphic fluids equilibrated with higher pressure flowed into newly-created open space, where a sudden decrease in pressure resulted in relatively rapid precipitation of granular quartz (Rimstidt, 1997). Earliest crack-seal veins began forming largely concomitantly with early granular quartz veins, suggesting that pressure conditions may be very local or cyclic.

Early quartz veins sealed newly formed fractures, and fluid pressure increased. Large-scale crack-seal vein-forming processes began shortly thereafter, as fluids re-equilibrated with prevailing pressure conditions. Inclusion bands within crack-seal veins demonstrate that cracking occurred on a micron to millimeter scale and that lithostatic pressure was such that large open space was not supported.

There are two principal lines of indirect evidence that suggest that a decrease in pressure contributed to the transition from crack-seal to granular veins. First, granular veins have generally similar or greater widths than crack-seal veins, but did not grow by

incremental crack-seal processes. This indicates that fluid and/or lithostatic pressures were such that larger fractures could be supported at similar depths. An increase in fluid pressure would in turn lead to an increase in CO_2 solubility, which is inconsistent with the large volume of carbonate present in the system. Therefore, a decrease in pressure, possibly related to fault rupture or increased fracture density due to continued crack-seal processes, would have likely contributed to an increase in quartz nucleation rates and the relatively rapid precipitation of granular quartz. This explanation is consistent with the interpreted post-peak metamorphic origin of the hydrothermal system.

A second line of evidence for granular quartz precipitation due to decreasing pressure is the increase in precipitation of carbonate minerals during granular quartz vein stages. While CO_2-bearing fluid inclusions are present in crack-seal veins, solubility of CO_2 was either too high or concentrations were too low to generate significant carbonate. Brittle failure triggered by fault rupture or increased fracture density could lead to a decrease in CO_2 solubility and subsequent loss of CO_2 present in hydrothermal fluids. Such a loss of CO_2 could lead to the precipitation of large volumes of bladed or massive carbonate (Tommy Thompson, pers. comm., November 2012). Alternatively, brittle failure could result in the introduction of increased CO_2 into the system. Increasing CO_2 could also lead to decreasing SiO_2 solubility, which could explain the greater occurrence of granular quartz veins relative to crack-seal quartz veins (Newton and Manning, 2000).

With the exception of rare bladed carbonate and vapor-dominant fluid inclusions, there is little evidence that boiling occurred, and decreasing CO_2 solubility due to fluid unmixing was not likely a major precipitation mechanism of gold. However, if gold was transported in a H_2S complex, a decrease in pressure and corresponding decrease in

ligand solubility could lead to gold precipitation, even in the absence of fluid unmixing or boiling (Loucks and Mavrogenes, 1999).

Vein relationships and mineralogy confirm that fluid chemistry changed several times throughout the development of the ore deposit, a fact that may explain the relative longevity of granular quartz vein formation. The first major change was the aforementioned introduction of larger volumes of carbonate. Carbonate, which does occur in crack-seal veins but shows no evidence of growth by crack-seal processes, is a major, typically late-stage constituent in nearly all granular quartz veins. The apparent increase in carbonate may be related to an increase in CO_2 or a decrease in CO_2 solubility. Alternatively, it may be related to an increase in the availability of complexing ions, such as Ca^{2+} or Fe^{2-3+}.

A second notable change in fluid chemistry was accompanied by the introduction of tourmaline and gold mineralization during stages 6 and 7. The sudden and short-lived appearance of tourmaline is somewhat enigmatic. It does not correspond with a notable increase in temperature, and it is indistinguishable from regional and vein-hosted tourmaline that is demonstrably earlier. The presence of dumortierite crosscutting tourmaline-bearing veins in the dumortierite-sericite schist of Lincoln Hill southeast of Spring Valley suggests that boron may have been remobilized during metamorphism. Thus, it is possible that continued metamorphism of earlier tourmaline and an influx of boron-bearing metamorphic fluids initiated a short-lived increase in the availability of boron at Spring Valley. Alternatively, boron may magmatic in origin and may have been introduced with the intrusion of the Rocky Canyon granodiorite, though there is no apparent boron mineralization associated with post-Koipato intrusives.

A third important change in fluid chemistry is recorded by the appearance of late Pb, Zn and Cu-bearing sulfides during stage 9. The appearance of sulfides does not correspond to a noticeable increase in homogenization temperature in fluid inclusions in quartz, nor was it accompanied by a change in alteration mineralogy. It is strongly correlated with gold mineralization in drillholes logged during the course of this study, though its true significance is not well understood.

Alteration

Hydrothermal alteration associated with mineralization in orogenic gold systems commonly consists of proximal sericite and carbonate, with pyrite and arsenopyrite dominant in igneous-hosted deposits, and pyrrhotite most commonly occurring in sedimentary-hosted deposits. Sericite-carbonate-pyrite ± arsenopyrite, pyrrhotite or chlorite alteration has been reported in the Wiluna area, and at the Racetrack and Golden Mile deposits, of the Yilgarn craton, Western Australia (McGoldrick, 1990; Chanter et al., 1998; Gebre-Mariam et al., 1993; Phillips, 1986), the Charters Towers district, North Queensland (Kreuzer, 2005; Kreuzer, 2006)and the Mother Lode of California (Hulin, 1930; Logan, 1935; Weir and Kerrick, 1987), among many others. Proximal sericite-carbonate-pyrite alteration at Spring Valley is consistent with alteration observed in these—and similar—systems.

Relatively abundant carbonate phases of varying composition are also common in orogenic systems (Goldfarb et al., 2005). At Spring Valley, carbonate is the second most abundant vein constituent and the third most abundant gangue mineral, and ranges in composition from calcite to Fe-calcite to ankerite. Though rare, bladed carbonate—

primarily calcite—does occur in granular and crack-seal veins. The presence of bladed calcite at mesothermal depths and the relative abundance of carbonate are indicative of high volumes of CO_2 in mineralizing fluids.

Tourmaline, long recognized as a common metamorphic product in greenschist- to amphibolite-facies rocks, is unsurprisingly a common alteration and vein constituent in orogenic deposits (Goldfarb et al., 2005; Dube and Gosselin, 2007; Slack and Trumball, 2011; van Hinsberg et al., 2011). It occurs in proximal alteration zones in the Golden Mile and Mount Charlotte deposits of the Kalgoorlie district of Western Australia, where it was used to constrain Sr isotope systematics of mineralizing fluids (Mueller et al., 1991; Bateman and Hagemann, 2004); in the Ballarat and Fosterville deposits of the Ballarat-Bendigo Zone of central Victoria, Australia (Bierlein et al., 2000); in gold-bearing quartz veins and adjacent selvages in the Sigma-Lamaque and Siscoe deposits in the Val d'Or district of the Abitibi greenstone belt (Robert and Brown, 1984; Olivo and William-Jones, 2002), among many others. At Spring Valley, schorl-variety tourmaline occurs in intermediate-stage quartz-carbonate veins and in adjacent selvages. Pre-ore tourmaline may also be present in healed breccias and in groundmass and clasts of volcaniclastic and sedimentary units.

Though less prominent than sericite, carbonate or tourmaline alteration, hematite is also known to occur in orogenic gold systems. At the Golden Mile deposit, hematite "dust" similar in character to nodular hematite in quartz-hematite altered zones at Spring Valley and lesser crystalline specularite occur proximal to mineralization with associated vanadian sericite, ankerite, quartz, siderite and pyrite (Bateman and Haggeman, 2004). It is known to impart a brick red to reddish-brown color that appears very similar to that of

quartz-hematite altered zones (Bateman and Haggeman, 2004). In Mesoproterozoic deposits of the Central Gawler Craton of South Australia, hematite occurs with chlorite and epidote in distal alteration zones, often as a hematite "dust" that stains feldspars red and as specularite in propylitic veins (Fraser et al., 2007). At the Charters Tower deposit, distal alteration is characterized by a chlorite-epidote-hematite assemblage, and feldspars are similarly stained red by microcrystalline hematite (Kruezer, 2005; Kruezer, 2006). Hematite-altered zones at Spring Valley locally contain elevated chlorite—typically in holes that occur peripheral to mineralized trends--and may, too, be analogous to propylitic alteration.

The origin of hematite and specularite alteration and the transition from proximal reduced sulfide-bearing assemblage to distal oxidized assemblages is not well understood. Espi et al. (2007) theorize that intermediate-stage hematite was introduced following either phase separation or mixing of mineralizing fluids with oxygenated groundwater. Similarly, Craw and Chamberlain (1996) identified isotopically heavier hematite-bearing veins in the Dalradian metamorphic belt of southwest Scotland and ascribed their formation to mixing of metamorphic fluids with oxidized meteoric fluids. They postulate that fluid mixing resulted in the precipitation of gold, though this theory is discounted by others (Goldfarb et al., 2005).

Alternative Reduced-Intrusion Related Gold Interpretation

The apparent close temporal association with Late Cretaceous magmatism suggests that Spring Valley may alternatively be a deep, intrusion-related gold system. The classification of reduced intrusion-related gold (RIRG) deposits is still in incipient

stages of development and significant overlap between orogenic classification and RIRG classification exists. This leads to considerable confusion over the assignment of newly discovered systems or reassignment of established systems to either style. Both may have an established temporal and spatial association to magmatism, and both may form at mesothermal depths (Hart and Goldfarb, 2005; Goldfarb et al., 2005). Alteration and gangue mineralogy between the two deposit styles are similar, as is characteristic low sulfide content (Hart and Goldfarb, 2005; Goldfarb et al., 2005). In addition, both are known to occur in greenschist-facies metamorphic belts, where they post-date deformation (Hart and Goldfarb, 2005; Goldfarb et al., 2005). The primary differences are an established connection between RIRG deposits and magmatism, the later timing of RIRG deposits relative to peak deformation, and the consistent association of gold in RIRG deposits with bismuth, antimony or arsenic.

Several lines of evidence suggest that Spring Valley may be a RIRG deposit. First, gold grades at Spring Valley are comparatively low and irregular and are more consistent with established RIRG deposits than with orogenic deposits (Hart and Goldfarb, 2005; Goldfarb et al., 2005). Second, vein geometry and distribution may be more aligned with RIRG classification, though discussion of vein geometry is currently limited by the lack of exposure. Extensional veins at Spring Valley have no close association to shear or fault-fill veins, and vein geometries and distribution are not consistent with oblique-extensional veins in other orogenic systems. Veins and associated mineralization also lack signs of deformation, which suggests they post-date metamorphism by a significant amount of time (Hart and Goldfarb, 2005). Thus, metamorphic vein textures identified during the course of this study may be more

indicative of formation in a mesozonal environment than formation related to orogenesis and/or widespread deformation. However, in a broader regional context, NE-trending quartz-Au veins and related foliation recorded throughout northwestern Nevada formed during a defined period of directed stress (Cheong, 1999; Wyld, 2001). Though commonly spatially and temporally associated with Late Cretaceous intrusives, the magnitude of deformation and the scale of affected areas suggest that it occurred independently of Late Cretaceous magmatism.

The most compelling evidence for classification of Spring Valley as a RIRG deposit is the apparent metal zoning within the region. RIRG deposits most commonly occur in tungsten-producing districts and show distinct zoning outward from Au-Bi-Te ± W, Mo hosted within causative intrusions, to proximal W±Cu±Au skarns and Au-As ± Sb veins, and distal Ag-base metal veins (Hart and Goldfarb, 2005; Goldfarb et al., 2005). Gold mineralization has been documented within the Rocky Canyon granodiorite, though it is apparently limited in extent and little information is available (Vikre and McKee, 1985). Late Cretaceous scheelite mineralization with greisen-like alteration strikingly similar to W-mineralization associated with RIRG deposits occurs most notably at Oreana, in limestone beds and pegmatite dikes related to the Rocky Canyon granodiorite stock. However, W mineralization is commonly associated with Late Cretaceous intermediate intrusives throughout northern Nevada and has yet to be linked to gold mineralization (Barton, 1987).

If mineralization at Spring Valley was part of a larger RIRG system, it would be analogous to proximal Au-As ± Sb mineralization in the zoning scheme outlined by Hart and Goldfarb (2005). However, As values are only slightly elevated over base levels and

As-bearing minerals are not present. Also, Sb does not occur at Spring Valley. Ag-base metal mineralization, such as that in the nearby Rochester and Wabash deposits, has been well-documented and may, in fact, be zoned distally from the Rocky Canyon granodiorite (Vikre and McKee, 1985). There is no established link between silver mineralization at Rochester and gold mineralization at Spring Valley, and an early gold event at Rochester may indicate that gold in the central Humboldt Range formed prior to silver mineralization (Tommy Thompson, pers. comm., 2012).

The possibility of district-wide metal zoning in orogenic deposits has been evaluated, though little consensus has been reached (Goldfarb et al., 2005). High-level Hg and Sb deposits may be epizonal expressions of both orogenic and reduced intrusion-related gold deposits. Thus, mercury mineralization at Cinnabar City and Little Linda deposits in the Spring Valley district and Sb mineralization in the Panther Canyon deposit of the Rye Patch district and the Black Warrior deposit of the Unionville district may be genetically associated with mesozonal gold mineralization at Spring Valley and elsewhere. In addition, increasing interest has been shown in the possibility of orogenic silver deposits. Deposits considered for classification as orogenic silver deposits are typically hosted in clastic metasedimentary rocks and have striking similarities to orogenic deposits, including occurrence in metamorphic belts, post-deformation timing, and CO2-rich fluids (Goldfarb et al., 2005).

Established RIRG deposits in the Tintina gold province of Alaska and the Northwest Territories and the Tasman fold belt of Australia are generally more mineralogically complex than Spring Valley and nearby gold deposits (McCoy et al., 1997; Goldfarb et al., 2005). At Fort Knox, gold occurs in multiple vein generations

associated with evolving alteration assemblages (Goldfarb et al., 2005). Early alteration manifests as K-feldspar in veins and groundmass, crosscut by later sericite-carbonate alteration (McCoy et al., 1997; Goldfarb et al., 2005). At Spring Valley, QSP-carbonate alteration is consistent for all vein types, with the exception of tourmaline-bearing veins that contain tourmaline in selvages. In addition, selvages adjacent to veins at Fort Knox and other RIRG deposits tend to be narrow and restricted even in areas of high vein density, while selvages at Spring Valley may extend tens of feet (Goldfarb et al., 2005). Admittedly, the extent of selvages may be controlled by reactivity of host rock.

Gold mineralization at Fort Knox is associated with a much broader range of sulfide compositions, including pyrite, marcasite, bismuthinite, arsenopyrite, molybdenite, and tellurides (McCoy et al., 1997; Goldfarb et al., 2005). Gold mineralization at Spring Valley is associated primarily with pyrite and lesser sphalerite and galena, with minor chalcopyrite and rare tetrahedrite. As-, Bi- and Te-bearing sulfides are not present, and mineralization is appears to only be associated with slightly elevated Pb, Zn and As (Neal and LeLacheur, 2010). Alteration and metal associations seen at Fort Knox and other intrusion-hosted RIRG deposits is similar to that seen in wall-rock hosted RIRG deposits (Robert et al., 2007).

The current level of understanding of RIRG deposits and the overlap in classification of orogenic and RIRG deposits, coupled with evidence gathered during the course of this and previous studies, suggests mineralization is orogenic or metamorphic in origin. Most notably, it is apparent that gold-bearing metamorphic veins in northwestern Nevada formed during a defined and directed deformational event. However, the district-wide similarities in metal zoning with established RIRG districts,

the apparent temporal association between mineralization and Late Cretaceous magmatism, and the timing of mineralization relative to orogenesis suggests a composite genetic model in which Late Cretaceous intrusives contributed all or part of mineralizing fluids or provided a source of heat. Further work is needed to conclusively link mineralization to Late Cretaceous magmatism.

In the absence of a reliable age of mineralization at Spring Valley, classification as either an orogenic or RIRG system is tenuous. If mineralization could be established as Late Cretaceous in age, than a RIRG interpretation is likely. However, if gold mineralization is significantly older than nearby silver mineralization and is Late Jurassic to Early Cretaceous in age, Spring Valley is likely an orogenic gold deposit.

Implications of Vein Orientations and Paragenesis on the Age of Mineralization

The majority of pre-ore ataxial quartz veins in the field area to the north of Spring Valley trend NW, which is consistent with formation during shearing under NW/SE-directed crustal shortening. In addition, previous logging conducted by site geologists suggests that many ataxial veins in core similarly trend NW. This indicates that some, if not all, ataxial veins may be associated with late Jurassic NW/SE directed emplacement of the Luning-Fencemaker allochthon. By contrast, the majority of crack-seal and granular quartz veins in Spring Valley trend northeast and likely formed during NE/SW-directed crustal shortening or NW/SE-directed extension associated with a distinct tectonic event.

The timing of this second event relative to emplacement of the Luning-Fencemaker allochthon is not well understood. Cheong (1999) noted similar temporal relationships between gold-bearing metamorphic quartz veins throughout northwestern Nevada and concluded that NW-trending veins predate NE-trending veins. Further, he concluded that NE-trending veins are middle to late Cretaceous in age (approximately 78-107 Ma in the Humboldt Range), based primarily on crosscutting relationships and K-Ar ages of sericite. In the Santa Rosa Range, Wyld et al. (2001) identified a second metamorphic event that postdated the emplacement of the Luning-Fencemaker allochthon. There, northwest-southeast compression is ascribed to weak underthrusting from the Sevier thrust belt to the east and is believed to have occurred synchronously with the emplacement of a ~102 Ma granitoid. This is consistent with the upper end of the sericite ages within the Humboldt Range. It should be noted that an overlap between the emplacement of the Luning-Fencemaker allochthon and the Sevier orogeny has been documented (Wyld, 2002; DeCelles, 2004).

An age of approximately 70 Ma was established for sericitic alteration of a plagioclase phenocryst in the Feldspar Porphyry at Spring Valley (Chris Henry, pers. comm., February 2012). In the absence of an established paragenetic relationship between analyzed sericitic and mineralization, and in light of the complex thermal history of the region, this age is somewhat suspect. It is broadly correlative with the range of K-Ar sericite ages for silver mineralization in the Humboldt Range, from ~114 to ~80 Ma, though these, too, are likely reset. The apparent association between NE-trending veins at Spring Valley and a post-Jurassic metamorphic event, coupled with regional context

provided by Wyld et al.(2001) and Cheong (1999), still suggest a strong possibility that mineralization is Late Cretaceous in age.

Alternatively, vein textures at Spring Valley suggest that it formed under an extensional tectonic regime. Thus, it is possible that metamorphic quartz veins at Spring Valley and elsewhere in Nevada formed during an extensional event that may predate or post-date Late Cretaceous deformation and that may be unrelated to Sevier deformation in the Santa Rosa Range. This event may have occurred closely following Late Jurassic orogenesis by relaxation of autochthonous crust; it may also be related to Late Cretaceous eastward migration of the volcanic arc and related plutonism. In the absence of a reliable age of mineralization, metamorphic veins at Spring Valley cannot be placed in a regional tectonic setting, and gold deposit style cannot be definitively constrained.

Conclusion

Spring Valley is a metamorphic quartz-gold deposit hosted within the volcanic, volcaniclastic, and intrusive units of the Permo-Triassic Koipato Group. Mineralization primarily occurs in the Quartz-eye Rhyolite, Welded Tuff, Agglomerate and Feldspar Porphyry units of the Rochester Formation, though mineralization has been intercepted in the Limerick Formation and in Rhyolite Porphyry dikes of the Weaver Formation. It is hosted within a series of crosscutting crack-seal and granular quartz veins associated with proximal QSP-carbonate ± tourmaline alteration.

Alteration is best developed in the Feldspar Porphyry. Proximal alteration consists of a pale green to greenish-gray quartz-sericite-pyrite-carbonate assemblage. Sericite occurs primarily in fine, anastomosing veinlets that extend outward from the vein at a high angle. It also occurs after groundmass K-feldspar and rimming and replacing K-feldspar and plagioclase phenocrysts. Biotite phenocrysts are pervasively altered to a mixture of sericite and lesser carbonate, hematite, leucoxene or pyrite. Fine- to medium-grained granular quartz occurs in small, irregular to rounded clusters within the groundmass and as discrete to intergrown granular grains replacing feldspar phenocrysts. Carbonate ranges in composition from calcite to Fe-calcite to ankerite and occurs as fine rhombic euhedra disseminated throughout the groundmass. Scaley, anhedral carbonate occurs after biotie and feldspar phenocrysts intergrown with sericite and after groundmass K-feldspar. Pyrite typically comprises between 0.5-2% and occurs as euhedral cubic to anhedral grains disseminated throughout the groundmass and after

biotite phenocrysts. Fine-grained, acicular to felty tourmaline is present in selvages adjacent to tourmaline-bearing veins.

QSP-carbonate ± tourmaline alteration grades outward into an intermediate to distal red-brown quartz-hematite assemblage. Similarly to proximal alteration zones, fine- to medium-grain granular quartz occurs in irregular to rounded clusters and after feldspar phenocrysts. It also occurs in fine veinlets with or without carbonate that locally crosscut sericite veinlets. Hematite occurs as very fine, nodular "dust" within groundmass and feldspar phenocrysts, lending a distinct brick red to brown coloration. Sericite and carbonate in quartz-hematite altered zones have similar occurrences to sericite and carbonate in QSP-carbonate altered zones, though sericite is far less abundant. Pyrite is generally absent, except in transition zones.

Red-brown quartz-hematite alteration grades outward into a distal dark gray quartz-specularite assemblage. Quartz-specularite alteration is similar to quartz-hematite alteration in quartz, sericite, carbonate and pyrite abundances and occurrences. The dark gray color of quartz-specularite altered wallrock is produced by very fine acicular to tabular specularite disseminated throughout the groundmass. Quartz-specularite alteration is irregularly distributed and is most commonly absent.

In the Agglomerate, alteration zoning is best developed in reactive greenstone clasts. Proximal to veins, it consists of a light green quartz-sericite-pyrite-carbonate-fuchsite ± tourmaline assemblage. Sericite is strongly pervasive and texturally destructive. It occurs intergrown with carbonate in groundmass and replacing biotite phenocrysts. Quartz occurs in irregular nodules within greenstone clasts. In groundmass, granular quartz may form cement or occur in vugs with coarse-grained sericite. Adjacent

to tourmaline-bearing veins, tourmaline flooding may occur in groundmass. QSP-carbonate-fuchsite alteration in greenstone clasts grades outward into a dark gray to black quartz-specularite/hematite alteration zone. Quartz occurs in groundmass intergrown with very fine-grained, acicular specularite. Minor, very fine-grained hematite 'dust" may be present.

In the Welded Tuff, proximal alteration consists of a light green to gray quartz-sericite-pyrite-carbonate ± tourmaline assemblage similar in mineralogy and occurrence to proximal alteration in the Feldspar Porphyry. At shallow depths, proximal alteration grades outward into relatively unaltered wallrock. At depth, proximal QSP-carbonate ± tourmaline alteration may grade outward into a dark purplish to reddish hematite- or specularite-bearing zone. In the Quartz-eye Rhyolite, proximal QSP-carbonate ± tourmaline alteration grades outward into relatively unaltered wallrock and is generally indistinguishable from greenschist-facies sericite-carbonate alteration except where pyrite is present.

Veins at Spring Valley consist of pre-ore ataxial metamorphic veins, and ore-stage crack-seal to granular quartz veins. Crack-seal veins consist of elongate-blocky quartz with or without early to late pyrite, or later carbonate, sericite or base metal sulfides. Discontinuous, parallel inclusion bands record cracking and mineral precipitation on a micron to millimeter scale. Crack-seal veins may host paragenetically late gold and base metal mineralization, particularly where adjacent to later mineralized granular quartz veins.

Granular quartz veins are typically 0.5mm to 40mm in width and consist of fine- to coarse-grained granular to subhedral quartz. Fine- to medium-grained granular to

subhedral quartz commonly lines vein margins. Veins are infilled by fine- to coarse-grained granular to euhedral quartz. Minor euhedral quartz occurs in carbonate-filled vugs. Granular quartz veins may also contain early to late sericite, tourmaline or pyrite, or late carbonate.

Though irregular, discontinuous veins are present locally, ore-stage veins at Spring Valley generally have planar or matching walls and likely formed under a brittle to brittle-ductile structural regime (Robert and Poulsen, 2001). Quartz vein textures and the relationship between quartz grain and vein margins suggests that they are extensional and likely formed at shallow mesothermal depths, between 5km and 10km (Robert and Poulsen, 2001). This is supported by the presence of carbonate and sericite in proximal alteration zones, which are common in orogenic deposits that form at relatively shallow depths (Goldfarb et al., 2005).

Eight vein stages were identified: 1. Pre-ore ataxial veins associated with moderately to strongly pervasive silicification, 2. Early granular gray quartz-tourmaline veins. 3. Early ore-stage gray elongate-blocky to granular quartz-carbonate ± pyrite veins, 4. White to gray elongate-blocky quartz ± carbonate-pyrite veins, 5. Gray granular quartz-carbonate ± pyrite veins, 6. Gray granular quartz-carbonate-tourmaline ± -pyrite veins, 7. White granular quartz-carbonate-tourmaline ± pyrite; 8. White granular quartz-carbonate-pyrite ± sphalerite-galena veins. Fluid inclusion analyses indicate that all vein stages had minimum temperature of formation between 210°C and 360°C.

Gold mineralization occurred in three phases during the formation of gray to white granular quartz veins. It was initiated by a quartz-tourmaline phase and continued throughout a white quartz phase, and temperature and chemistry of mineralizing fluids

and pressure of the system likely played an import role in the transport and precipitation of gold. Where it was observed in polished section and core, gold was always late. It commonly occurs replacing earlier sulfides, pyrite, sphalerite and galena, or in fractures between quartz grain boundaries.

Fluctuations in pressure, recorded by quartz grain morphology and the sequence of veining events, may have played an important role in the precipitation of gold. Elongate-blocky quartz growth is favored where crystal growth rates exceed nucleation rates under steady-state conditions (Vearncombe, 1993). Granular, or non-directional, quartz formation occurs when nucleation rates exceed growth rates (Vearncombe, 1993). Changes in pressure, temperature or fluid composition can propel nucleation rates relative to growth rates (Vearncombe, 1993).

Though no analytical data supporting fluctuations was obtained, indirect evidence suggests that the transition between crack-seal and granular veins was related to changes in pressure: 1. Granular veins have similar widths as crack-seal veins but did not growth by incremental crack-seal processes, which indicates that fluid and/or lithostatic pressures at the time of granular vein formation were such that larger fractures could be supported at similar depths; 2. High volumes of carbonate in granular veins relative to crack-seal veins suggest that CO_2 solubility either decreased following crack-seal vein growth, resulting in the loss of CO_2, or CO_2 concentrations in mineralizing fluids increased, both of which could be achieved by a sudden decrease in pressure related to fault rupture. The complex structural history of Spring Valley and evidence of movement along structures both prior to and following mineralization supports this interpretation.

Changes in fluid chemistry may have prolonged granular quartz vein forming event. The first change in fluid chemistry is recorded by the introduction--or reintroduction--of carbonate following the cessation of the crack-seal vein forming event. Though carbonate is present in crack-seal veins, it did not grow by incremental crack-seal processes and is always a late vein-filling phase. As mentioned previously, this change in fluid composition may have been triggered by a sudden decrease in pressure with CO_2 loss. They second notable change in fluid chemistry is recorded by the appearance of tourmaline during stage 6. The introduction of tourmaline does not correspond with an increase in temperature and may be related to an influx of boron released at greater depths into the system. The third change in fluid chemistry is recorded by the appearance of sphalerite and galena during stage 9. Similarly to the appearance of tourmaline, sphalerite and galena introduction was not accompanied by a significant increase in temperature. The source of base metals and the implications of this event are not known.

Vein orientations and paragenesis have important implications for the age of mineralization. Ataxial veins commonly trend NW and are thus possibly related to Late Jurassic NW-SE-directed crustal shortening. Alteration at Spring Valley is clearly retrograde relative to greenschist-facies metamorphism and thus likely post-dates the late Jurassic emplacement of the Luning-Fencemaker allochthon. Ore-stage veins crosscut earlier ataxial veins and are associated with a distinct event. Cheong (1999) identified a likely late Cretaceous orogenic gold event that occurred throughout northwestern Nevada and produced NE-trending, gold-bearing quartz veins that crosscut regional metamorphic fabrics related to the development of the Luning-Fencemaker thrust. This is consistent

with a previously obtained K-Ar age of approximately 70 Ma from sericite in altered wallrock at Spring Valley (Chris Henry, pers. comm., 2012).

Exploration Implications

Exploration for similar deposits on a regional scale may follow several models dependent on the classification of Spring Valley as an orogenic or reduced intrusion-related gold deposit. Fortunately, significant overlap exists between the two deposits, and similarities may provide the basis for an exploration program. Both orogenic and reduced intrusion-related gold deposits share the following characteristics (Hart and Goldfarb, 2005; Goldfarb, 2005):

1. Association with greenschist-facies host rocks and occurrence in collisional orogenic belts;
2. Post-metamorphic timing of gold mineralization;
3. Formation at mesothermal depths and development of metamorphic vein textures;
4. Sericite-carbonate-pyrite alteration, though in RIRG deposits, sericitization is typically predated by K-feldspar alteration.

Regardless of classification, deposits similar to Spring Valley are likely hosted in greenschist-facies metamorphic rocks in broad, collisional orogenic belts. In addition, mineralization should clearly postdate peak deformation. Prospective hosts in northern Nevada were likely metamorphosed during emplacement of the Luning-Fencemaker allochthon. If Spring Valley is an orogenic system, mineralization likely occurred within several million years of peak deformation. By contrast, if it is a RIRG deposit, then mineralization may postdate deformation by tens of millions of years.

Reactive felsic units of the upper Koipato Group appear to be favorable hosts for gold mineralization in the Humboldt Range, though absent the identification of systems similar to Spring Valley, it is too early to comment on favorable hosts. If Spring Valley is a RIRG deposit related to Late Cretaceous magmatism, then mineralization elsewhere may be hosted within causative intrusions. It may also be hosted within reactive wallrock adjacent to intrusions.

Vein features

Mineralization at Spring Valley is distinct from the majority of gold deposits in Nevada in that it formed at mesothermal depths. This is evident in the textures of ore-stage veins. Deposits similar to Spring Valley should lack quartz textures indicative of formation at epithermal depths, including colloform, crustiform, or comb-textured quartz. Rather, quartz textures should reflect formation at depth under high pressure and include fibrous, elongate-blocky or non-directional (granular) quartz.

Vein textures at Spring Valley are not only indicative of formation in a mesothermal setting, but are also indicative of formation in a favorable brittle-ductile to brittle regime where lithostatic pressure and temperature are conducive to gold precipitation. Deposits similar to Spring Valley should have internal and external vein features that reflect brittle deformation and possibly formation during extension. Such features include:

1. Relatively planar, matching vein walls;
2. Quartz textures indicative of formation in open space, such as elongate-blocky quartz or granular quartz that did not form by replacement;

3. Evidence of brittle cracking, i.e. wallrock inclusion bands;
4. Elongated quartz growing perpendicular to slightly oblique to vein walls, indicating oblique to orthogonal extension.

Displacement-controlled veins similar to pre-ore ataxial veins at Spring Valley will not likely host mineralization elsewhere, primarily due to the fact that they formed under high pressure where open space was not supported, and pressure fluctuations necessary for gold precipitation did not occur. Also, it is likely that they formed during peak deformation, rather than after. If Spring Valley is an orogenic system, there will almost certainly be larger shear or fault-fill veins that host mineralization and do not exhibit the same vein features. Refer to Robert and Poulson (2001) for complete descriptions of vein textures associated with orogenic gold deposits. If Spring Valley is a RIRG system, mineralized veins may exhibit a much broader range of internal features and geometries, though they will likely occur in sheeted sets, stockworks or vein swarms.

NE-trending, metamorphic quartz-Au veins similar to those at Spring Valley have been identified throughout northwestern Nevada. Notable occurrences are present in the Humboldt Range, the Kamma Mountains to the west of the Humboldt Range and in the East Range to the east of the Humboldt Range. In the Humboldt Range, metamorphic quartz-Au veins have been documented in the Spring Valley, Imlay and Star districts (Cheong, 1999). In the Kamma Mountains, metamorphic quartz-Au veins have been identified in the Jungo, Sulfur, Rosebud, Rabbit Hole, Scossa, Placerites, Arabia and Trinity districts (Cheong, 1999). In the East Range, similar quartz veins have been documented in the Sierra and Willow Creek districts (Cheong, 1999). In addition,

metamorphic quartz-Au veins have been documented in the Pine Forest Range, the Eugene Mountains, the Slumbering Hills and the Ten Mile Hills area (Cheong, 1999).

The Haystack deposit in the Jungo District bears several similarities to mineralization at Spring Valley, though it should be noted that exploration at Haystack is still in incipient stages (Crosby, 2010). First, mineralization is hosted within NNE, NW and NS-trending, gently dipping veins that area generally less than 1 m in thickness and are composed of massive to finely granular quartz (Crosby, 2010). Veins are typically subparallel and may occur in stockwork or sheeted swarms (Crosby, 2010). In addition, they may contain fine, acicular tourmaline and are associated with sericitic and argillic alteration (Crosby, 2010). In contrast to Spring Valley, mineralization at Haystack is hosted within a Cretaceous granodiorite intrusive and is associated with bismuthinite (Crosby, 2010). The Haystack deposit was classified as a reduced intrusion-related gold system, based on the above characteristics, a clear association with Late Cretaceous magmatism, and the strong correlation between gold and bismuth (Crosby, 2010).

Alteration, gangue and ore mineralogy

Spring Valley is distinct from other deposits in the Humboldt Range. It is mineralogically simple, with gold primarily associated with pyrite, sphalerite and galena, and contains virtually no silver. Deposits similar to Spring Valley may have similar gold and base metal associations; however, if it is part of a larger zoned system, mineralogy of related deposits could conceivably vary.

Distal to intermediate quartz-hematite or quartz-specularite alteration is only consistent within the Feldspar Porphyry unit at Spring Valley. By contrast, quartz-

sericite-pyrite-carbonate alteration is consistent throughout all host rocks and all ore-stage veins. Deposits similar to Spring Valley would have multiple generations of veins—possibly varying in texture—with sericite-carbonate-pyrite selvages. Though tourmaline is not a reliable indicator of mineralization on a district scale, the presence of schorl-variety tourmaline in veins and selvages elsewhere may be a valuable exploration tool.

Metal zoning and associated mineralization

The most compelling argument for classification of Spring Valley as an RIRG deposit is the apparent metal zoning outward from the Rocky Canyon granodiorite stock to the northwest. Late Cretaceous intrusions in Nevada are commonly associated with tungsten mineralization, similarly to intrusions related to RIRG deposits. If gold mineralization is related to the Rocky Canyon granodiorite, then exploration elsewhere should be focused in and around known tungsten producing districts. Tungsten mineralization related to Late Cretaceous intrusions occur throughout northern Nevada, including the Mill City district of the Eugene Mountains, the Trinity district of the Kamma Mountains, and the Awakening district of the Slumbering Hills, all of which contain documented metamorphic quartz-Au veins.

Both orogenic and RIRG deposits are commonly associated with extensive placer deposits. The Placerites, Arabia and Rabbit Hole districts in the Kamma Mountains are all known placer districts in which metamorphic quartz veins have been identified. In the East Range, both placer deposits at metamorphic quartz-Au veins have been documented in the Sierra district.

References

Barker, A.J., 1998, Introduction to Metamorphic Textures and Microstructures: London, Chapman and Hall, 243 p.

Barth, A.P., and Wooden, J.L., 2006, Timing of magmatism following initial convergence at a passive margin, southwestern U.S. Cordillera, and ages of lower crustal magma sources: The Journal of Geology, v. 114, pp. 231–245.

Barton, M.D., 1987, Lithophile element mineralization associated with Late Cretaceous two-mica granite in the Great Basin: Geology, vol. 15. Pp. 337-340.

Bateman, R., and Haggeman, S., 2004, Gold mineralisation throughout about 45 Ma of Archaean orogenesis: protracted flux of gold in the Golden Mile, Yilgarn craton, Western Australia: Mineralium Deposita, v. 39, pp. 536–559.

Bierlein, F.P., Arne, D.C., McKnight, S., Lu, J., Reeves, S., Besanko, J., Marek, J., and Cooke, D., 2000, Wall-Rock Petrology and Geochemistry in Alteration Halos Associated with Mesothermal Gold Mineralization, Central Victoria, Australia: Economic Geology, vol. 95, pp. 283-312.

Bons, P.D., 2000. The formation of veins and their microstructures. *in*: Jessell, M.W., Urai, J.L. (Eds.), Stress, Strain and Structure, A Volume in Honour of W.D. Means. Journal of the Virtual Explorer, vol. 2. http://virtualexplorer.com.au/2000/volume2/www/contribs/bons/index.html.

Bons, P.D., 2001, Development of crystal morphology during unitaxial growth in a progressively widening vein: I. The numerical model: Journal of Structural Geology, vol. 23, p. 865-872.

Burke, D.B., and Silberling, N.J., 1973, The Auld Lang Syne Group of Late Triassic and Jurassic (?) age, north-central Nevada: U.S. Geological Survey Bulletin B 1394-E, 14 p.

Campbell, D.F., 1939, Geology of the Bonanza King Mine, Humboldt Range, Pershing County, Nevada: Economic Geology, vol. 34, no. 1, p. 96-112.

Chadwick, T.H., 2011, Geologic Map of the Spring Valley Project Area, Barrick in-house company report.

Chanter, S C; Eilu, P; Erickson, M E; Jones, G F P; Mikucki, E., 1998, Bulletin gold

deposit: Monograph Series - Australasian Institute of Mining and Metallurgy, vol. 22 pp. 105-110.

Cox, S.F., Etheridge, M.A., Wall, V.J., 1986. The role of fluids in syntectonic mass transport, and the localization of metamorphic vein-type ore deposits. Ore Geology Reviews 2, 65–86.

Cheong, S., 1999, Structural setting and fluid characteristics of metamorphic gold-quartz veins in northwest Nevada: Unpublished Ph.D. dissertation, University of Nevada, Reno, 332 p.

Chevillon, V., 2007, Follow Up host Rock Petrography, Spring Valley Gold Deposit, Pershing County, Nevada: Unpublished report for Midway Gold Corp, 15 p.

Craw, D., and Chamberlain, C.P., 1996, Meteoric incursion and oxygen fronts in the Dalradian metamorphic belt, southwest Scotland: a new hypothesis for regional gold mobility: Mineralium Deposita, v. 31, pp. 365-373.

Crosby, R., 2010, NI 43-101 Technical Report Haystack Deposit: Ironwood Gold Corp.

DeCelles, P.G., 2004, Late Jurassic to Eocene Evolution of the Cordilleran Thrust Belt and Foreland Basin System, Western U.S.A.: American Journal of Science, Vol. 304, pp. 105–168

Dickinson, W.R., 2006, Geotectonic evolution of the Great Basin: Geosphere, v. 2, no. 7. pp. 353–368.

Drury, M.R. and Urai, J.L., 1990, Deformation-related recrystallization processes: Tectonophysics, vol. 172, pp. 235-253.

Dubé, B., and Gosselin, P., 2007, Greenstone-hosted quartz-carbonate vein deposits: *in* Goodfellow, W.D. (eds.), Mineral Deposits of Canada: A Synthesis of Major Deposit-Types, District Metallogeny, the Evolution of Geological Provinces, and Exploration Methods: Geological Association of Canada, Mineral Deposits Division, Special Publication No. 5, pp. 49-73.

Espi, J.O., Hayashi, K.I., Komuro, K, Murakami, H., and Kajiwara, Y., 2007, Geology, Wall-Rock Alteration and Vein Paragenesis of the Bilimoia Gold Deposit, Kainantu Metallogenic Region, Papua New Guinea: Resource Geology, vol. 57, no. 3, pp. 249-268.

Fairbanks, E.E., 1926, Dumortierite from Nevada: American Mineralogist 11, pp. 93-96.

Fisher, D.M, and Brantley, S.L., 1992, Models of Quartz Overgrowth and Vein

Formation: Deformation and Episodic Fluid Flow in an Ancient Subduction Zone: Journal of Geophysical Research, vol. 97, no. B13, pp. 20,043-20, 06.

Fraser, G.L., Skirrow, R.G., Schmidt-Mumm, A., and Holm, O., 2007, Mesoproterozoic Gold in the Central Gawler Craton, South Australia: Geology, Alteration, Fluids and Timing: Economic Geology, vol. 102, pp. 1511-1539.

Gebre-Mariam, M., Groves, D.I., McNaughton, N.J., Mikucki, E.J., Vearncombe, J.R., 1993, Archaean Au-Ag mineralisation at Racetrack, near Kalgoorlie, Western Australia; a high crustal-level expression of the Archaean composite lode-gold system: Mineralium Deposita, vol. 28, no. 6, pp. 375-387.

Goldfarb, R.J., Baker, T., Dubé, B., Groves, D.I., Hart, C.J.R., and Gosselin, P., 2005, Distribution, Character and Genesis of Gold Deposits in Metamorphic Terranes, *in* Hedenquist, J.W., Thompson, J.F.H., Goldfarb, R.J., and Richards, J.P. (eds.), Economic Geology 100th Anniversary Volume, pp. 407-450.

Groves, D.I., Goldfarb, R.J., Gebre-Mariam, M., Hagemann, S.G., and Robert, F., 1998, Orogenic gold deposits: A proposed classification in the context of their crustal distribution and relationship to other gold deposit types: Ore Geology Reviews, v. 13, p. 7–27.

Groves, D.I., Goldfarb, R.J., Robert, F., and Hart, C.J.R., 2003, Gold Deposits in Metamorphic Belts: Overview of Current Understanding, Outstanding Problems, Future Research, and Exploration Significance: Economic Geology, vol. 98, pp. 1-29.

Hart, C.J.R., Goldfarb, R.J., 2005. Distinguishing intrusion-related from orogenic gold systems. New Zealand Minerals Conference Proceedings, p. 125–133.

Hogdson, C.J., 1989, The Structure of Shear-Related, Vein-type Gold Deposits: A Review: Ore Geology Reviews, v. 4, pp. 231-273.

Hulin, C.D., 1930, A Mother Lode Gold Ore: Economic Geology, vol. 25, pp. 348-355.

Johnson, M.G., 1977, Geology and Mineral Deposits of Pershing County, Nevada: Nevada Bureau of Mines and Geology Bulletin 89, 115 p.

Jones, J.C., 1928, The Deposit of Dumortierite in Humboldt Queen Canyon, Pershing County, Nevada: University of Nevada Bulletin, vol. 22, no. 2, pp. 23-26.

Kistler, R.W., and Speed, R.C., 2000, 40Ar/39Ar, K-Ar, Rb-Sr Whole-Rock and Mineral Ages, Chemical Composition, Strontium, Oxygen and Hydrogen Isotopic

Systematics of Jurassic Humboldt Lopolith and Permian (?) and Triassic Koipato Group rocks, Pershing and Churchill Counties, Nevada: U.S. Geological Survey Open-File Report 00-217, 14 p.

Kruezer, O.P, 2005, Intrusion-Hosted Mineralization in the Charters Towers Goldfield, North Queensland: New Isotopic and Fluid Inclusion Constraints on the Timing and Origin of the Auriferous Veins: Economic Geology, v. 100, pp. 1583–1603.

Kruezer, O.P., 2006, Textures, paragenesis and wall-rock alteration of lode-gold deposits in the Charters Towers district, north Queensland: implications for the conditions of ore formation: Mineralium Deposita, v. 40, pp. 639-663.

LeLacheur, E., Mosch, D., Edelin, J., and McMillin, S., 2011, Spring Valley Project NI 43-101 Technical Report: Midway Gold Corp, 104 p.

Logan, C., 1935, Mother Lode gold belt of California, California Department of Natural Resources, Division of Mines Bulletin vol. 108, 240 p.

Loucks, R.R., and Mavrogenes, J.A., 1999, Gold Solubility in supercritical hydrothermal brines measured in synthetic fluid inclusions: Science, v. 284, p. 2159-2163.

Ludington, S., McKee, E.H., Cox, D.P., Moring, B.C., and Leonard, K.R., 1996, Pre-Tertiary Geology of Nevada, in Singer D.A., ed., An Analysis of Nevada's Metal Bearing Resources, Nevada Bureau of Mines and Geology Open File Report 96-2, p. 4-1-4-9.

McGoldrick, P.J., 1990, Wiluna gold deposits: Monograph Series - Australasian Institute of Mining and Metallurgy, vol. 14, pp. 309-312.

Mueller, A.G., de Laeter, J.R., and Groves, D.I., 1991, Strontium Isotope Systematics of Hydrothermal Minerals from Epigenetic Archean Gold Deposits in the Yilgarn Block, Western Australia: Economic Geology, vol. 86, pp. 780-809.

Muntean, J.L, and Einaudi, M.T, 2000, Porphyry gold deposits of the Refugio district, Maricunga belt, northern Chile: Economic Geology, vol. 95, pp. 1445–1472.

Neal, B., and LeLacheur, E., 2010, Geologic overview of the Spring Valley gold deposit, Pershing County, NV: Geological Society of Nevada 2010 Symposium, pp. 625-635.

Newton, R.C., and Manning, C.E., 2000, Quartz solubility in H2O-NaCl and H2O-CO2 solutions at deep crust-upper mantle pressures and temperatures: 2–15 kbar and 500–900°C: Geochemica et Cosmochemica Acta, vol. 64, no. 17, pp. 2993-3005.

Olivo, G.R., and William-Jones, A.E., 2002, Genesis of the Auriferous C Quartz-

Tourmaline Vein of the Siscoe Mine, Val d'Or District, Abitibi Subprovince, Canada: Structural, Mineralogical and Fluid Inclusion Constraints: Economic Geology, vol. 97, pp. 929-947.

Passchier, C. W. and Trouw, R.A.J., 1996, Microtectonics: Berlin, Springer-Verlag., 289 p.

Phillips, G.N., 1986, Geology and alteration in the Golden Mile, Kalgoorlie: Economic Geology, vol. 81, no. 4, pp. 779-808.

Potter, R.W. II, 1977, Pressure corrections for fluid-inclusion homogenization temperatures based on the volumetric properties of the system NaCl-H2O: Journal of Research of the U.S. Geological Survey, v. 5, no. 5, pp. 603-607.

Ramsay, J. G., 1980, The crack-seal mechanism of rock deformation: Nature, vol. 284, pp. 135-139.

Rimstidt, J.D., 1997, Gangue mineral transport and deposition, in: Barnes, H.L. (Ed.), Geochemistry of Hydrothermal Ore Deposits, pp. 487–515.

Robert, F., Brommecker, R., Bourne, B.T., Dobak, P.J., McEwan, C.J., Rowe, R.R., and Zhou, X., 2007, Models and exploration methods for major gold deposit types: Exploration 07: Fifth Decennial International Conference on Mineral Exploration, Toronto, 2007, Proceedings, p. 691–711.

Robert, F., and Brown, A.C., 1984, Progressive alteration associated with gold-quartz-tourmaline veins at the Sigma Mine, Abitibi Greenstone Belt, Quebec: Economic Geology, vol. 79, p. 393-399.

Robert, F., and Poulsen, K.H., 2001, Vein Formation and Deformation in Greenstone Gold Deposits: Reviews in Economic Geology, v. 14, pp. 111-155.

Ross, K.V., 2006: Petrographic Report on the Spring Valley Property, Pershing County, Nevada. Unpublished report for Midway Gold Corp, 55 p.

Slack, J.F., and Trumbull, R.B., 2011, Tourmaline as a Recorder of Ore-Forming Processes: Elements, vol. 7, pp. 321-326.

Silberling, N.H., and Wallace, R.E., 1969, Stratigraphy of the Star Peak Group (Triassic) and overlying lower Mesozoic rocks, Humboldt Range, Nevada: U.S. Geol. Survey Prof. Paper 592, 50 p.

Silberling, N.H., and Nichols, K.M., 1982, Middle Triassic Molluscan Fossils of Biostratigraphic Significance from the Humboldt Range, Northwestern Nevada:

U.S. Geological Survey Professional Paper 1207, 77 p.

Silberling, N.J., and Roberts, R.J., 1962, Pre-Tertiary stratigraphy and structure of northwestern Nevada: Geological Society of America Special Paper 72, 58 p.

Silberling, N.J., and Wallace, R. E., 1967, Geologic map of the Imlay quadrangle, Pershing County, Nevada: U .S. Geological Survey Map GQ-666.

Sillitoe, R.H., 2008, Major gold deposits and belts of the North and South American Cordillera: Distribution, tectonomagmatic settings, and metallogenic considerations: Economic Geology, vol. 103, p. 663–687.

Simmons, S.F., White, N.C., and John, D.A., 2005, Geological Characteristics of Epithermal Precious and Base Metal Deposits: *in* Hedenquist, J.W., Thompson, J.F.H., Goldfarb, R.J., and Richards, J.P. (eds.), Economic Geology 100th Anniversary Volume, pp. 485-522.

Skalbeck, J.D., 1985, Paleomagnetism of the early Triassic Koipato Group, western Nevada, and its tectonic implications: Unpublished thesis, Western Washington University, 206 p.

Tatlock, D.B., 1961, Redistribution of K, Na, and Al in Some Felsic Rocks in Nevada and Sweden: Mining Engineering, vol. 13, p. 1256.

van Hinsberg, V.J., Henry, D.J., and Dutrow, B.L., 2011, Tourmaline as a Petrologic Forensic Mineral: A Unique Recorder of Its Geologic Past: Elements, vol. 7, pp. 327-332.

Vearncombe, J.R., 1993, Quartz vein morphology and implications for formation depth and classification of Archaean gold-vein deposits: Ore Geology Reviews, vol. 8, pp. 407-424.

Vetz, N.Q., 2011, Geochronologic and Isotopic Investigation of the Koipato Formation, Northwestern Basic, Nevada: Implications for Late Permian-Early Triassic Tectonics Along the Western U.S. Cordillera: Abstract, Boise State University, 147 p.

Vikre, P., 1977, Geology and silver mineralization of the Rochester district, Pershing County, Nevada: Unpublished Ph.D. dissertation, Stanford University, 404 p.

Vikre, P., 1981, Silver Mineralization in the Rochester District, Pershing County, Nevada: Economic Geology, vol. 76, pp. 580-609.

Vikre, P.G., and McKee, E.H., 1985, Zoning and Chronology of Hydrothermal Events in the Humboldt Range, Pershing County, NV: Isochron/West, no. 44, p. 17-24.

Wallace, R.E., Tatlock, D.B., and Silberling, N. J., 1960, Intrusive rocks of Permian and Triassic age in the Humboldt Range, Nevada: U.S. Geol. Survey Prof. Paper 400-B, p.B291-B293.

Wallace, R.E., Tatlock, D. B., Silberling, N.J., and Irwin, W. P., 1969a, Geologic map of the Unionville quadrangle, Pershing County, Nevada: U.S. Geological Survey Map GQ-820.

Wallace, R.E., Tatlock, D. B., Silberling, N.J., and Irwin, W. P., 1969b, Geologic map of the Buffalo Mountain quadrangle, Pershing and Churchill Counties, Nevada: U.S. Geological Survey Map GQ-821.

Weir, R.H. Jr., and Kerrick, D.M., 1987, Mineralogic, Fluid Inclusion, and Stable Isotope Studies of Several Gold Mines in the Mother Lode, Tuolumne and Mariposa Counties, California: Economic Geology, vol. 82, pp. 328-344.

Wilson, S.E., 2010, Technical Report, Lincoln Hill, Pershing County, Nevada: NI-43-101 Technical Report, 70 p.

Wyld, S.J., 2002, Structural evolution of a Mesozoic backarc fold-and-thrust belt in the U.S. Cordillera: New evidence from northern Nevada: GSA Bulletin; v. 114; no. 11; p. 1452–1468

Wyld, S.J., Rogers, J.W., and Copeland, P., 2003, Metamorphic Evolution of the Luning-Fencemaker Fold-Thrust Belt, Nevada: Illite Crystallinity, Metamorphic Petrology, and 40Ar/39Ar Geochronology: The Journal of Geology, volume 111, p. 17–38.

Wyld, S.J., Rogers, J.W., and Wright, J.E., 2001, Structural evolution within the Luning-Fencemaker fold-thrust belt, Nevada: progression from back-arc basin closure to intra-arc shortening: Journal of Structural Geology, vol. 23, pp. 1971-1995.

Appendix A - U-Pb CA-TIMS results

The chemical abrasion isotope dilution thermal ionization mass spectrometry (CA-TIMS) U-Pb dating method was used to obtain zircon ages of host rocks within the Rochester and Weaver formations and of spatially associated intrusive bodies. CA-TIMS dating was performed by Dr. Jim Crowley at the Isotope Geology Laboratory at Boise State University. Results are presented below.

Notes (see tables A1-A6 below)

(a) z1, z2, etc. are labels for analyses composed of single zircon grains that were annealed and chemically abraded (Mattinson, 2005).

Fraction labels in bold denote analyses used in the weighted mean calculations.

(b) Model Th/U ratio calculated from radiogenic 208Pb/206Pb ratio and 207Pb/235U date.

(c) Pb* and Pbc are radiogenic and common Pb, respectively. mol % ^{206}Pb* is with respect to radiogenic and blank Pb.

(d) Measured ratio corrected for spike and fractionation only. Fractionation correction is 0.18 ± 0.03 (1 sigma) %/amu (atomic mass unit) for single-collector Daly analyses, based on analysis of EARTHTIME 202Pb-205Pb tracer solution

(e) Corrected for fractionation, spike, common Pb, and initial disequilibrium in 230Th/238U. Common Pb is assigned to procedural blank with composition of 206Pb/204Pb = 18.35 ± 1.50%; 207Pb/204Pb = 15.60 ± 0.75%; 208Pb/204Pb = 38.08 ± 1.00% (1 sigma). 206Pb/238U and 207Pb/206Pb ratios corrected for initial disequilibrium in 230Th/238U using Th/U [magma] = 3.

(f) Errors are 2 sigma, propagated using algorithms of Schmitz and Schoene (2007) and Crowley et al. (2007).

(g) Calculations based on the decay constants of Jaffey et al. (1971). 206Pb/238U and 207Pb/206Pb dates corrected for initial disequilibrium in 230Th/238U using Th/U [magma] = 3.

Table A-1: U-Pb CA-TIMS isotopic data from sample BC-1 (Quartz-eye Rhyolite)

	Th/U (b)	$^{206}Pb^*$ x10^{-13} mol (c)	mol % $^{206}Pb^*$ (c)	Pb^*/Pb_c (c)	Pb_c (pg) (c)	$^{206}Pb/^{204}Pb$ (d)	Radiogenic Isotope Ratios: $^{208}Pb/^{206}Pb$ (e)	$^{207}Pb/^{206}Pb$ (e)	% err (f)	$^{207}Pb/^{235}U$ (e)	% err (f)	$^{206}Pb/^{238}U$ (e)	% err (f)	corr. coef.
	0.481	3.5020	99.89%	264	0.33	16121	0.153	0.051177	0.089	0.278274	0.145	0.039436	0.070	0.893
	0.351	8.8498	99.92%	347	0.61	21885	0.113	0.052436	0.074	0.291507	0.152	0.040319	0.098	0.914
	0.382	9.1609	99.93%	426	0.52	26689	0.121	0.051201	0.072	0.278425	0.133	0.039439	0.069	0.940
	0.339	5.4568	99.86%	212	0.61	13462	0.107	0.051145	0.093	0.277929	0.150	0.039412	0.071	0.884
	0.466	5.8808	99.91%	340	0.43	20846	0.148	0.051218	0.079	0.278634	0.138	0.039456	0.069	0.927
	0.379	4.4800	99.85%	189	0.57	11842	0.120	0.051172	0.100	0.278105	0.154	0.039416	0.069	0.866

Sample (a)	Isotopic Dates: ± (f)	$^{207}Pb/^{235}U$ (g)	± (f)	$^{206}Pb/^{238}U$ (g)	± (f)
BC-1					
z1					
z3	1.68	259.74	0.35	254.81	0.25
z4	1.67	249.41	0.30	249.36	0.17
z5	2.15	249.01	0.33	249.19	0.17
z6	1.81	249.57	0.31	249.46	0.17
248.58	2.31	249.15	0.34	249.21	0.17

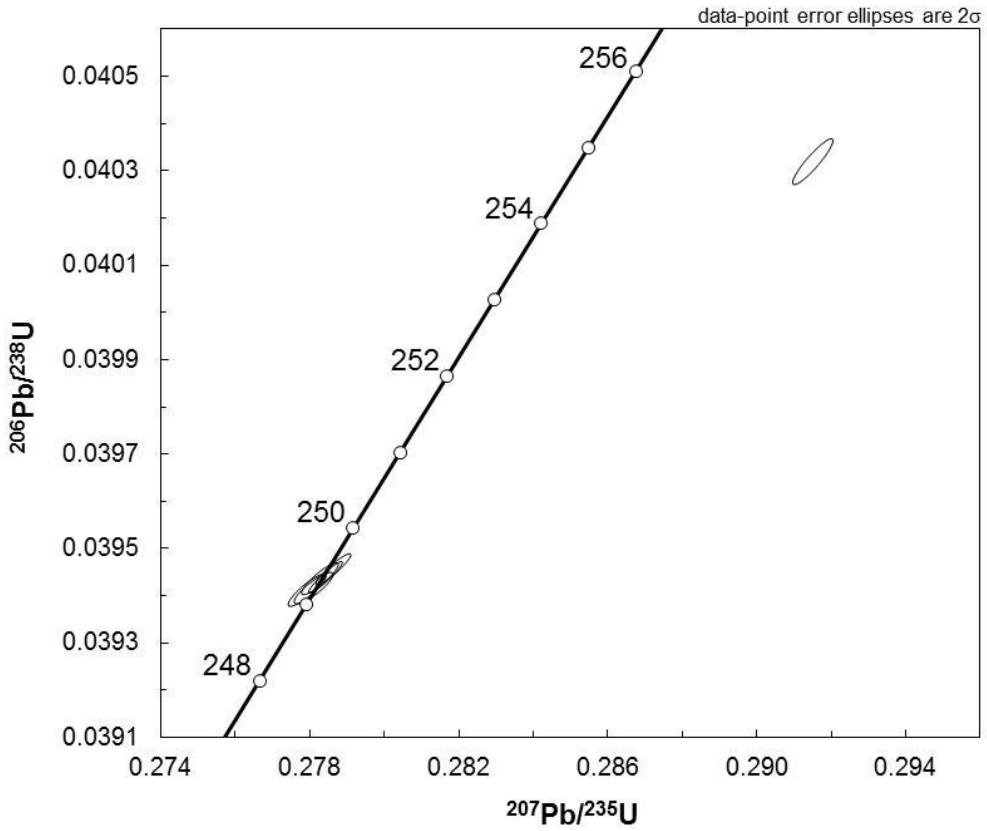

Fig. A-1: CA-TIMS Isochron plot of zircon grains from sample BC-1 (Quartz-eye Rhyolite).

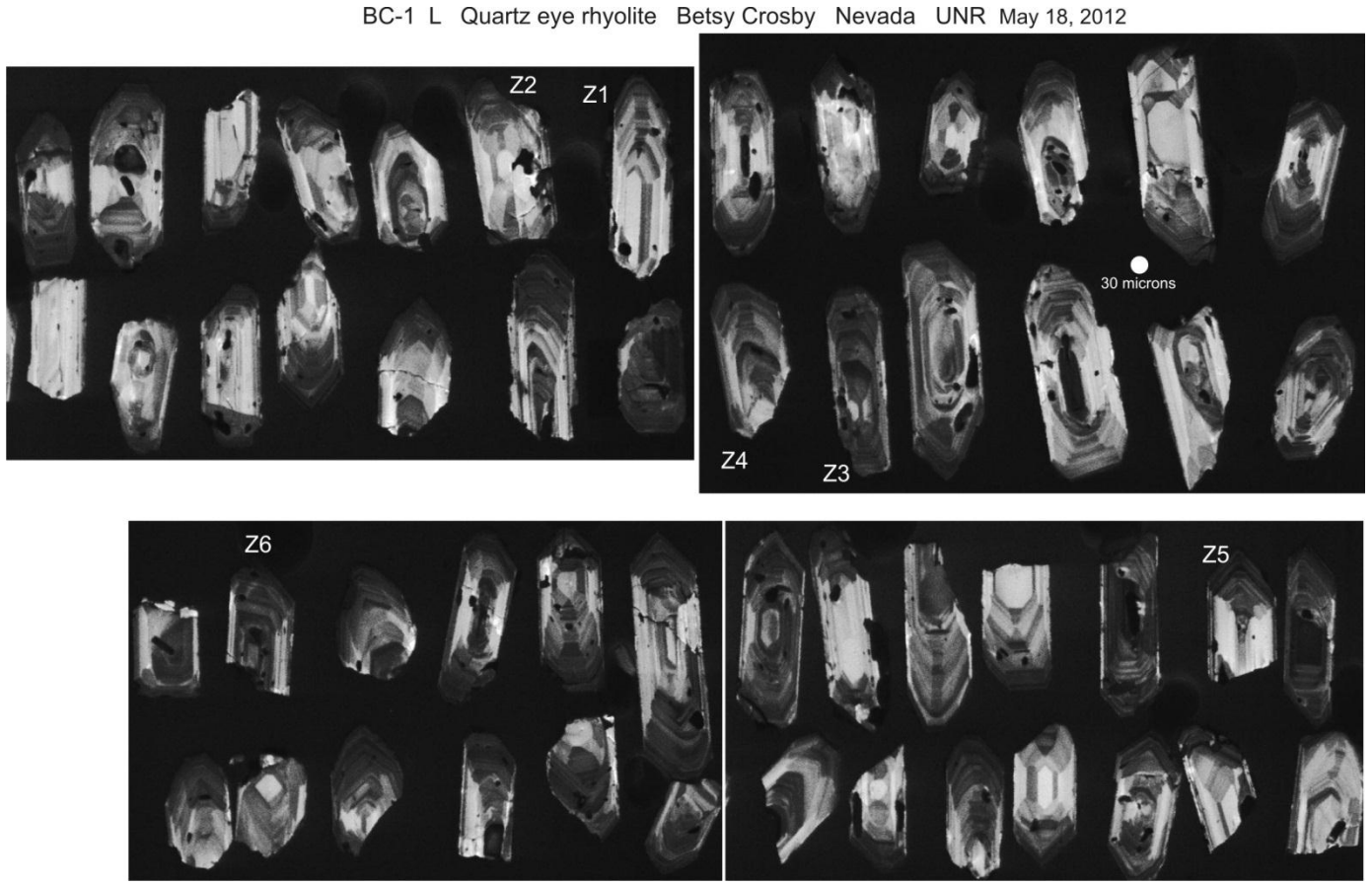

Figure A-2: Cathodeluminescence images zircon grains separated from sample BC-1. Labeled grains were selected for analyses.

Table A-2: U-Pb CA-TIMS isotopic data from sample BC-3 (Feldspar Porphyry)

Sample (a)	Th/U (b)	$^{206}Pb^*$ x10^{-13} mol (c)	mol % $^{206}Pb^*$ (c)	Pb^*/Pb_c (c)	Pb_c (pg) (c)	$^{206}Pb/^{204}Pb$ (d)	Radiogenic Isotope Ratios: $^{208}Pb/^{206}Pb$ (e)	$^{207}Pb/^{206}Pb$ (e)	% err (f)	$^{207}Pb/^{235}U$ (e)	% err (f)	$^{206}Pb/^{238}U$ (e)	% err (f)	corr. coef.
BC-3														
z1	0.456	1.5736	99.68%	92	0.42	5674	0.145	0.051190	0.181	0.278516	0.227	0.039461	0.070	0.748
z2	0.462	1.9147	99.69%	95	0.50	5859	0.146	0.051132	0.173	0.277962	0.219	0.039427	0.070	0.743
z3	0.609	1.5929	99.66%	90	0.45	5323	0.193	0.051253	0.192	0.278772	0.236	0.039448	0.073	0.702
z4	0.632	1.8354	99.66%	90	0.52	5320	0.200	0.051130	0.185	0.277982	0.230	0.039431	0.070	0.724
z5	0.575	1.0250	99.49%	61	0.43	3632	0.182	0.051005	0.271	0.277387	0.315	0.039443	0.074	0.660
z6	0.644	2.0408	99.78%	141	0.37	8262	0.204	0.051222	0.131	0.278457	0.181	0.039427	0.069	0.820

Isotopic Dates

Sample (a)	± (f)	$^{207}Pb/^{235}U$ (g)	± (f)	$^{206}Pb/^{238}U$ (g)	± (f)
BC-3	4.16	249.48	0.50	249.49	0.17
z1	3.99	249.04	0.48	249.28	0.17
z2	4.42	249.68	0.52	249.41	0.18
z3	4.26	249.06	0.51	249.30	0.17
z4	6.25	248.58	0.69	249.38	0.18
z5	3.00	249.43	0.40	249.28	0.17
z6					

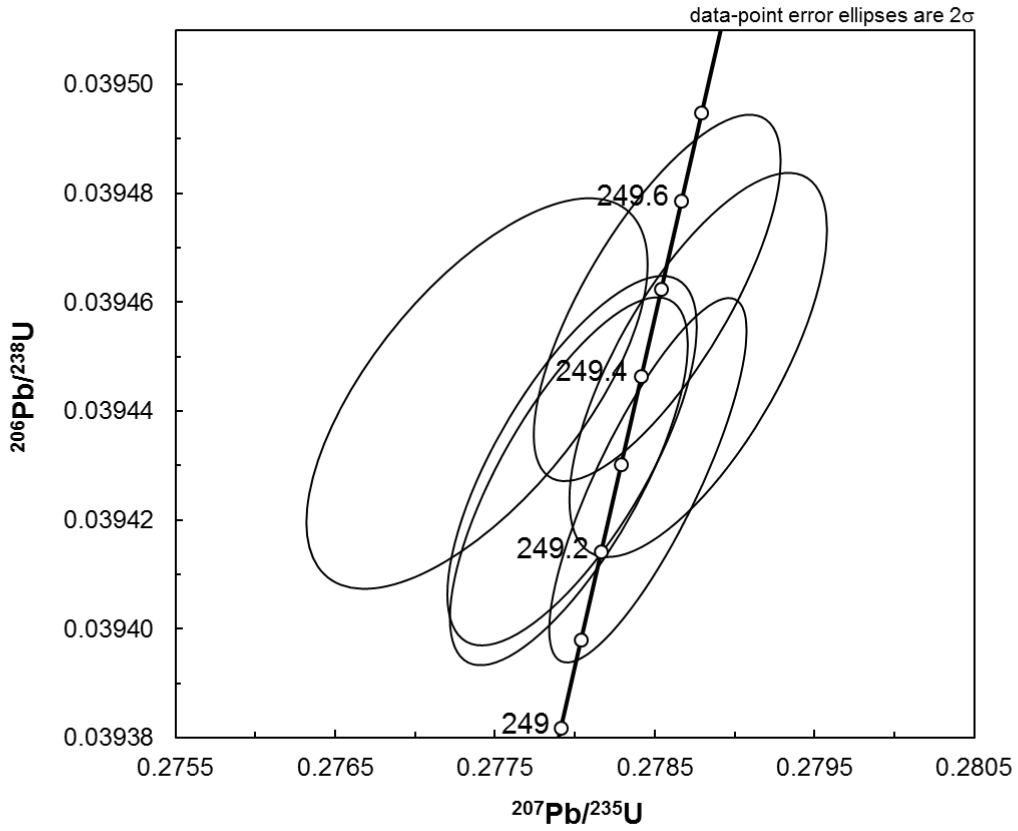

Figure A-3: CA-TIMS Isochron plot of zircon ages from sample BC-3 (Feldspar Porphyry)

Figure A-4: CL images of zircon grains from sample BC-3. Labeled grains were selected for CA-TIMS analyses.

Table A-3: U-Pb CA-TIMS isotopic data from sample BC-4 (Rhyolite Porphyry)

Sample (a)	Th/U (b)	$^{206}Pb^*$ x10^{-13} mol (c)	mol % $^{206}Pb^*$ (c)	Pb^*/Pb_c (c)	Pb_c (pg) (c)	$^{206}Pb/^{204}Pb$ (d)	Radiogenic Isotope Ratios: $^{208}Pb/^{206}Pb$ (e)	$^{207}Pb/^{206}Pb$ (e)	% err (f)	$^{207}Pb/^{235}U$ (e)	% err (f)	$^{206}Pb/^{238}U$ (e)	% err (f)	corr. coef.
BC-4														
z1	0.680	1.8864	99.74%	123	0.40	7159	0.216	0.051220	0.150	0.278922	0.197	0.039495	0.071	0.762
z3	0.838	1.3058	99.53%	70	0.50	3936	0.266	0.051181	0.243	0.278046	0.286	0.039401	0.073	0.671
z4	0.451	2.4118	99.80%	146	0.41	9010	0.143	0.051172	0.125	0.278317	0.174	0.039447	0.070	0.813
z5	0.529	1.2942	99.49%	60	0.55	3611	0.168	0.051135	0.266	0.278053	0.309	0.039438	0.074	0.661
z6	0.667	1.0705	99.55%	70	0.40	4072	0.211	0.051099	0.251	0.278176	0.295	0.039482	0.074	0.670
z7	0.538	0.9168	99.44%	54	0.43	3282	0.170	0.051062	0.319	0.277697	0.364	0.039443	0.075	0.660
z8	0.909	2.1266	99.76%	137	0.43	7541	0.288	0.051092	0.151	0.277903	0.198	0.039449	0.071	0.766

Isotopic Dates

Sample (a)	± (f)	$^{207}Pb/^{235}U$ (g)	± (f)	$^{206}Pb/^{238}U$ (g)	± (f)
BC-4					
z1	3.46	249.80	0.44	249.70	0.17
z3	5.60	249.11	0.63	249.12	0.18
z4	2.87	249.32	0.39	249.40	0.17
z5	6.13	249.11	0.68	249.35	0.18
z6	5.79	249.21	0.65	249.62	0.18
z7	7.35	248.83	0.80	249.38	0.18
z8	3.47	248.99	0.44	249.42	0.17

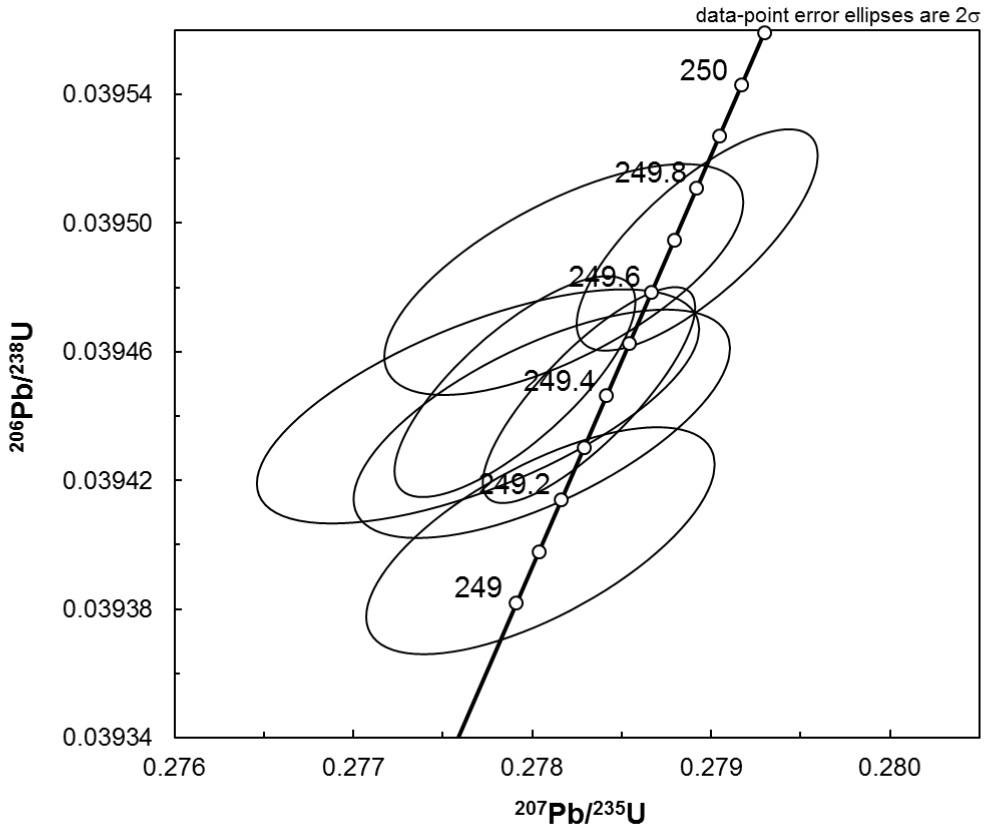

Figure A-5: CA-TIMS Isochron plot of ages of zircon grains from sample BC-4 (Rhyolite Porphyry)

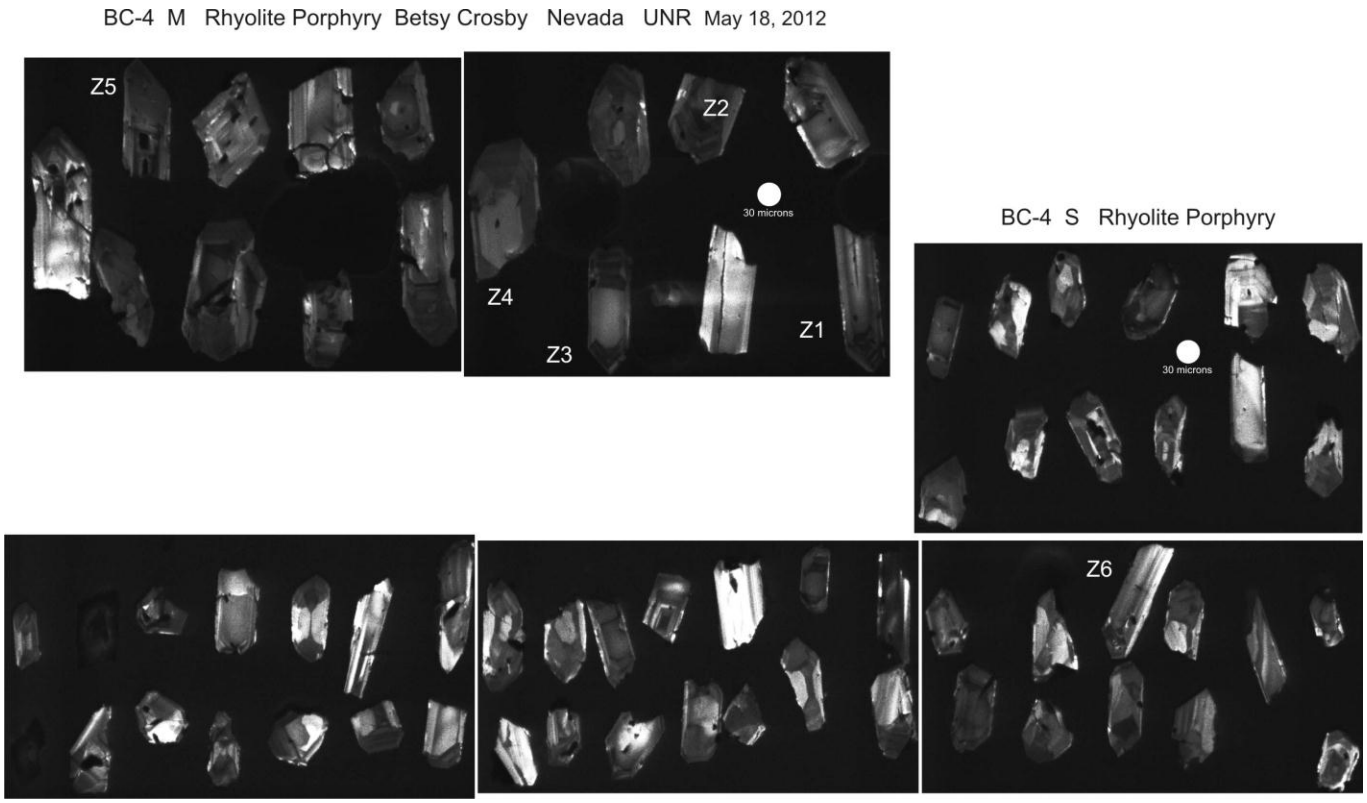

Figure A-6: CL images of zircon grains from sample BC-4. Labeled grains were selected for analyses.

Table A-4: U-Pb CA-TIMS isotopic data from sample BC-5 (Leucogranite)

Sample (a)	Th/U (b)	$^{206}Pb^*$ x10^{-13} mol (c)	mol % $^{206}Pb^*$ (c)	Pb^*/Pb_c (c)	Pb_c (pg) (c)	$^{206}Pb/^{204}Pb$ (d)	Radiogenic Isotope Ratios: $^{208}Pb/^{206}Pb$ (e)	$^{207}Pb/^{206}Pb$ (e)	% err (f)	$^{207}Pb/^{235}U$ (e)	% err (f)	$^{206}Pb/^{238}U$ (e)	% err (f)	corr. coef.
BC-5														
z1	0.437	4.5401	99.84%	186	0.60	11477	0.139	0.051243	0.106	0.278385	0.161	0.039401	0.073	0.846
z2	0.433	6.5957	99.92%	357	0.45	22074	0.137	0.051199	0.076	0.278156	0.136	0.039403	0.069	0.929
z3	0.511	2.2686	99.49%	59	0.96	3594	0.162	0.051135	0.258	0.278588	0.299	0.039513	0.072	0.652
z4	0.535	4.2453	99.82%	168	0.64	10086	0.170	0.051242	0.112	0.278615	0.164	0.039434	0.071	0.835
z5	0.668	2.5288	99.69%	103	0.64	6002	0.211	0.051144	0.168	0.280446	0.214	0.039770	0.073	0.733
z6	0.457	1.4382	99.71%	101	0.35	6230	0.145	0.051199	0.167	0.278144	0.213	0.039401	0.071	0.752
z7	0.766	1.4166	98.68%	24	1.56	1395	0.242	0.051082	0.651	0.277469	0.706	0.039396	0.088	0.661
z9	0.467	2.4395	99.76%	122	0.49	7492	0.148	0.051140	0.147	0.277658	0.195	0.039377	0.070	0.775

Sample (a)	Isotopic Dates: ± (f)	$^{207}Pb/^{235}U$ (g)	± (f)	$^{206}Pb/^{238}U$ (g)	± (f)
BC-5					
z1	2.44	249.38	0.36	249.12	0.18
z2	1.76	249.19	0.30	249.13	0.17
z3	5.93	249.54	0.66	249.81	0.18
z4	2.57	249.56	0.36	249.33	0.17
z5	3.87	251.01	0.48	251.41	0.18
z6	3.84	249.18	0.47	249.12	0.17
z7	14.99	248.65	1.56	249.08	0.22
z9	3.38	248.80	0.43	248.97	0.17

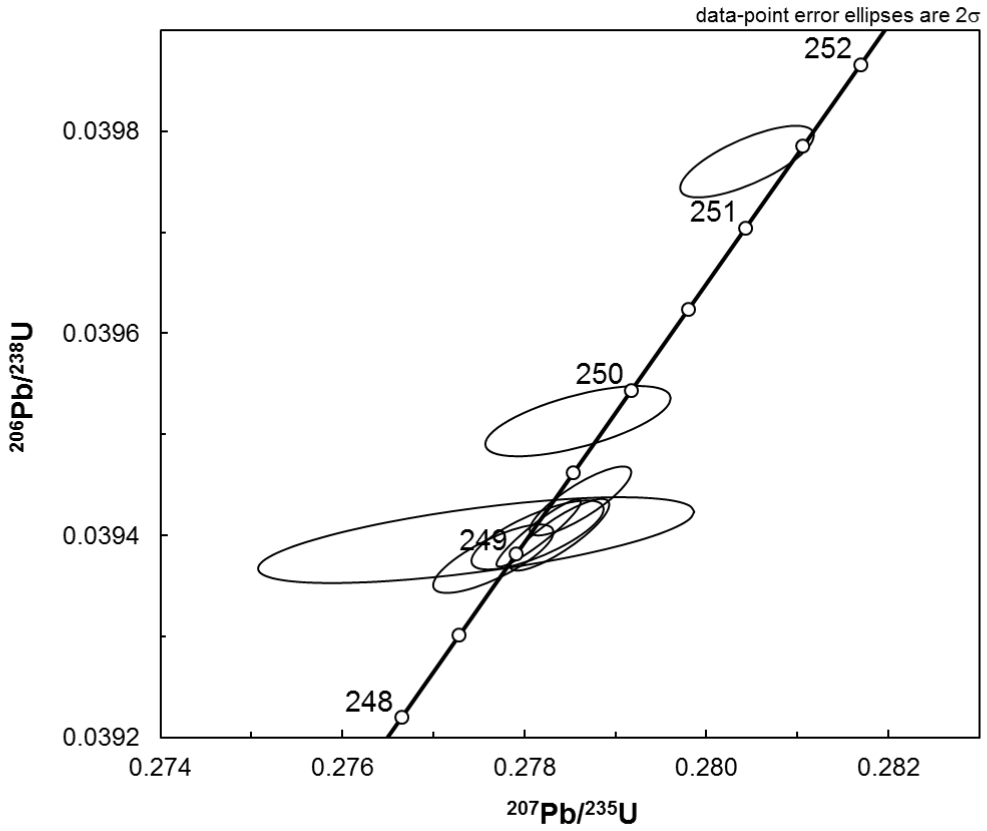

Figure A-7: CA-TIMS Isochron plot of ages of zircon grains from sample BC-5 (Leucogranite)

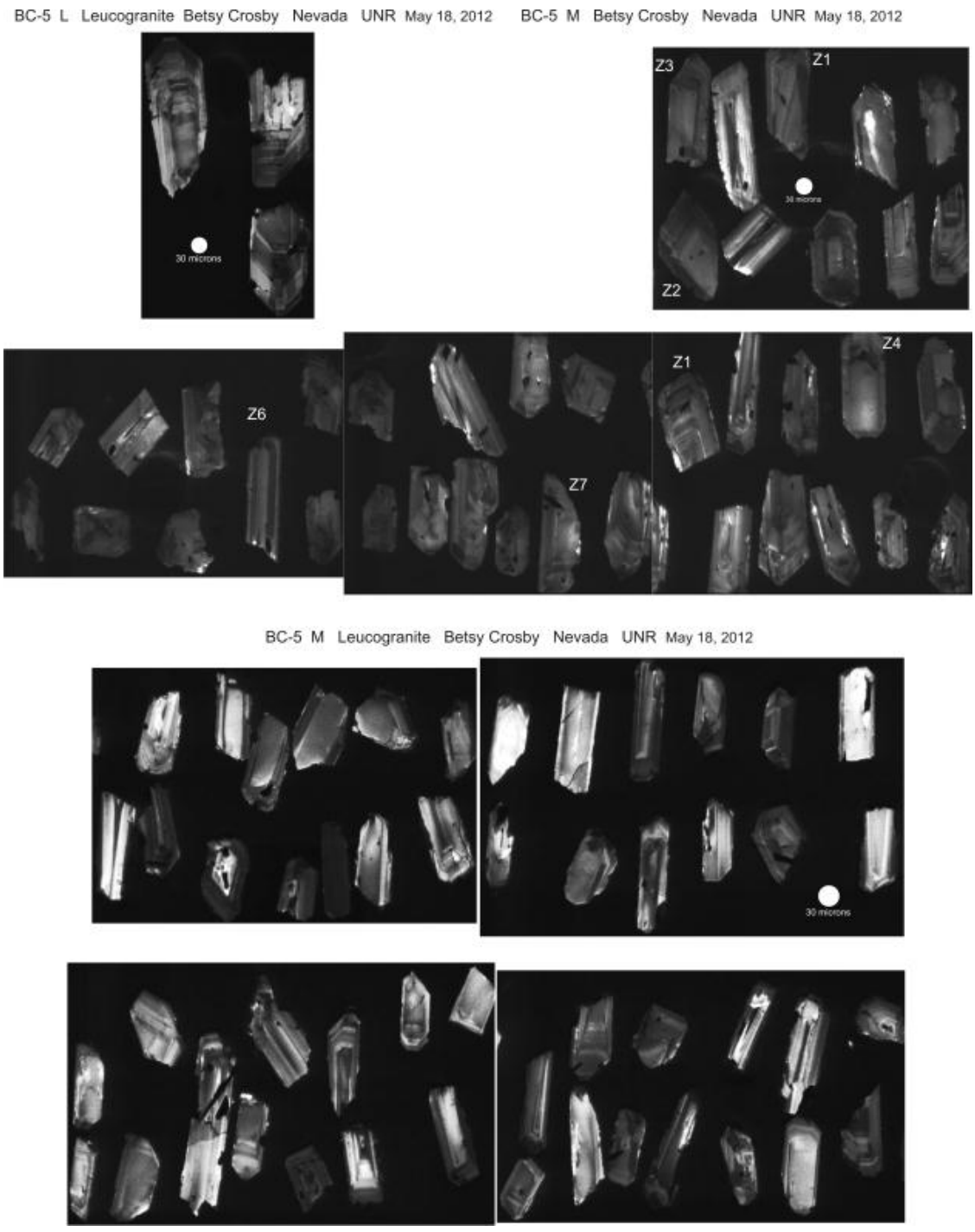

Figure A-8: CL images of zircon grains from sample BC-5. Labeled grains were selected for analyses.

Table A-5: U-Pb CA-TIMS isotopic data from sample BC-6 (Rocky Canyon granodiorite)

Sample (a)	Th/U (b)	$^{206}Pb^*$ x10^{-13} mol (c)	mol % $^{206}Pb^*$ (c)	Pb^*/Pb_c (c)	Pb_c (pg) (c)	$^{206}Pb/^{204}Pb$ (d)	Radiogenic Isotope Ratios: $^{208}Pb/^{206}Pb$ (e)	$^{207}Pb/^{206}Pb$ (e)	% err (f)	$^{207}Pb/^{235}U$ (e)	% err (f)	$^{206}Pb/^{238}U$ (e)	% err (f)	corr. coef.
BC-6														
z1	0.264	6.5221	99.91%	300	0.51	19399	0.086	0.049247	0.083	0.130894	0.142	0.019277	0.070	0.907
z2	0.270	4.2141	99.85%	196	0.51	12644	0.088	0.049034	0.095	0.122687	0.152	0.018147	0.071	0.889
z3	0.227	3.9870	99.85%	191	0.48	12538	0.073	0.048095	0.109	0.098888	0.161	0.014912	0.073	0.827
z4	0.299	1.6561	99.68%	90	0.43	5822	0.096	0.047807	0.186	0.091675	0.232	0.013908	0.071	0.727
z5	0.266	2.8468	99.82%	157	0.42	10177	0.086	0.050056	0.116	0.169122	0.168	0.024504	0.070	0.831
z6	0.232	3.3740	99.84%	176	0.44	11512	0.075	0.048943	0.113	0.120824	0.166	0.017905	0.072	0.838

Sample (a)	Isotopic Dates: ± (f)	$^{207}Pb/^{235}U$ (g)	± (f)	$^{206}Pb/^{238}U$ (g)	± (f)
BC-6					
z1	1.95	124.90	0.17	123.09	0.09
z2	2.23	117.51	0.17	115.93	0.08
z3	2.57	95.75	0.15	95.42	0.07
z4	4.42	89.06	0.20	89.04	0.06
z5	2.70	158.66	0.25	156.06	0.11
z6	2.64	115.82	0.18	114.40	0.08

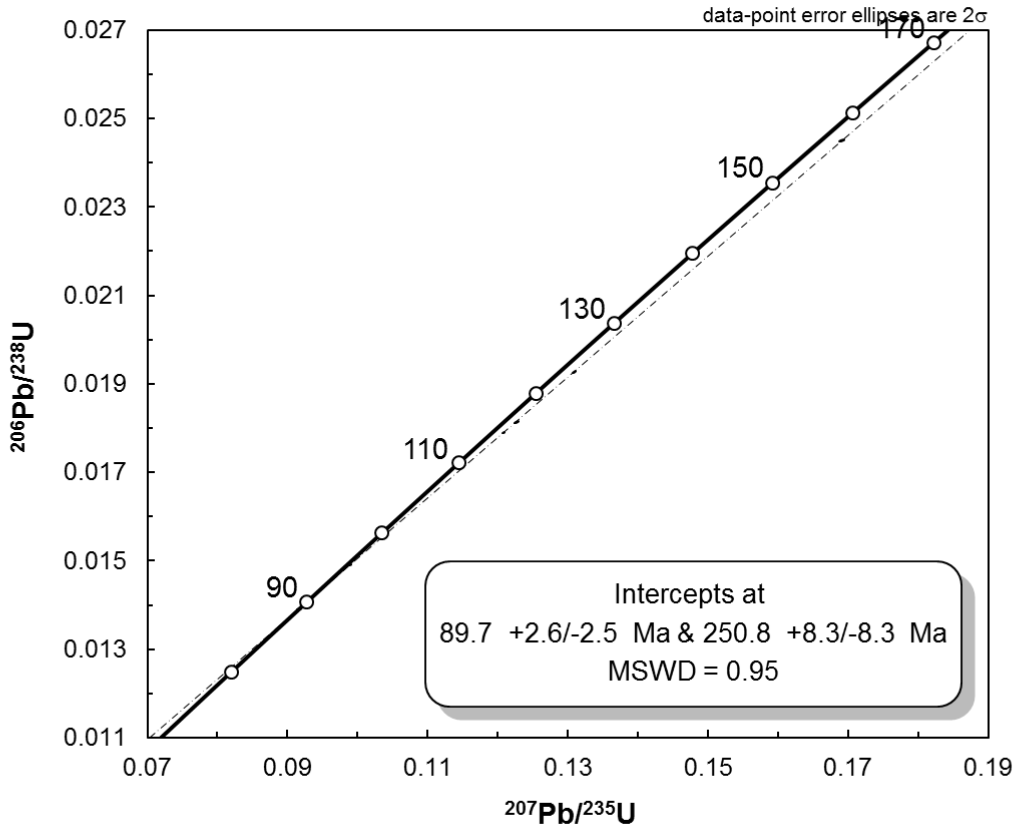

Figure A-9: CA-TIMS Isochron plot of ages of zircon grains from sample BC-6 (Rocky Canyon granodiorite)

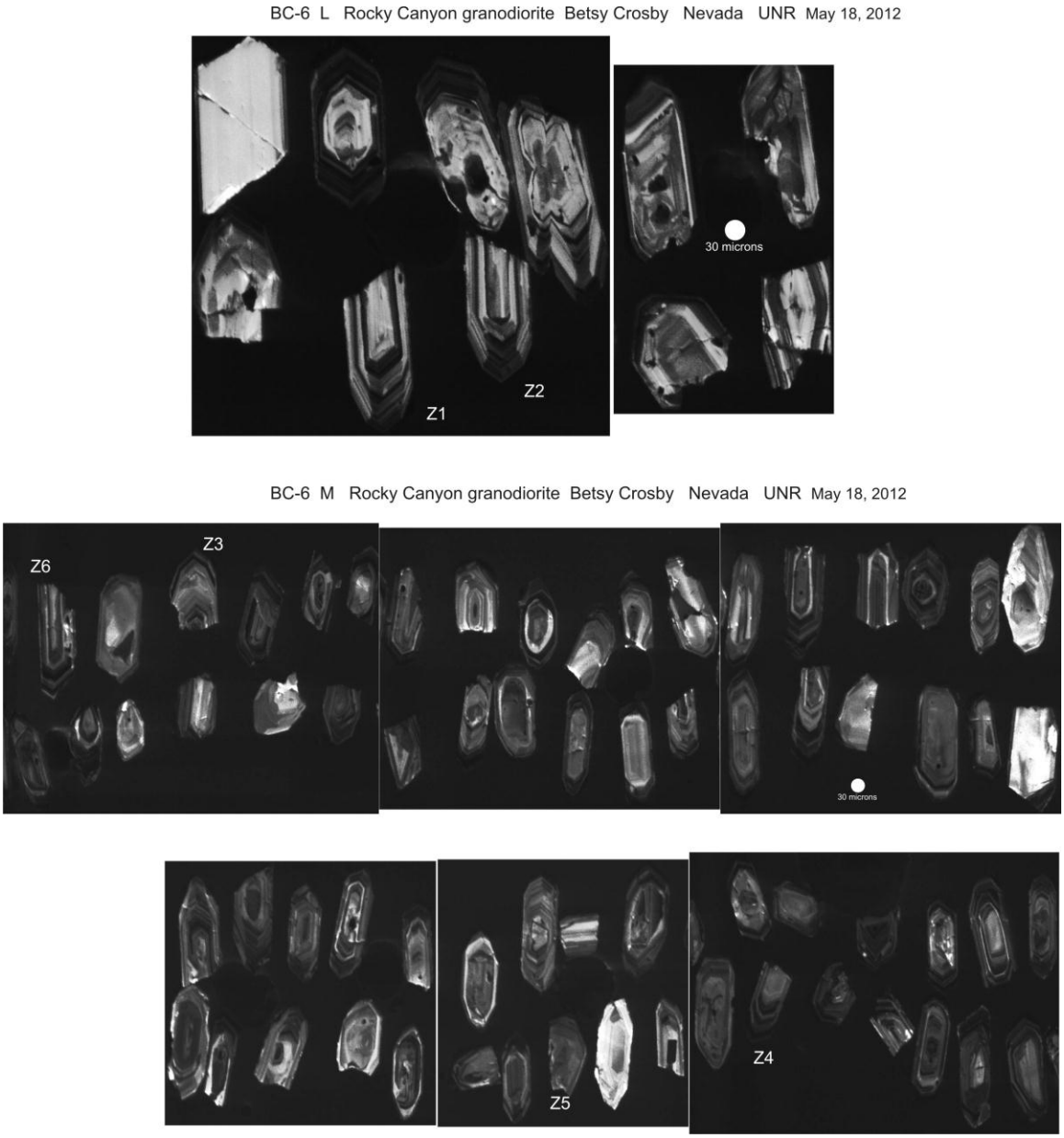

Figure A-10: CL images of zircon grains from sample BC-6. Labeled grains were selected for analyses.

Table A-6: U-Pb CA-TIMS isotopic data from sample BC-7 (Canyon monzonite)

							Radiogenic Isotope Ratios							
	$\frac{Th}{U}$	$^{206}Pb^*$ x10^{-13} mol	mol % $^{206}Pb^*$	$\frac{Pb^*}{Pb_c}$	Pb_c (pg)	$\frac{^{206}Pb}{^{204}Pb}$	$\frac{^{208}Pb}{^{206}Pb}$	$\frac{^{207}Pb}{^{206}Pb}$	% err	$\frac{^{207}Pb}{^{235}U}$	% err	$\frac{^{206}Pb}{^{238}U}$	% err	corr. coef.
	(b)	(c)	(c)	(c)	(c)	(d)	(e)	(e)	(f)	(e)	(f)	(e)	(f)	
	1.539	0.5629	99.24%	50	0.36	2402	0.495	0.046682	0.429	0.032114	0.472	0.004989	0.078	0.620
	1.487	0.2515	97.55%	15	0.52	749	0.480	0.046905	1.371	0.032246	1.463	0.004986	0.109	0.852
	1.790	0.7703	99.29%	56	0.46	2568	0.574	0.046618	0.404	0.032086	0.447	0.004992	0.078	0.614
	1.505	0.2474	97.69%	16	0.48	795	0.486	0.046923	1.272	0.032275	1.357	0.004989	0.107	0.805
	1.493	0.3114	96.74%	11	0.87	562	0.478	0.046509	1.819	0.031992	1.932	0.004989	0.131	0.870
	1.349	0.3335	98.14%	20	0.52	986	0.432	0.046522	1.144	0.031990	1.220	0.004987	0.102	0.768

	Isotopic Dates				
Sample	±	$\frac{^{207}Pb}{^{235}U}$	±	$\frac{^{206}Pb}{^{238}U}$	±
(a)	(f)	(g)	(f)	(g)	(f)
BC-7					
z1	10.26	32.10	0.15	32.08	0.02
z2	32.75	32.22	0.46	32.06	0.03
z3	9.69	32.07	0.14	32.10	0.02
z4	30.38	32.25	0.43	32.08	0.03
z5	43.61	31.98	0.61	32.08	0.04
z6	27.42	31.97	0.38	32.07	0.03

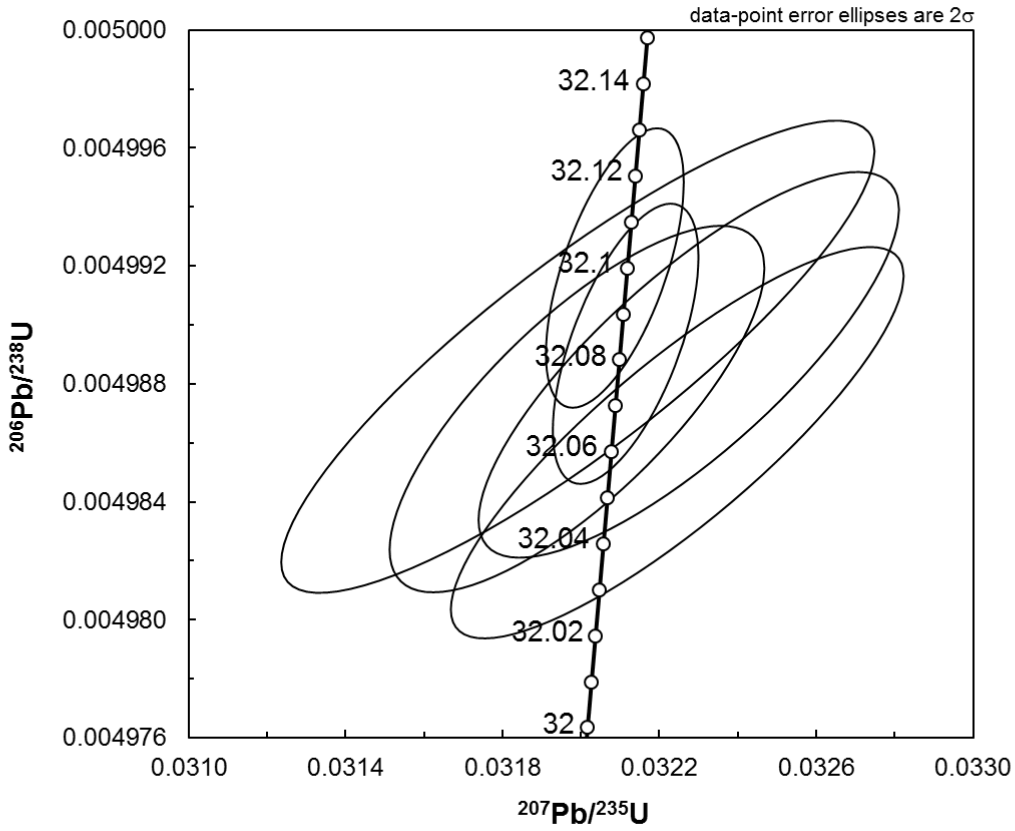

Figure A-11: CA-TIMS Isochron plot of ages of zircon grains from sample BC-7 (Canyon monzonite)

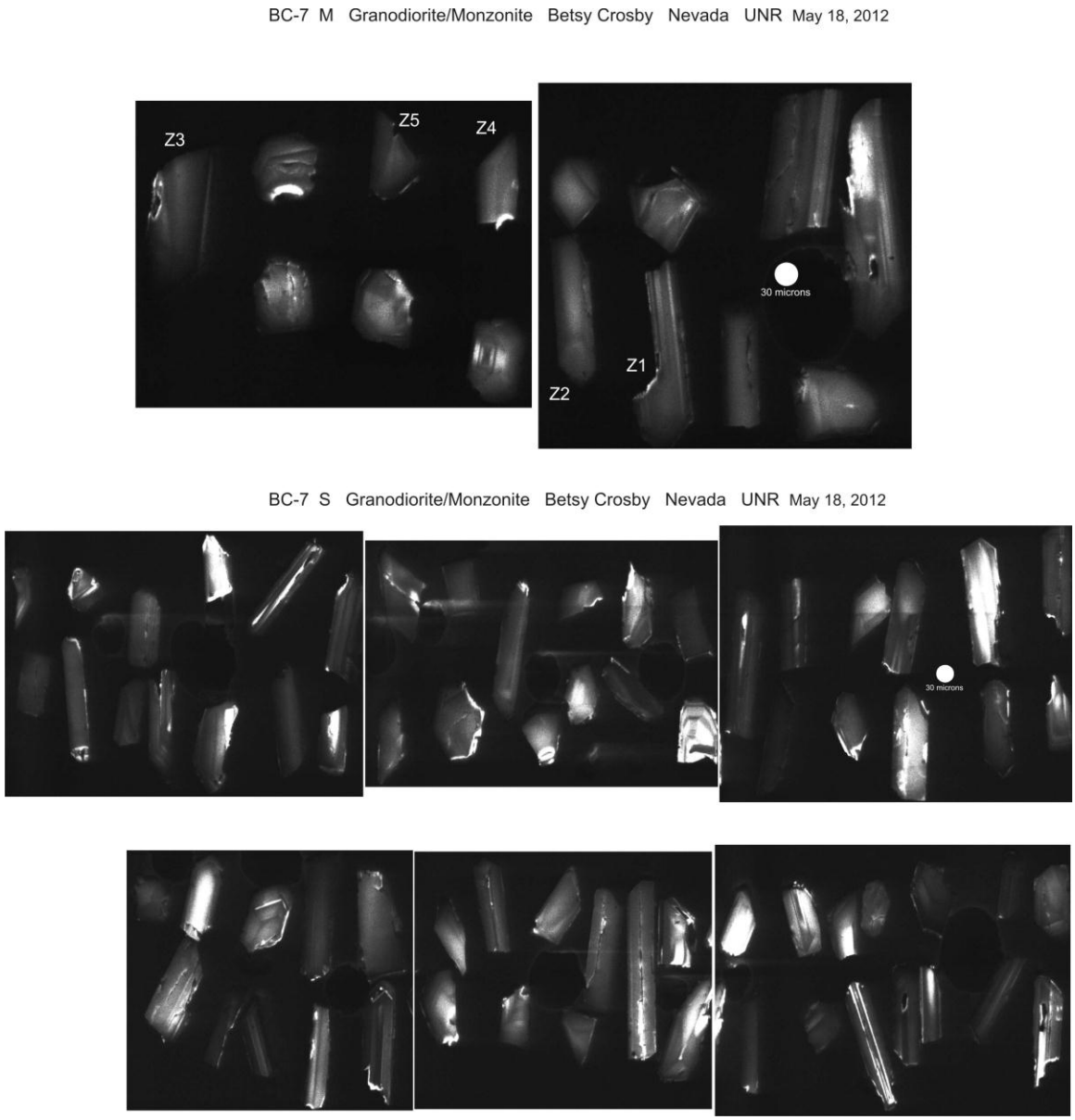

Figure A-12: CL images of zircon grains from sample BC-7. Labeled grains were selected for analyses.

Appendix B - Alteration Geochemistry

Ten samples from select alteration transects were sent to ALS Chemex for borate fusion analyses of trace element, metal, and major element geochemistry. The purpose of these analyses was to determine the geochemical associations of different alteration assemblages and to identify major and trace element changes from relatively unaltered to vein-distal altered to vein-proximal altered wallrock. Results of these analyses are presented below. See text for discussion.

Table B-1: Trace element compositions of samples from selected alteration zones. . ***(All values reported in ppm)***

SAMPLE	Ag	Ba	Ce	Co	Cr	Cs	Cu	Dy	Er	Eu	Ga
FP-1[3]	<1	920	111.5	1.3	10	4.83	<5	4.67	2.65	1	16.9
FP-2[1]	2	1135	100	1.9	10	5.79	39	4.88	2.75	0.81	15.7
FP-3[1]	5	1095	101.5	2.1	10	5.66	30	4.46	2.56	0.8	15.2
FP-5[2]	<1	1140	104	1.1	10	4.45	5	4.77	2.63	1.12	11.3
FP-6[3]	<1	1530	125	1.6	10	8.03	<5	3.4	2.25	0.76	21.3
FP-8[1]	<1	1255	112.5	1.6	<10	5.93	20	2.82	1.63	0.77	15
FP-9[1]	2	1215	95.5	2.1	10	7.22	16	3.33	1.92	0.77	19.8
FP-10[2]	<1	1315	125	2.1	10	5.77	<5	3.37	2.07	0.81	13.6
FP-11	<1	695	95.3	1.8	<10	3.52	9	3.48	2.23	0.72	12.9
FP-12	<1	733	121	2.3	10	8.37	<5	4.94	2.86	0.98	18.4

SAMPLE	Gd	Hf	Ho	La	Lu	Mo	Nb	Nd	Ni	Pb	Pr
FP-1[3]	5.8	7.6	0.94	58.5	0.43	<2	16.4	42.5	<5	8	12.05
FP-2[1]	5.67	6.3	0.92	52.1	0.39	3	15	38.1	<5	205	10.95
FP-3[1]	5.32	6	0.84	53.7	0.35	3	14.9	38.4	<5	2160	11.1
FP-5[2]	6.01	6.5	0.95	54.3	0.38	2	14.2	41.5	<5	18	11.5
FP-6[3]	4.58	7.9	0.73	65.7	0.43	<2	17.3	47.8	<5	19	13.7
FP-8[1]	4.33	5.8	0.56	59.3	0.3	<2	11.7	41.7	<5	12	12.05
FP-9[1]	4.36	5.7	0.67	50.4	0.35	<2	11.7	36.1	<5	602	10.35
FP-10[2]	4.73	6.5	0.7	66.5	0.35	2	14.2	47.4	<5	14	13.6
FP-11[4]	4.56	6.9	0.75	49.8	0.39	6	14.6	36.9	<5	30	10.4
FP-12[4]	6.17	7.1	1	62.8	0.43	<2	16.2	46.4	<5	12	13.2

[1] Proximal QSP-carbonate alteration

[2] Intermediate quartz-hematite alteration

[3] Distal quartz-specularite alteration

[4] Unaltered

Table B-1, cont'd: Trace element compositions of samples from selected alteration zones. ***(All values reported in ppm)***

SAMPLE	Rb	Sm	Sn	Sr	Ta	Tb	Th	Tl	Tm	U	V
FP-1[3]	169.5	7.41	3	79	1.4	0.86	28.4	0.6	0.41	6.11	9
FP-2[1]	200	6.78	3	55	1.2	0.85	24.1	0.8	0.4	11.45	10
FP-3[1]	199.5	6.6	4	41	1.1	0.78	22.5	0.8	0.37	18.55	10
FP-5[2]	158	7.73	3	90.9	1.3	0.87	25.3	0.7	0.38	7.06	9
FP-6[3]	248	7.26	4	50.1	1.5	0.6	30.8	1	0.36	7.03	15
FP-8[1]	193	6.38	2	46.6	1.1	0.54	21.6	0.8	0.26	7.94	12
FP-9[1]	220	6	3	38.5	1	0.6	20.7	0.8	0.3	9.34	14
FP-10[2]	180.5	7.26	3	69.4	1.2	0.61	26	0.8	0.31	6.58	9
FP-11[4]	86.5	6.23	3	90.4	1.3	0.62	25.6	<0.5	0.35	7.88	5
FP-12[4]	181	8.11	4	47.1	1.4	0.89	28.2	0.6	0.43	8.01	11

SAMPLE	W	Y	Yb	Zn	Zr
FP-1[3]	4	28.4	2.76	25	289
FP-2[1]	8	26.8	2.5	831	216
FP-3[1]	8	25.2	2.31	46	208
FP-5[2]	4	27.8	2.46	22	225
FP-6[3]	5	19.7	2.56	43	276
FP-8[1]	6	16.6	1.78	28	201
FP-9[1]	9	19.6	2.06	420	194
FP-10[2]	4	20.3	2.19	40	236
FP-11[4]	4	22.3	2.51	54	243
FP-12[4]	3	29.5	2.8	56	251

[1] Proximal QSP-carbonate alteration

[2] Intermediate quartz-hematite alteration

[3] Distal quartz-specularite alteration

[4] Unaltered

Table B-2: Major element compositions of samples from selected alteration zones.

SAMPLE	SiO2	Al2O3	Fe2O3	CaO	MgO	Na2O	K2O	Cr2O3	TiO2	MnO	P2O5
FP-1[3]	70	13.3	3.1	0.85	0.25	3.62	5.5	<0.01	0.28	0.02	0.1
FP-2[1]	75.3	12.65	2.4	0.28	0.17	2.3	5.73	<0.01	0.23	<0.01	0.07
FP-3[1]	75.1	11.8	3.88	0.22	0.23	1.64	5.65	<0.01	0.22	0.01	0.06
FP-5[2]	74.2	12.2	2.36	0.78	0.13	2.83	5.33	<0.01	0.22	0.03	0.05
FP-6[3]	71.8	13.6	2.84	0.47	0.51	1.61	6.27	<0.01	0.27	0.04	0.06
FP-8[1]	75.1	11.4	2.54	0.74	0.33	1.57	5.13	<0.01	0.19	0.03	0.06
FP-9[1]	72.8	12.05	3.19	1.13	0.56	0.96	5.13	<0.01	0.19	0.04	0.06
FP-10[2]	72.2	12.95	2.16	0.67	0.37	2.77	5.52	<0.01	0.2	0.04	0.06
FP-11[4]	70.9	14	2.23	1.84	0.37	5.21	2.48	<0.01	0.23	0.06	0.07
FP-12[4]	74.3	13.05	2.61	1.1	0.51	2.8	3.66	<0.01	0.26	0.04	0.08

SAMPLE	SrO	BaO	LOI	Total
FP-1[3]	0.01	0.12	1.44	98.59
FP-2[1]	0.01	0.14	1.59	100.87
FP-3[1]	<0.01	0.14	2.28	101.23
FP-5[2]	0.01	0.14	1.31	99.59
FP-6[3]	0.01	0.19	1.64	99.31
FP-8[1]	<0.01	0.15	1.88	99.12
FP-9[1]	<0.01	0.15	3.04	99.3
FP-10[2]	0.01	0.15	1.63	98.73
FP-11[4]	0.01	0.08	2.57	100.05
FP-12[4]	0.01	0.09	3.01	101.52

[1] Proximal QSP-carbonate alteration

[2] Intermediate quartz-hematite alteration

[3] Distal quartz-specularite alteration

[4] Unaltered

Table B-3: Metal concentrations in selected samples

SAMPLE	Ag	As	Cd	Co	Cu	Mo	Ni	Pb	Sc	Zn
FP-1[3]	<0.5	5	<0.5	2	1	2	4	9	6	27
FP-2[1]	1.7	45	7	2	37	2	3	211	5	915
FP-3[1]	4.7	60	<0.5	2	29	2	4	2320	5	47
FP-5[2]	<0.5	5	<0.5	1	3	2	4	19	5	27
FP-6[3]	<0.5	<5	<0.5	1	2	2	3	19	6	42
FP-8[1]	<0.5	34	<0.5	2	18	2	3	12	4	28
FP-9[1]	1.4	10	4.9	2	14	2	3	626	6	490
FP-10[2]	<0.5	<5	<0.5	2	2	2	3	12	4	42
FP-11	<0.5	11	<0.5	2	9	2	4	30	4	58
FP-12	<0.5	<5	<0.5	2	2	2	3	12	6	61